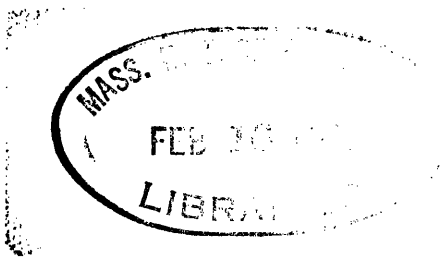

THE EARLY STAGES OF PLASTIC FLOW IN COPPER

by

William Thomas Brydges III

S.B., S.M., Massachusetts Institute of Technology
(1963)

SUBMITTED IN PARTIAL FULFILLMENT
OF THE REQUIREMENTS FOR THE
DEGREE OF DOCTOR OF
SCIENCE

at the

MASSACHUSETTS INSTITUTE OF TECHNOLOGY

Signature of Author . . . . . .
Department of Mechanical Engineering, October 31, 1966

Certified by . . . . . .
Thesis Supervisor

Accepted by . . . . . .
Chairman, Departmental Committee
on Graduate Students

THE EARLY STAGES OF PLASTIC FLOW IN COPPER

by

William Thomas Brydges III

Submitted to the Department of Mechanical Engineering on October 31, 1966 in partial fulfillment of the requirements for the degree of Doctor of Science.

ABSTRACT

The early stages of plastic flow in copper single crystals have been explored by dislocation etch pit experiments.

By twisting crystals to introduce known forest dislocation densities, the tension yield stress has been related to the forest density in the form

$$\tau_y = \tau_{yo} + \alpha_y G b \sqrt{N_f}$$

where $\tau_{yo} \approx 5$ g/mm^2 and $\alpha_y \approx 0.65$, indicating a strong interaction between primary and forest dislocations.

The motion of dislocations and their arrangement in multipole clusters have been studied as a function of stress in the pre-yield and easy glide regimes. Below the multiplication stress, about five per cent of the initial dislocations move, on slip planes subjected to a finite stress, distances comparable to the spacing of forest dislocations ($25 \cdot 10^{-4}$ cm). Above the multiplication stress, pre-yield strain is due to dislocations moving the order of ten forest spacings. In easy glide, dislocation multiplication experiments suggest that the distance of motion is constant and comparable to the crystal size (0.5 cm), and not sensitive to strain rate and temperature.

The dislocation motion accounting for the strain recovered on unloading has been determined. The distance of dislocation back motion decreases from about 60 to $25 \cdot 10^{-4}$ cm in the pre-yield region, and becomes constant at about $15 \cdot 10^{-4}$ cm in easy glide. The dislocation density in motion during unloading increases as the square root of strain through the pre-yield and easy glide regions.

The results support the view that the flow stress is determined by the forest dislocation density, and is the stress necessary for primary dislocations to move large distances through the forest.

Thesis Supervisor: Ali S. Argon
Title: Associate Professor of Mechanical Engineering

TABLE OF CONTENTS

LIST OF FIGURES

LIST OF TABLES

I. INTRODUCTION

It was recognized by Orowan (1934), Polanyi (1934), and Taylor (1934) that dislocations in a crystal lattice are responsible for values of the yield strength of crystals being several orders of magnitude lower than the theoretical lattice shear strength. Yet after thirty years of investigation of the relationships between dislocations and the plasticity of crystals, the initial portion of the stress-strain curve is quantitatively little understood. The tensile shear stress-shear strain curve for a copper single crystal used in this study is shown in Figure 1-1, with the characteristic parameters labelled. The attention of this work is directed to the pre-yield region (below τ_o, the macroscopic yield point), and to easy glide (Stage I).

Several factors contributed to the choice of copper for the study. It is a face-centered cubic metal which exhibits three stage hardening at room temperature and on which a considerable literature exists about mechanical behavior; it can be obtained in spectrographic purity and grown into single crystals of controlled orientation by standard techniques; and, of primary importance for this work, on certain crystallographic surfaces the points of emergence of dislocations can be revealed reliably by pits produced by chemical attack.

Experiments in the early stages of plastic deformation are afflicted by at least two inherent difficulties. First, mechanical properties in these regimes are strongly dependent on the initial structure of the crystals, and experimentally there is always some variation in structure

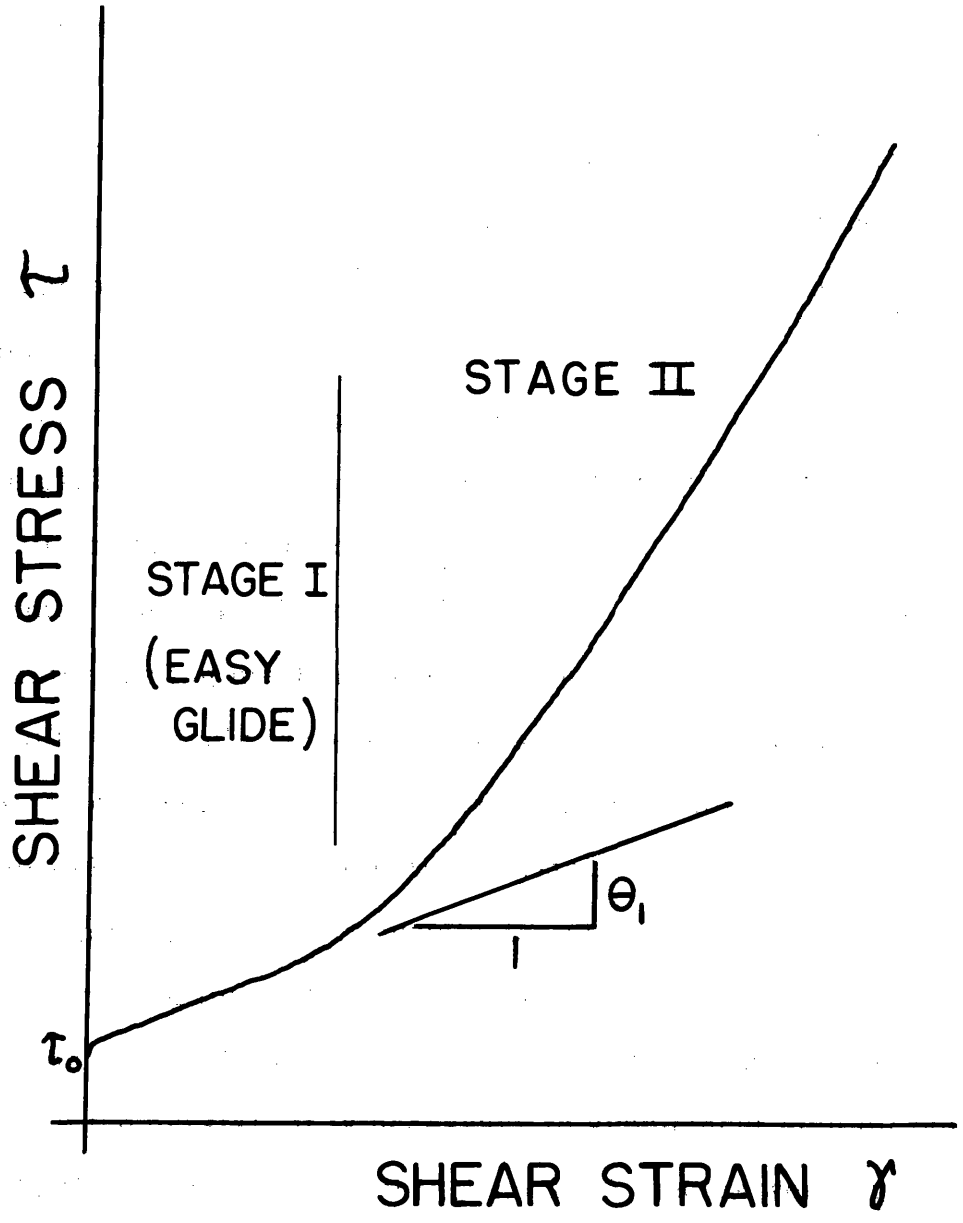

Fig. 1-1. Shear stress-shear strain curve for a copper single crystal with characteristic parameters labelled.

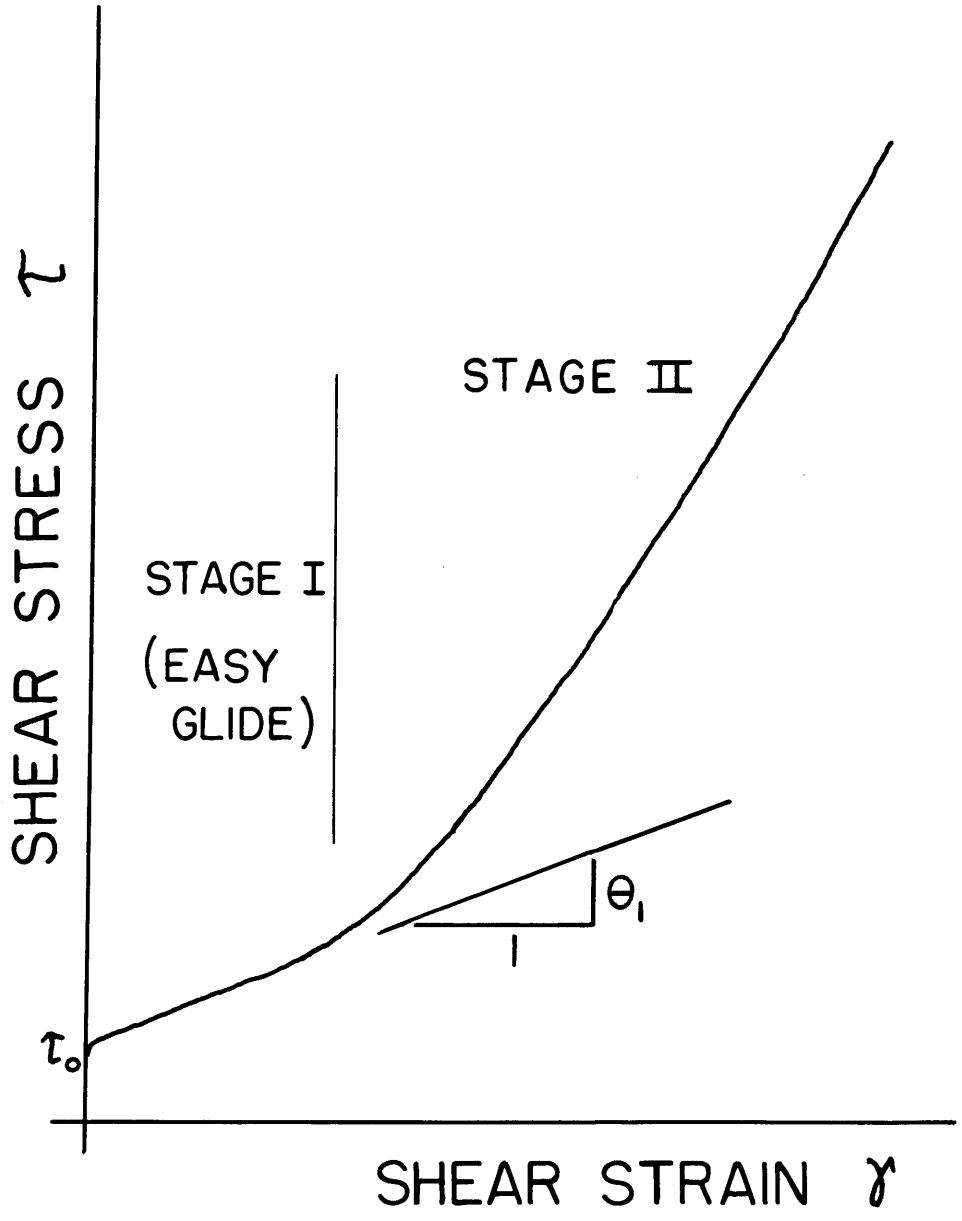

Fig. 1-1. Shear stress-shear strain curve for a copper single crystal with characteristic parameters labelled.

between crystals grown or annealed in different batches. Second, because the stresses required to alter the initial structure are exceedingly low, handling of the crystals presents difficulties. Ideally, measurements of all parameters would be made on each crystal, using techniques which require a minimum of specimen handling, the measurements being reproduced on as many crystals of similar initial structure as possible. Practically, it is usually not possible to make measurements of all desired quantities on each crystal; hence, when observations from different crystals are put together, the variability in crystals and their handling is a latent variable.

The dislocation etch-pitting technique is particularly suitable for studies in the early stages of plastic flow. The technique is non-destructive, permits repetitive observations on the same crystal, and requires a minimum of specimen handling. It is possible also to perform etching while a crystal is in the testing machine, and even under load. The technique is best applied to relatively large specimens in which the danger of handling stresses is reduced. It has its best resolution at low dislocation densities, and furnishes a view of the entire crystal. These are unique advantages etch-pitting has over transmission electron microscopy (TEM). The major limitation of the etch pit technique is that only surface observations are being made. In order to gain a complete picture of dislocation configurations in the crystal, it is necessary to supplement etch pit observations with TEM observations. Although no TEM studies were made, the etch pit results of this work are compatible with the TEM findings of others, as will be discussed.

Following Section II, Crystal Preparation and General Experimental

Procedure, the experimental results are described in Section III, divided as follows: 3.1, Dislocation Multiplication in Easy Glide; 3.2, Dislocation Arrangements as a Function of Stress; 3.3, Microstrain Measurements; 3.4, Dislocation Motion Accounting for Recovered Unloading Strain; 3.5, Relation of the Yield Stress to the Forest Dislocation Density.

The Discussion (Section IV) and Conclusions (Section V) are followed by five appendices describing experimental procedures and findings which have no direct bearing on the understanding of the early stages of plastic flow in copper.

II. CRYSTAL PREPARATION AND GENERAL EXPERIMENTAL PROCEDURE

The starting material was obtained from the Johnson, Matthey Company in the form of rods 5 mm in diameter and 15 cm long (Johnson, Matthey catalogue designation JM 30). The impurity analysis of the copper, supplied by the manufacturer, is shown in Table 2-1.

Crystals were grown in vacuum (10^{-1} microns Hg) from a seed which had been mechanically cut from a large single crystal of the same material and then annealed. Prior to growth the charge was cut into small pieces, polished in nitric acid, rinsed in water and then methanol, and dried in a warm air stream. The charge was placed in an antechamber above the mold and cast into the mold after the vacuum was attained. It was then re-melted in place and solidification begun. A modified Bridgman growth technique consisted of holding the mold stationary in a furnace having a temperature gradient (10°C per cm) and moving the solidification front upwards relative to it by continuously decreasing the power supplied to the furnace. The growth rate was 0.5 cm per hour. An impurity analysis of an as-grown crystal is given in Table 2-1.

The mold was dry-machined from Carbone Corporation graphite having a total impurity content less than ten parts per million (manufacturer's specifications). Twenty 1/4" × 1/4" × 3 1/2" crystals were grown at a time by branching from a header region connected to the seed. The yield of single crystals retaining the seed orientation was usually 15/20. After growth the crystals were mechanically sawed off the header while

Table 2-1. Impurity content of copper in various stages of preparation.

ırity ment	As Purchased (supplier's analysis)	After Growth (crystal 5-3)	(3-4)	After Anneal (5-15)	(5-1(
rographic Analyses					
	2 ppm	1	1	1	1
›n	1	1-10	10-100	1-10	1
'	1	1	1	1	1
esium	<1	1-10	1	1-10	1-1
um	ND	1	1	1	10
	ND	1	ND	1	1
anese	ND	1	ND	1	1
inum	ND	ND	1	1	ND
:l	ND	ND	10	ND	ND
.ical Analyses					
›n	NA	NA	<1	NA	NA
:n	ND	NA	NA	NA	<5

NA: not analyzed ND: not detected

still confined in the channels of the mold. This procedure insured that there would be no large-scale deformation to the crystals in the cutting operation. Deformation introduced by the sawing at one end of the crystal was tolerated because (1) the crystals were to be annealed before testing, and (2) the grips covered 1/2" from each end of the crystal in testing. Crystals were numbered for reference in the manner '4-13', indicating the crystal in mold position thirteen in the fourth batch grown. A more detailed description of the furnace, mold and method of crystal growth has been given previously (Brydges 1963).

Before testing, crystals were annealed five days at 1000°C in a vacuum of 2.10^{-2} microns Hg, followed by cooling to 300°C at a rate of 15°C per hour, then to room temperature by furnace cooling. During annealing the crystals were laid horizontally on a slab of graphite of the same purity used in the mold. The $\{111\}$ side faces, which were later to be etched, were vertical. The slab was placed in a Vycor test tube, which in turn was put in the hot zone of a quartz tube furnace. A piece of commercial purity copper sheet was used as a roof over the boat to prevent products from the devitrification of the Vycor tube from falling on the crystals. An impurity analysis of crystals after annealing is shown in Table 2-1.

The crystal orientation was selected to fulfill two requirements: (1) allow easy glide by having one $\{111\}<110>$ slip system more highly stressed by the applied tension than the rest, and (2) provide surfaces close to $\{111\}$ for dislocation etching of the crystal. Figure 2-1 shows the location of the crystal axis on a standard stereographic projection and indicates the nomenclature for the various slip planes. The Schmid factors

CRYSTAL ORIENTATION FOR EASY-GLIDE INVESTIGATION

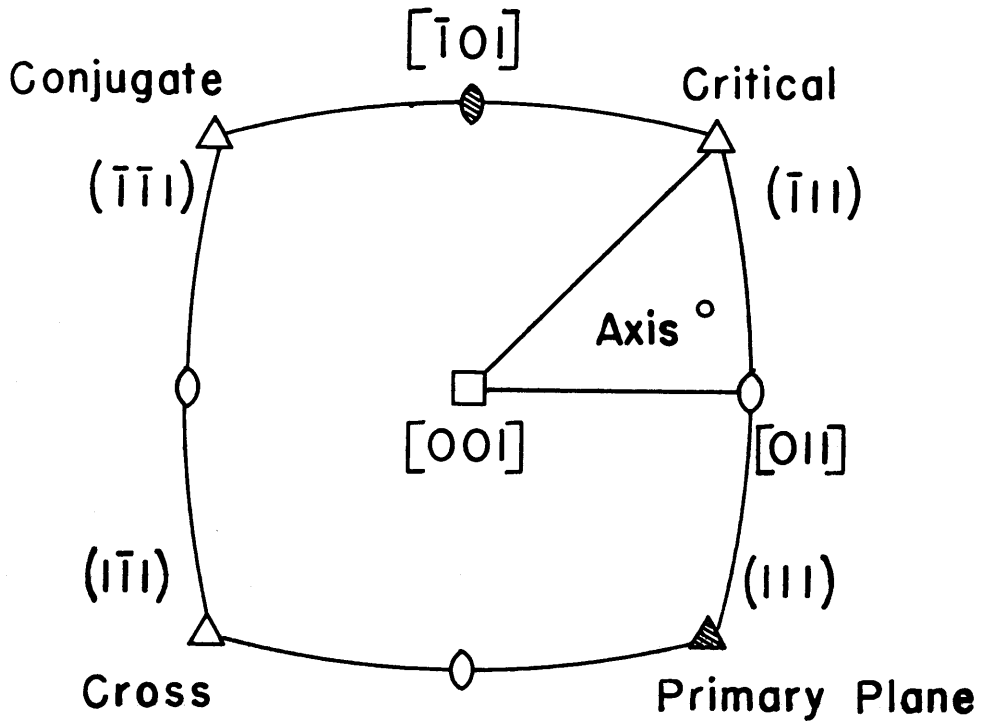

Primary Slip System: (111) [$\bar{1}$01]

Schmid Factor on Primary System: 0.46

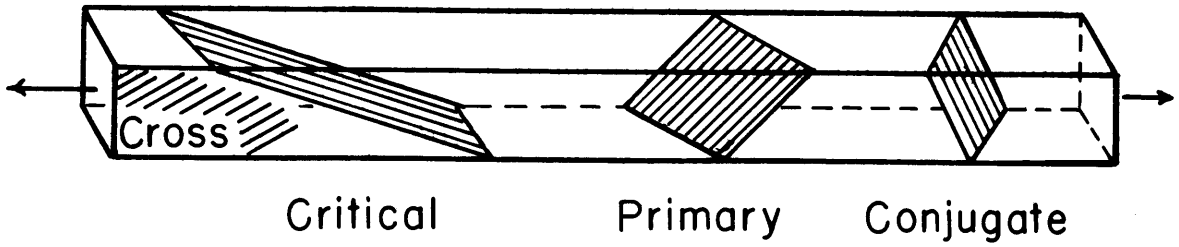

Fig. 2-1. Crystal orientation and nomenclature for {111} slip planes.

for all slip systems for this orientation are given in Table 2-2. If two side faces were exactly $(1\bar{1}1)$, the cross-slip system would be entirely unstressed by applied tension. However, the etching faces of the crystals were off $(1\bar{1}1)$ orientation by one degree, with an uncertainty of one degree, as determined from Laue back reflection x-ray photographs; in the table the Schmid factor for the cross system is shown for the worst case – two degrees off.

To prepare crystals for etching, they were electropolished in a solution of 50% orthophosphoric acid and 50% tap water. The electrolyte was stirred with a magnetic stirrer and the specimen, suspended vertically from one end, was rotated counter to the electrolyte flow with a motor-driven device. A copper screen was used as cathode. It was found that mirror-like polishes could be obtained either at 1.5 to 2.0 volts (on the usual polishing plateau), or at 5.0 volts where bubble evolution occurred. To protect the grips during etching they were coated with Miccrostop lacquer. If the crystal was to be etched immediately after polishing, it was rinsed in tap water and then etched wet; if it was to be etched at a later time, it was rinsed in tap water, then methanol, then dried in a warm air stream. As a matter of good laboratory practice the running water, methanol, and etchant were maintained within 1°C of room temperature, although the polishing bath became somewhat warmer. An experiment in which a crystal was polished, rinsed and etched, and then re-polished, rinsed in cold water and etched again showed that the different temperatures of solutions did not cause any dislocations to be introduced into the crystal.

The dislocation etchant employed was made according to Livingston's

Table 2-2. Schmid factors for all {111}<110> slip systems.

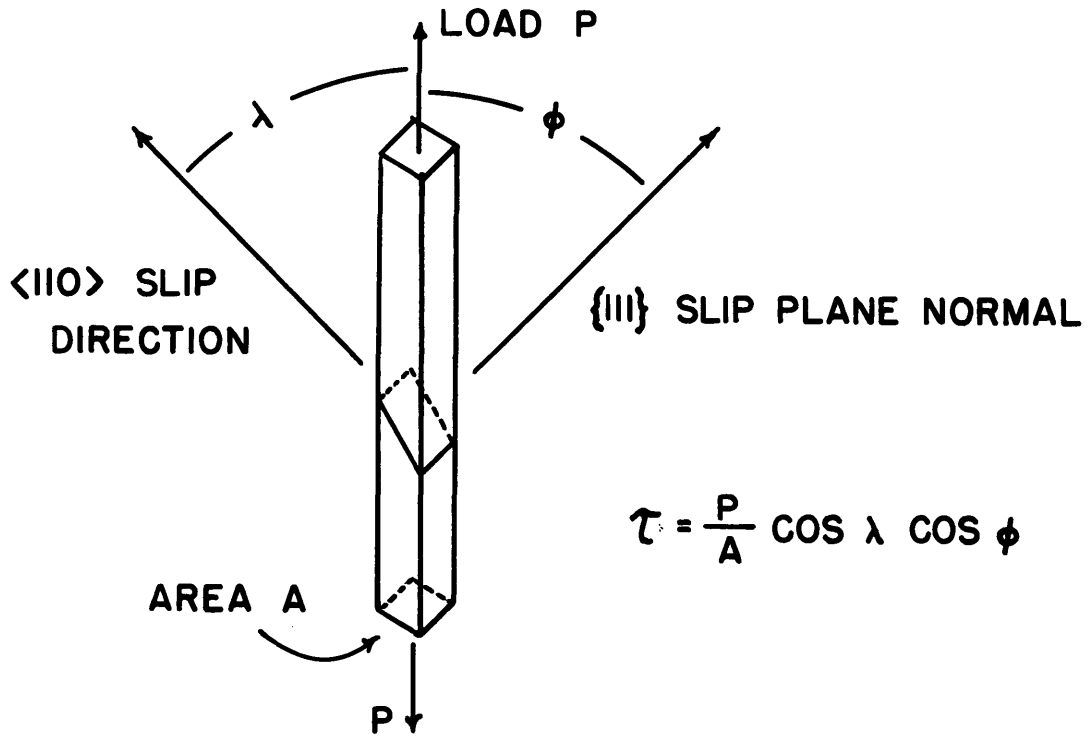

Slip Plane	Slip Direction	Schmid Factor ($\cos\lambda \cos\phi$)
111 (Primary)	$\bar{1}01$	0.46
	$0\bar{1}1$	.06
	$\bar{1}10$	.39
$\bar{1}11$ (Critical)	$\bar{1}\bar{1}0$	.25
	$0\bar{1}1$	.08
	101	.34
$\bar{1}\bar{1}1$ (Conjugate)	$\bar{1}10$	.12
	011	.20
	101	.08
$1\bar{1}1$ (Cross and Etching)	$\bar{1}\bar{1}0$	.01
	$\bar{1}01$	.02
	011	.03

(1962b) formula: 90 parts water, 25 hydrochloric acid, 15 acetic acid and 1 bromine. After etching, the crystal was rinsed in tap water, then in methanol, and dried in a warm air stream. A detailed account of the etching process is given in Appendix A.

Etch pit counts were generally made from Polaroid photographs taken on either a Leitz Panphot or a Zeiss Ultraphot microscope. No preset number of photographs was taken for a particular data point; rather, the number (and the magnification) was adjusted to give what was felt to be a valid sample of the particular pit distribution.

After annealing the crystal exhibited an etch pit density (excluding dislocations in sub-boundaries) of about 10^5 per cm^2. The range was from $7 \cdot 10^4$ to $4 \cdot 10^5$ per cm^2. The structure of an annealed crystal is revealed in Figure 2-2. A variation in sub-structure was evident along the growth direction. In general, one or more growth striations or sub-boundaries ran the whole length of the crystal, more or less parallel to the axis. Small cells (dimension about 1 mm) were most numerous at the end of the crystal first solidified. It was established by etching the cross plane and the primary plane (exposed by spark-sectioning, see Appendix B) that the dislocation density after annealing was isotropic.

This structure was comparable to or more perfect than that in crystals employed by other investigators using starting material of similar purity. The differences are likely due to growth and annealing conditions. In general, investigators using etch pit techniques obtain crystals of higher starting perfection than investigators utilizing transmission electron microscopy. Young (1962c), Livingston (1962b), Hordon (1962), and Basinski and Basinski (1964), all utilizing etch pits, experimented on

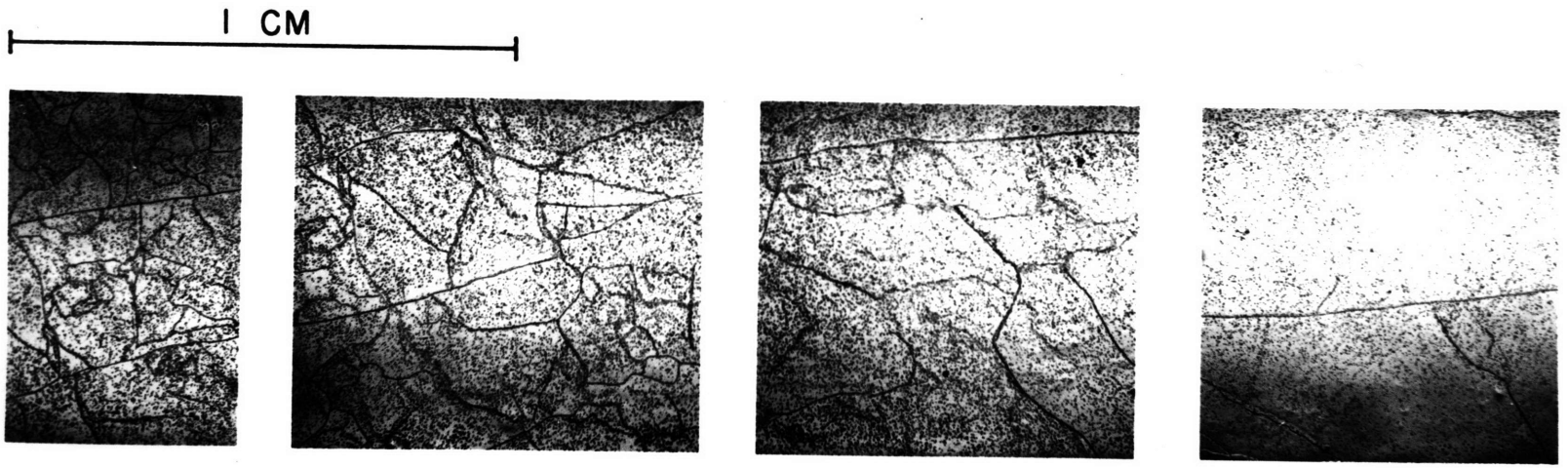

Fig. 2-2. Sub-structure in an annealed crystal. The growth direction is from left to right.

crystals with starting densities of 10^5 per cm^2 or less. Essmann (1965) and Steeds (1966), for transmission work, used crystals with initial densities in excess of 10^6 per cm^2. Also with the higher initial density group are some investigators who have performed mechanical property tests without examining the structures which develop, such as Bilello (1965) who measured an initial etch pit density of $2 \cdot 10^6$ per cm^2.

The testing procedure varied depending on the experiment and will be described in later sections, but the method of gripping the specimens for tension tests was the same throughout. The crystals were soft-soldered into one-half inch long brass collars and were loaded through knife-edge grips as shown in Figure 2-3. The axis of the knife edges was normal to the $(1\bar{1}1)$ specimen surfaces, which contain the primary slip system Burgers vector. The knife edges could pivot about an axis normal to their own through a pin joint. These two degrees of freedom were introduced to allow the grips to rotate to accommodate the crystal lattice rotation during deformation. Even with these precautions, however, bending occurred in the specimen to a distance of one specimen thickness from the grips. This was observed by etch pits which showed polygonization of dislocations of opposite signs (shown by black and white pits, see Appendix A) on opposite faces of the crystal, Figure 2-4. In studying dislocation structures developed from deformation no observations were taken in these end regions.

It was also found that bending was introduced into the specimen by asymmetric loading if the crystal was soldered into the grips on three sides. This was due to unbalanced loading – the tractions on the odd face were not paired on its opposite face and a moment was generated. This

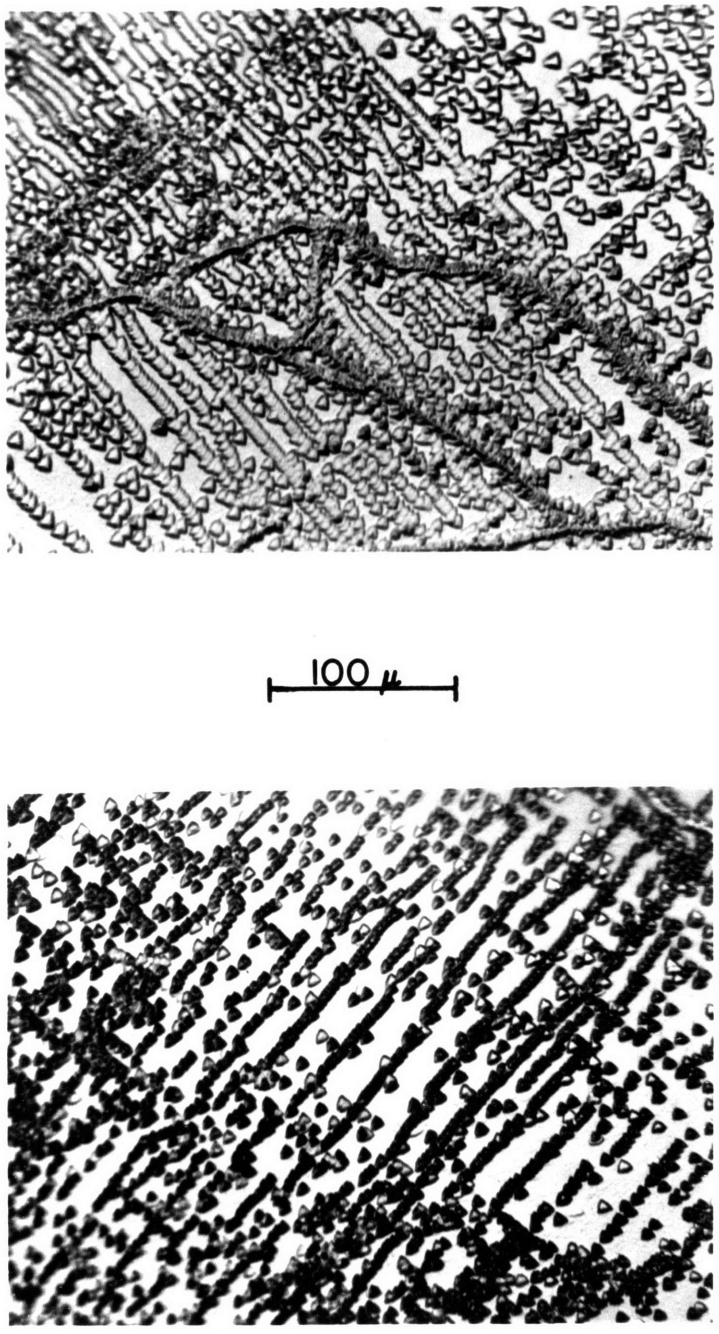

Fig. 2-4. Polygonization of dislocations of opposite sign on opposite faces near crystal grips.

was confirmed by tests on lead cast in the shape of the specimens and glued into the grips, first on three sides and then on two. In the final grip design, soldering on only two faces was accomplished by relieving the bottom of the groove with a second groove, leaving two thin ledges on which the specimen rested.

Tensile tests were performed on electric-motor-driven machines of 1000-pound capacity. Two machines of essentially the same construction were employed. One was equipped with strain-gauge load and machine displacement cells; the other had only a load cell. The actual manner in which stress and strain were determined for any particular experiment will be discussed in the experimental results sections.

Although loading was in tension for the experiments to be reported, the effective stress for plastic flow is the shear stress resolved on the slip plane and in the slip direction of the dislocations whose motion accounts for the strain. Because in the early stages of straining the predominant motion is that of dislocations with Burgers's vector $[\bar{1}01]$ on the primary slip plane (111), the stress values which will be reported are shear stresses resolved to this system by multiplying the normal stress by the primary system Schmid factor 0.46. The strain values to be reported are shear strains resolved to this system by dividing the normal strain by the same Schmid factor. Stress and strain were not corrected for lattice rotation, the correction terms being negligibly small (Schmid and Boas 1950, p. 59).

Etch pit densities are denoted by N when they are densities observed on the cross plane $(1\bar{1}1)$, and by N_f when they are observed on the primary slip plane (111) exposed by spark-sectioning (Appendix C).

In general, these etch pit measurements have been used to interpret the mechanical behavior of the crystals through their correlation with dislocation densities and thus with plastic strains due to the motion of dislocations. These relations will now be analyzed.

Although there may be considered to be a one-to-one correspondence between etch pits on a $\{111\}$ surface and dislocations intersecting the surface (Livingston 1960), the etch pit density on a surface is not, in general, equal to the dislocation length per unit volume in the crystal. In the simple case of dislocation lines intersecting an etching plane at right angles, the intersection etch pit density N_{normal} (cm^{-2}) would be equal to the dislocation volume length density ρ (cm/cm^3). However, if the dislocation lines make an angle θ with the etching plane normal, the intersection etch pit density will be related to the length density (or, equivalently, to the intersection density N_{normal} on a plane normal to the dislocation lines) by the equation

$$N = \rho \cdot \cos \theta.$$

If the dislocation lines are isotropically distributed in space, an integration of this geometric relation yields the result that the intersection density on any plane will be one-half the volume length density. A corresponding relation can be worked out for any given distribution of dislocation lines with respect to an etching surface. In the particular case of (111) $[\bar{1}01]$ dislocations intersecting the $(1\bar{1}1)$ etching plane, the dislocations make an angle of 70.5 degrees (the $\{111\}$ interplanar angle) with the etching surface, and the relation between the observed etch pit density and the density on a plane normal to the dislocation lines is

$$N = \rho \cos (19.5°) = \frac{\rho}{1.06}.$$

The plastic shear strain γ due to motion through an average distance ℓ of a length density ρ of dislocations with Burgers vector b is (Cottrell 1953, p. 18)

$$\gamma = b\rho\ell.$$

To relate this strain to etch pit densities and displacements observed on the etching face, the particular dislocations whose motion contributed to the strain must be known. If the strain is produced by the motion of primary system edge dislocations alone, the relation between N and ρ is as worked out above, and the distance of motion x observed on the $(1\bar{1}1)$ etching face is identical to the distance of motion measured normal to the dislocation lines. Thus the relation between the shear strain γ resolved on the primary system, etch pit densities N observed on $(1\bar{1}1)$, and distances of movement x observed on $(1\bar{1}1)$ becomes

$$\gamma = 1.06\ bNx.$$

Because the uncertainties in etch pit density measurements are usually greater than 10%, the factor 1.06 will usually be taken as unity.

Considerable use will be made of these relations in later sections. Also recurring in calculations will be the numerical values of the Burgers vector b $\left(\frac{1}{2}\langle 110\rangle\right) = 2.5 \cdot 10^{-8}$ cm, and the shear modulus $G = 4.9 \cdot 10^{11}$ dynes/cm^2 $= 5 \cdot 10^6$ g/mm^2 (Friedel 1964, p. 455).

III. EXPERIMENTAL RESULTS

3.1 Dislocation Multiplication in Easy Glide

Dislocation multiplication is particularly amenable to study by etch pit techniques; Livingston (1962b), Young (1962b), Hordon (1962), and Basinski and Basinski (1964) have performed experiments to measure etch pit densities as functions of stress and strain. The experiments reported here are similar to these in technique but introduce the additional parameters of temperature and strain rate.

The procedure was to polish and etch a crystal to determine the initial density N_o on the $(1\bar{1}1)$ surfaces, then to deform the crystal into the easy glide range, unload, re-polish and etch, and determine the etch pit density N. The sequence was repeated with successive strain increments through easy glide or until the technique began to fail either because the etch pit density became unresolvable by light microscopy or because the side faces became un-etchable due to rounding from successive polishings.

Crystals were tested at three strain rates at each of three temperatures. The specimen length between grips was nearly constant, 6 cm, and the shear strain rates based on this length were $1.4 \cdot 10^{-6}$, $8.0 \cdot 10^{-5}$, and $5.0 \cdot 10^{-3}$ per second. The temperatures were room temperature, 298°K; the equilibrium temperature of dry ice and alcohol, 195°K; and the equilibrium temperature of liquid nitrogen and its vapor, 77°K. The baths were contained in a Dewar flask which surrounded the lower portion of the testing machine frame, the bath being in direct contact with

the specimen. The experiments were performed on the machine equipped with load and displacement cells, the outputs of which were fed into a Sanborn recorder and then into an X-Y recorder to provide a load-elongation curve which could be monitored during the test. The actual strains were measured by observing with an optical cathetometer the change in separation of two pin scratches made across the gauge section on the irrational specimen surfaces. Prior to adopting this method it was shown with etch pits that although dislocations are introduced into the crystal by scratching, subsequent straining occurs without multiplication of these dislocations. Presumably the scratching introduces dislocations of many systems which are in a highly work-hardened configuration.

Table 3.1-1 shows the parameters measured in the tests. The strain rates have been abbreviated S (for the slowest), M (medium) and F (fast). The initial etch-pit density N_o does not include dislocations in sub-boundaries. The value of the yield stress, τ_o, was obtained from a construction on the X-Y recording as the point of intersection of two lines, one coincident with the loading slope prior to yielding, the other coincident with the easy glide slope. Although the yielding process is a gradual one (as will be discussed in a later section), on the X-Y plot the yield point appears rather sharp because the strain scale is compressed. The easy glide strain-hardening coefficient θ_1 was computed from the true strain values. The extent of easy glide was determined only in those cases when the accumulated strain increments showed an upward turn in the X-Y load elongation recording. The dislocation multiplication rate $\frac{dN}{d\gamma}$ was taken from a straight line fit to the etch pit density versus strain plot. The etch pit density at the yield point, N_y, was determined by

Table 3.1-1. Parameters determined for crystals in easy glide multiplication experiments.

Temp (°K)	Strain Rate	Crystal	N_o (10^5 cm^{-2})	τ_o (g/mm^2)	θ_1 (kg/mm^2, γ)	Extent of Easy Glide (% γ)	$\frac{dN}{d\gamma}$ (10^8 cm^{-2})	$\frac{1}{N_o}\frac{dN}{d\gamma}$ (10^3)	N_y (10^5 cm^{-2})
77	S	3-8	1.6	31	0.8	>4.1	1.7	1.1	1.5
	M	3-2	0.7	35	1.0	7.4	0.7	1.0	4.0
	F	3-5	1.3	40	1.4	6.5	1.5	1.2	5.0
195	S	5-2	1.6	43	1.9	1.7	1.6	1.0	10.0
	M	3-11	7.0	110	2.8	>0.7	2.9	0.4	—
	M	3-12	2.6	57	1.4	4.0	1.0	0.4	6.5
	F	5-20	2.8	82	1.1	>4.2	1.4	0.5	11.0
298	S	3-9	3.4	31	1.3	3.9	0.9	0.3	0.0
	M	3-19	2.0	47	1.7	>2.7	0.9	0.4	3.5
	M	3-6	2.3	32	1.5	3.5	0.8	0.3	11.0
	F	3-1	3.8	31	2.5	2.2	0.9	0.2	0.0

extrapolating this line to zero strain. In almost all cases this intercept was considerably above the initial etch pit density value.

Dislocation multiplication data may be presented in a variety of ways, some having a more straightforward physical interpretation than others.

The approximately linear relation between the increase in etch pit density after yielding, $N-N_y$, and the plastic strain is shown in Figure 3.1-1, which includes the data for all crystals tested. A linear increase of etch pit density with strain implies that the mean free path λ for dislocation motion is constant. This follows from the geometric equation for strain in terms of dislocation density and motion; if dislocation density increases linearly with strain, each dislocation will, on the average, have moved the same distance. Taking $N \approx \rho$ and $\lambda = x$ the geometric strain equation becomes

$$\gamma = bN\lambda$$

and for the unity slope line in Figure 3.1-1, $\lambda = 5$ mm, which is on the order of the specimen thickness. If the total etch pit density is plotted instead of the increase in density after yielding, the density-strain correlation is not linear because of the pre-yield multiplication.

The value of mean free path just calculated is larger than the subgrain size. Evidence that dislocations are able to penetrate sub-boundaries is presented in Figure 3.1-2, where dislocation clusters at successive sub-boundaries appear to be associated across the crystal. It was observed that the character and amount of slip were roughly the same throughout a crystal, with no apparent dependence on sub-structure.

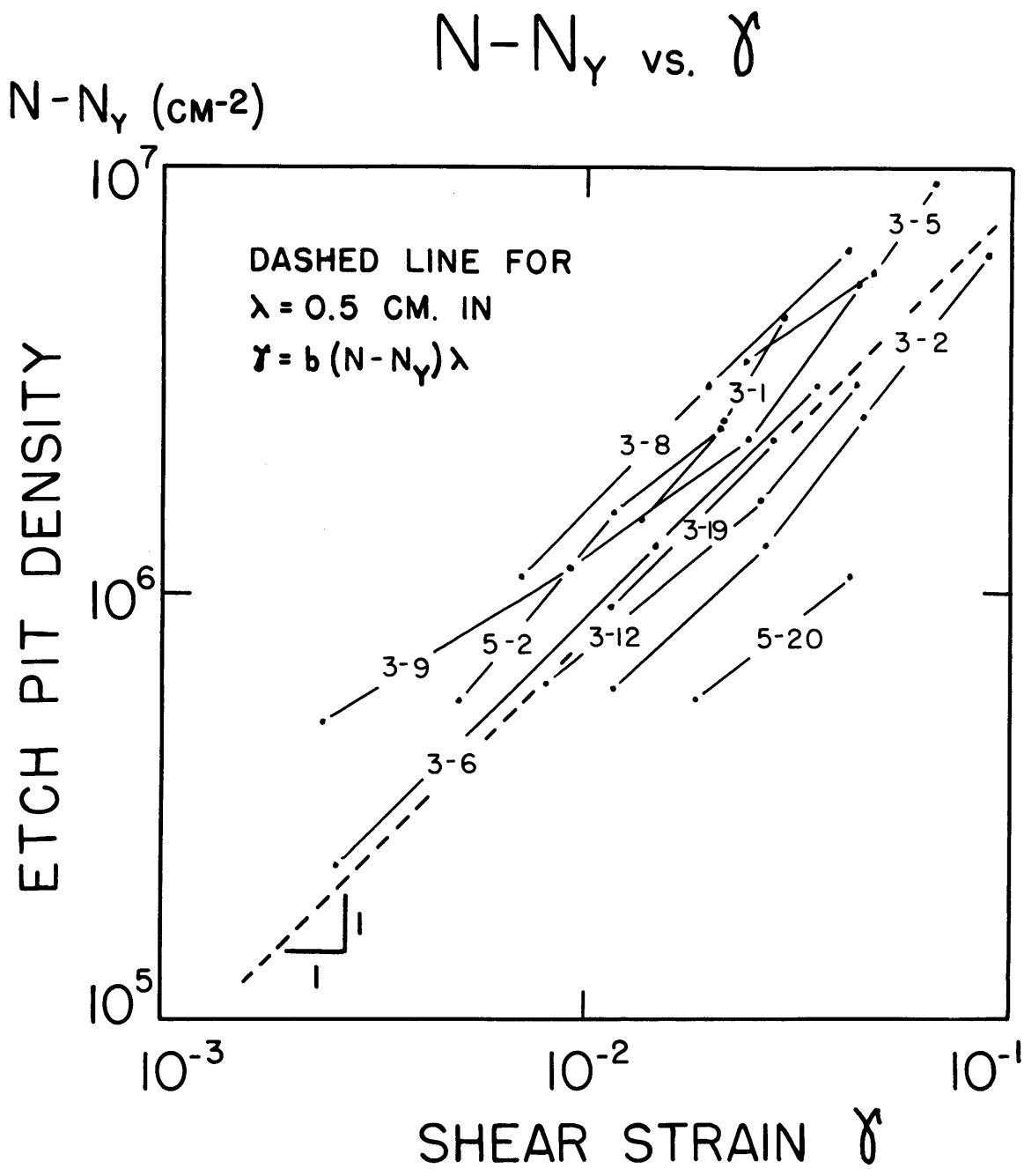

Fig. 3.1-1. Relation between the increase in etch pit density after yielding and shear strain for all crystals tested in easy glide multiplication experiments.

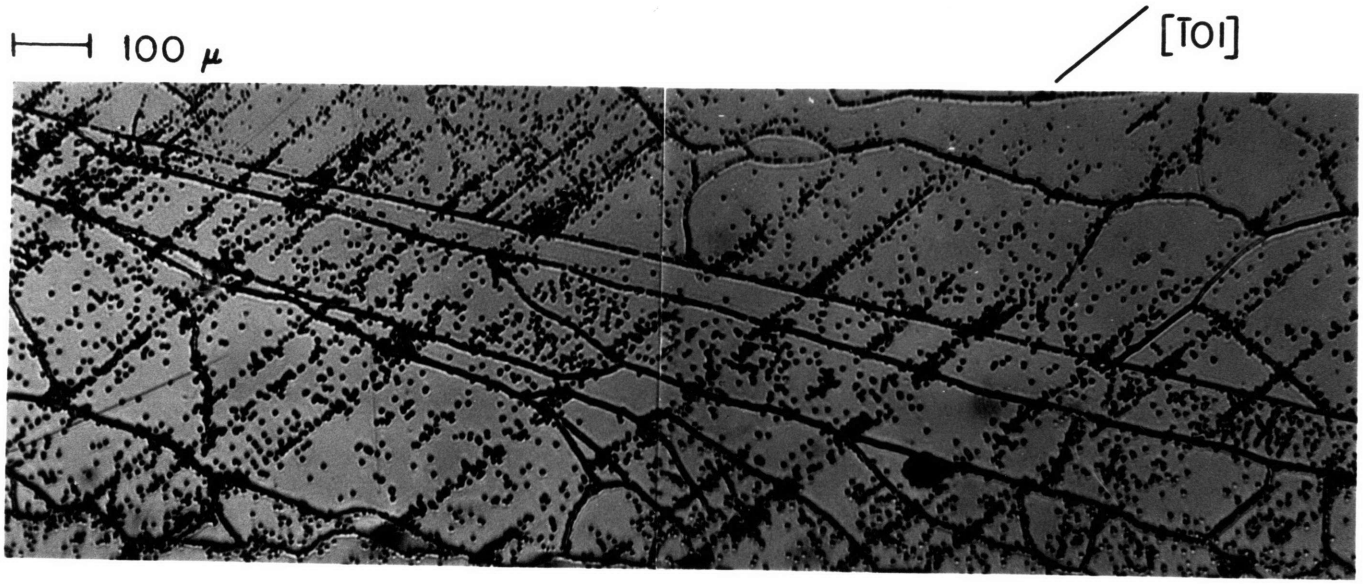

Fig. 3.1-2. The interaction of dislocations with sub-boundaries in easy glide, crystal 5-17.

The relation between total etch pit density and shear stress resolved on the primary slip system is shown in Figure 3.1-3. The correlation line shown is that given by Livingston (1963) to represent his (1962b) data and that of Young (1962b).

The physical importance of this correlation between the flow stress and the square root of the etch pit density measured on the cross plane is uncertain. Clearly, the data here has too much scatter and is over too limited a range to allow drawing any conclusions about the accuracy of the correlation. Basinski and Basinski (1964), while agreeing with Livingston that a square root correlation is valid in Stage II, find that in easy glide such a correlation is valid only for the forest dislocation etch pit density (the density measured on the primary plane), and that the density measured on the cross plane does not satisfy the relation. They report that the forest density-stress correlation is in fact valid throughout easy glide and Stage II. In a later section experiments will be reported which indicate that the yield stress is determined by a square-root correlation with the forest density. The cumulative effect of these observations is to suggest that the forest density correlation is the more physically significant.

The temperature and strain rate dependence of the dislocation multiplication rate $\frac{dN}{d\gamma}$ is shown in Figure 3.1-4. Although less than a factor of two separates all the rates, a general trend toward higher multiplication rates at lower temperatures does seem tenable. There is no reason to suppose that there is a transition in strain rate effect for the strain rates applied, so it is concluded that the difference in multiplication parameter for different strain rates at the same temperature is due to

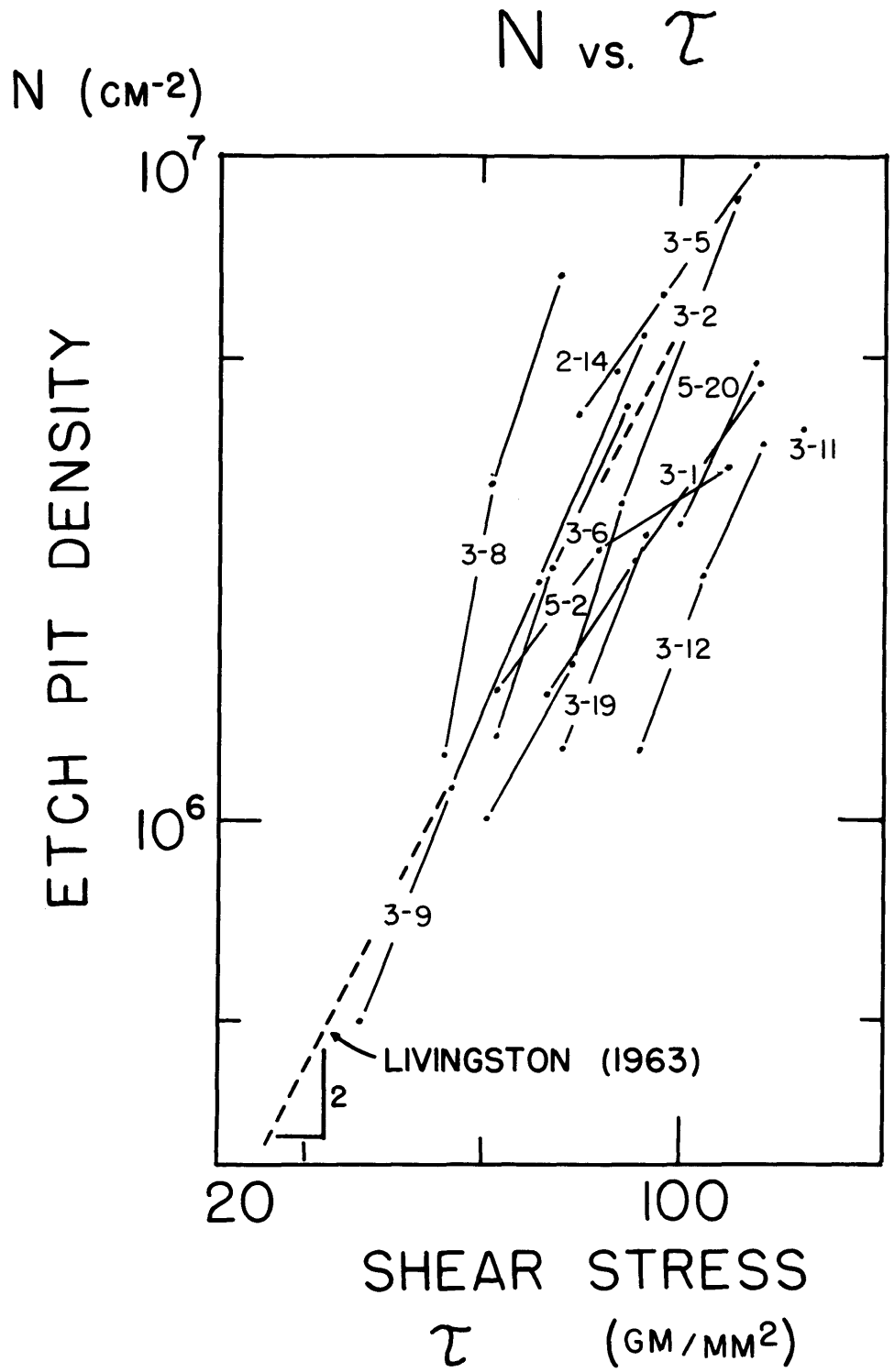

Fig. 3.1-3. Relation between the etch pit density and shear stress for all crystals tested in easy glide multiplication experiments.

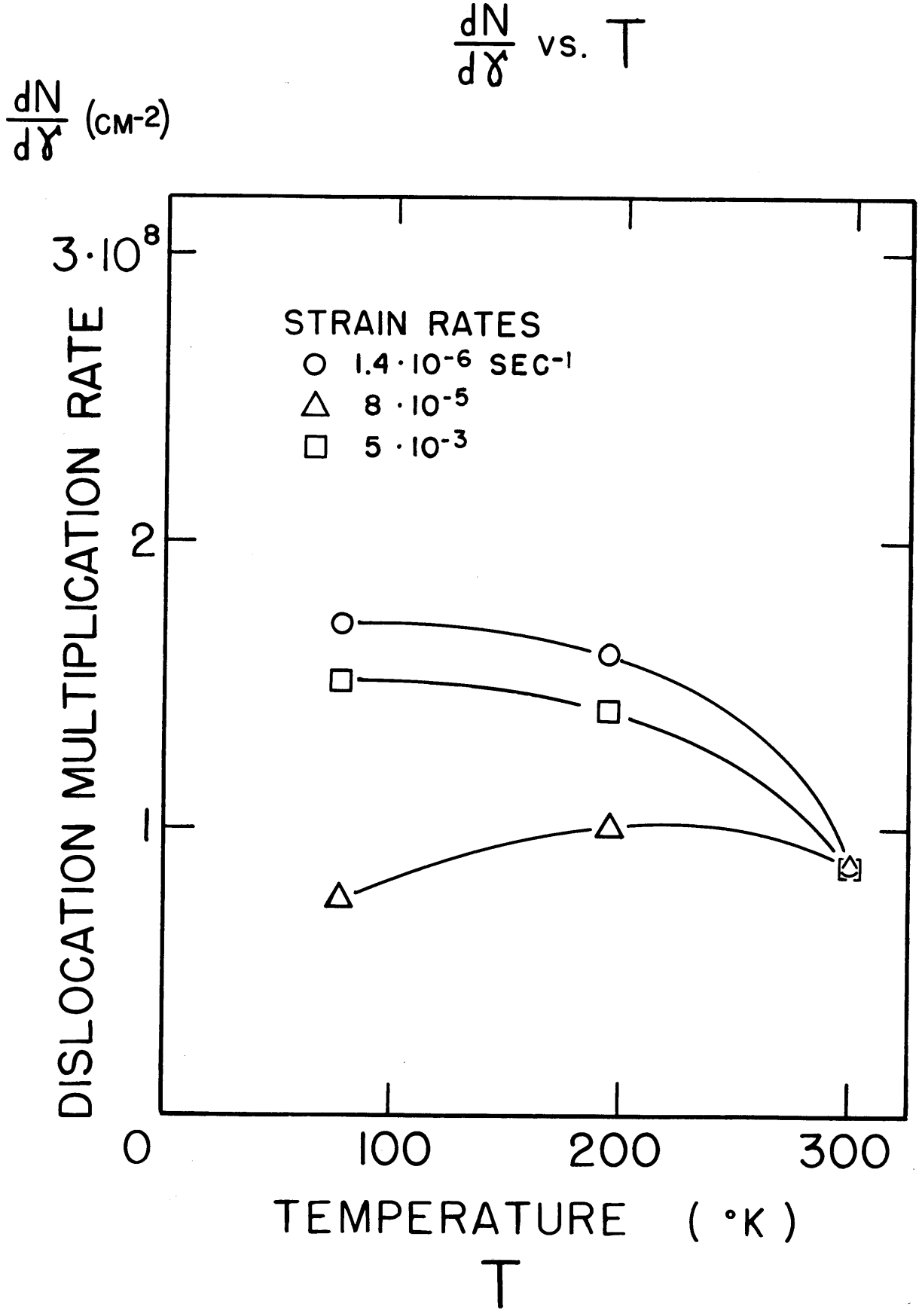

Fig. 3.1-4. Relation between the dislocation multiplication rate and temperature in easy glide.

unanalyzed differences between crystals and experimental errors.

It has been suggested by Reid, Gilbert and Rosenfield (1965) that the rate of dislocation multiplication depends on the initial grown-in dislocation density. Figure 3.1-5 illustrates the result of normalizing the dislocation multiplication rates by dividing them by the initial etch pit density. Apart from one point, this normalization has had the effect of accentuating the difference between multiplication rates at differing temperatures. Extrapolation on the 1/T plot predicts that at high temperature the normalized multiplication rate becomes very small.

3.2 Dislocation Arrangements As a Function of Stress

The multiplication experiments have been presented without attention being given to the manner in which the dislocations are arranged in the deformed crystal. In this section will be presented the results of a systematic study of the development of dislocation arrangements from the pre-yield through the easy-glide regimes. The only etch pit study to overlap these regions has been that of Young (1962b), who measured etch pit densities but not distributions. In a separate study examining the pre-yield region, Young (1961b) also was concerned mainly with dislocation numbers and not arrangements.

The tests to be described were made on crystal 4-8, which was polished, etched and examined before loading, then re-polished. Loading was performed on the machine without a displacement cell; no measurement was made of strain. The load signal was fed into the Sanborn recorder. The procedure was to etch the electropolished crystal while it

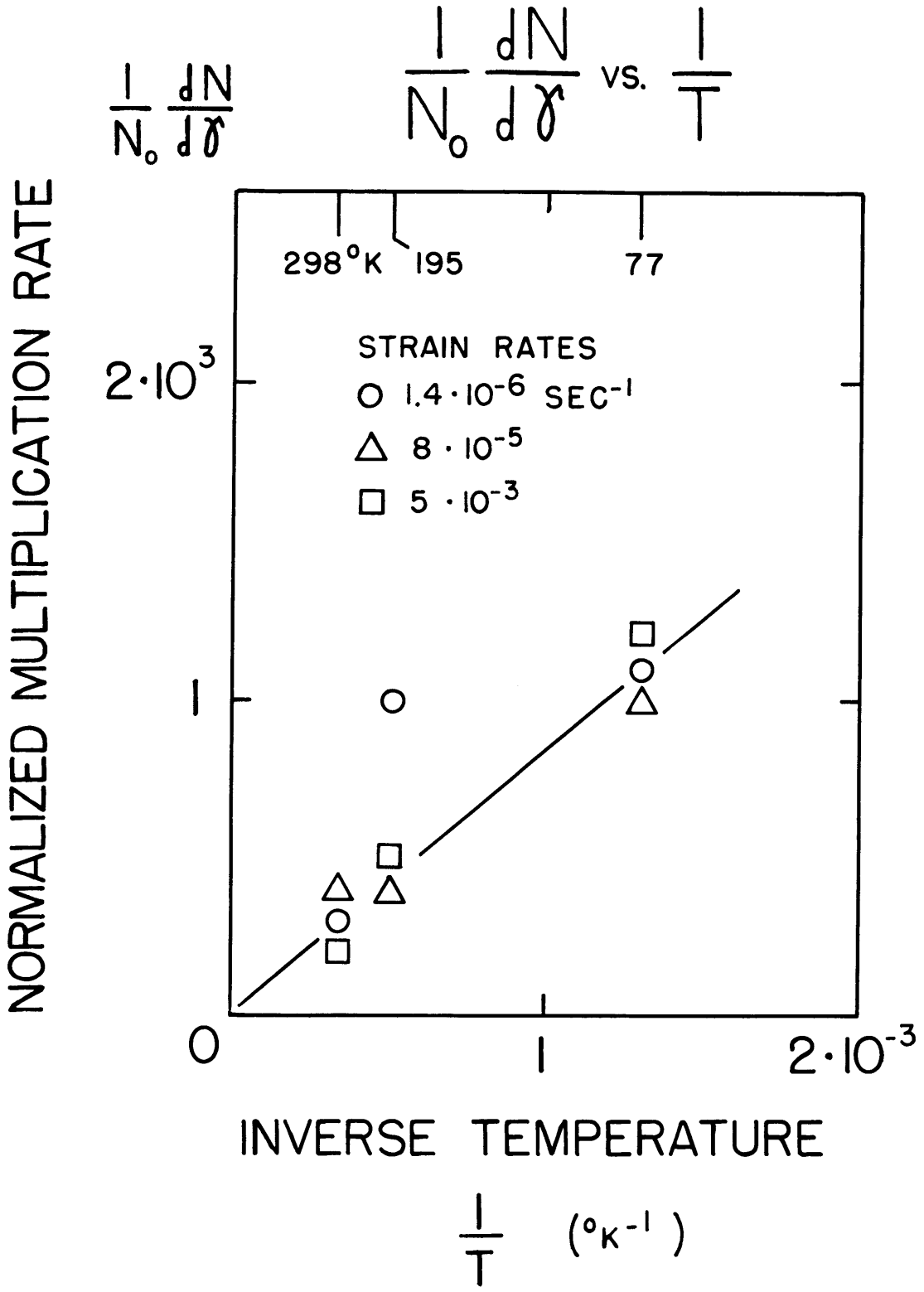

Fig. 3.1-5. Relation between the normalized dislocation multiplication rate and inverse temperature in easy glide.

was in the machine prior to loading, remove the etch (which was in a beaker), load to a predetermined value, unload, re-etch the crystal while it was still in the machine, rinse in water and methanol and dry in an air stream. The crystal was then removed from the machine and microscope observations made of the dislocation motion which had occurred. The density of dislocations which moved during the straining increment was determined by counting the flat-bottomed pits; such pits mark the initial sites of dislocations which moved. The distance moved by a dislocation was identified as the distance between such a flat-bottomed pit and a (generally) nearby smaller, pointed-bottom pit which was on a line parallel to a $<110>$ slip direction from the flat pit. The formation of flat-bottomed and new pointed-bottomed pits in a double-etching experiment is described more fully in Appendix A.

In the double-etched condition etch pit resolution is not optimum, both because of the several types of pits showing, and because a double-etching does not leave clean, sharp pits (see Appendix A). Consequently, the crystal was electropolished and etched again so that more accurate etch pit counts could be made and etch pit clusters analyzed. The crystal, electropolished again, was then ready for the next loading increment.

The shear stress resulting from the first loading increment was 5 g/mm^2. Subsequent loadings were to stresses of 10, 16, 17, 21, 30, 39, 50, 65 and 89 g/mm^2. The macroscopic yield point of the crystal was 34 g/mm^2. This was determined from the point on the load-time chart of the Sanborn recorder at which the loading rate sharply decreased (the crosshead displacement rate of the testing machine was constant).

The etch pit density observed through this stress range is shown in

Figure 3.2-1. In this plot, N represents an average of the densities measured at several points in the crystal, the same regions being used each time. It can be seen that the etch pit density did not increase from its initial value of about 2.10^5 per cm^2 until the stress reached about 17 g/mm^2, which agrees well with Young's (1961b) similar observation. Above this stress the density increased rapidly.

Below the multiplication stress there was always some motion of dislocations initially present. At $\tau = 10$ g/mm^2, about five per cent of the dislocations moved. The fraction of dislocations which moved did not increase with stress below the multiplication value. Below τ_m motion was not confined to the primary system: Figure 3.2-2 shows motion on both the primary and conjugate planes. The plane of a moving dislocation was determined as the plane whose $<110>$ line of intersection with the etching face $(1\bar{1}1)$ was parallel to the pit movement. The number of dislocations moving on the different systems was measured and it appeared that there was a transition from motion on three $\{111\}$ planes to motion almost exclusively on the primary plane at the multiplication stress. The relative frequencies of motion observed for $\{111\}$ planes are shown in Table 3.2-1. Motion on the cross plane could not, of course, be detected since that was the etching plane. The counting for these determinations was done on the projection screen of the microscope. The crystal was scanned to locate flat-bottomed pits and then a search was made for a small pointed-bottomed pit in one of the three $<110>$ slip directions away from it. When it was questionable to which flat pit a fresh pit corresponded, it was not included in the count. At $\tau = 16$ g/mm^2, 91 associations were made; at 21 g/mm^2, a lesser number 27, were made because after

Figure 3.2-1. In this plot, N represents an average of the densities measured at several points in the crystal, the same regions being used each time. It can be seen that the etch pit density did not increase from its initial value of about 2.10^5 per cm^2 until the stress reached about 17 g/mm^2, which agrees well with Young's (1961b) similar observation. Above this stress the density increased rapidly.

Below the multiplication stress there was always some motion of dislocations initially present. At $\tau = 10$ g/mm^2, about five per cent of the dislocations moved. The fraction of dislocations which moved did not increase with stress below the multiplication value. Below τ_m motion was not confined to the primary system: Figure 3.2-2 shows motion on both the primary and conjugate planes. The plane of a moving dislocation was determined as the plane whose $<110>$ line of intersection with the etching face $(1\bar{1}1)$ was parallel to the pit movement. The number of dislocations moving on the different systems was measured and it appeared that there was a transition from motion on three $\{111\}$ planes to motion almost exclusively on the primary plane at the multiplication stress. The relative frequencies of motion observed for $\{111\}$ planes are shown in Table 3.2-1. Motion on the cross plane could not, of course, be detected since that was the etching plane. The counting for these determinations was done on the projection screen of the microscope. The crystal was scanned to locate flat-bottomed pits and then a search was made for a small pointed-bottomed pit in one of the three $<110>$ slip directions away from it. When it was questionable to which flat pit a fresh pit corresponded, it was not included in the count. At $\tau = 16$ g/mm^2, 91 associations were made; at 21 g/mm^2, a lesser number 27, were made because after

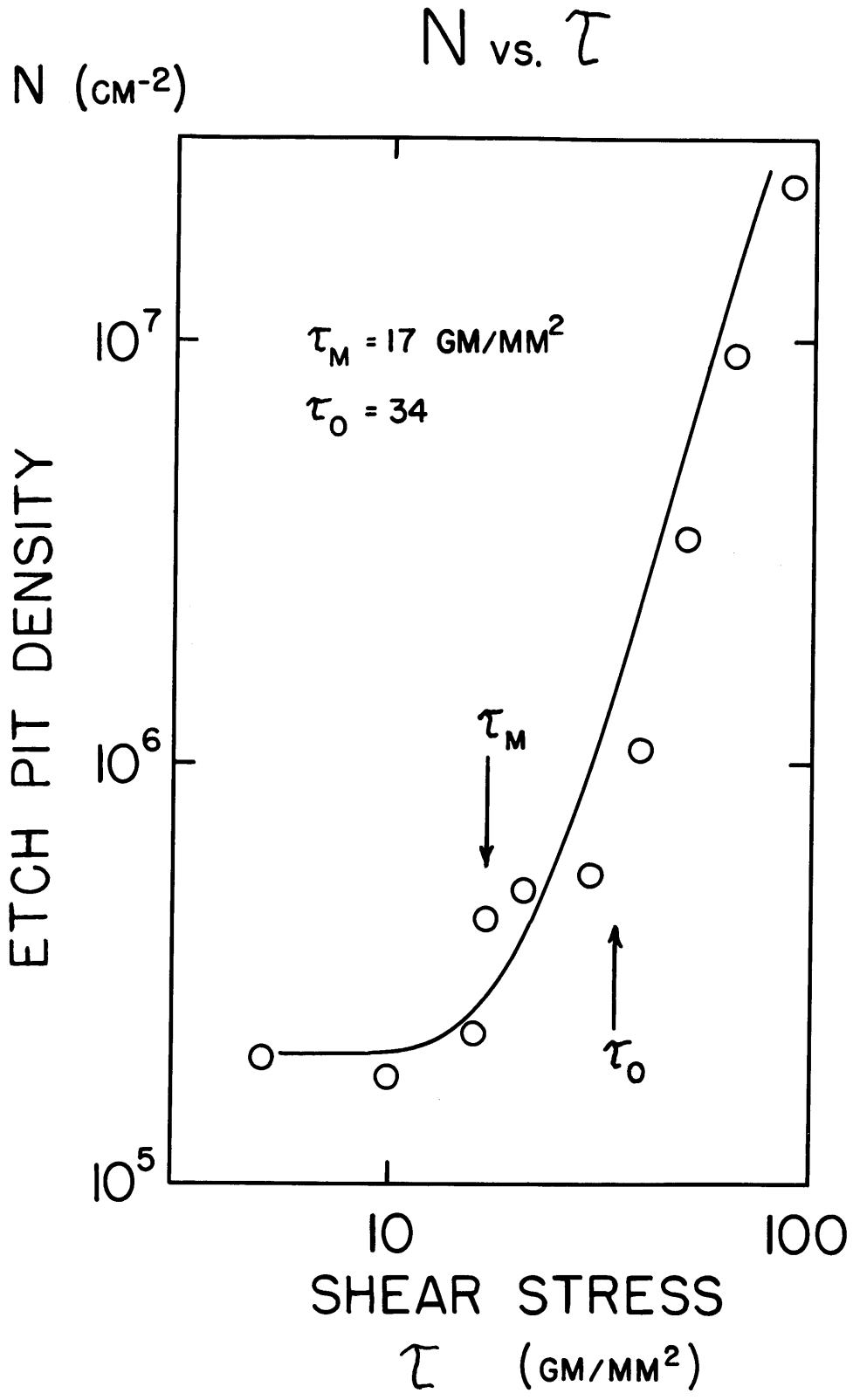

Fig. 3.2-1. Relation between etch pit density and shear stress in the pre-yield and easy glide regions, crystal 4-8.

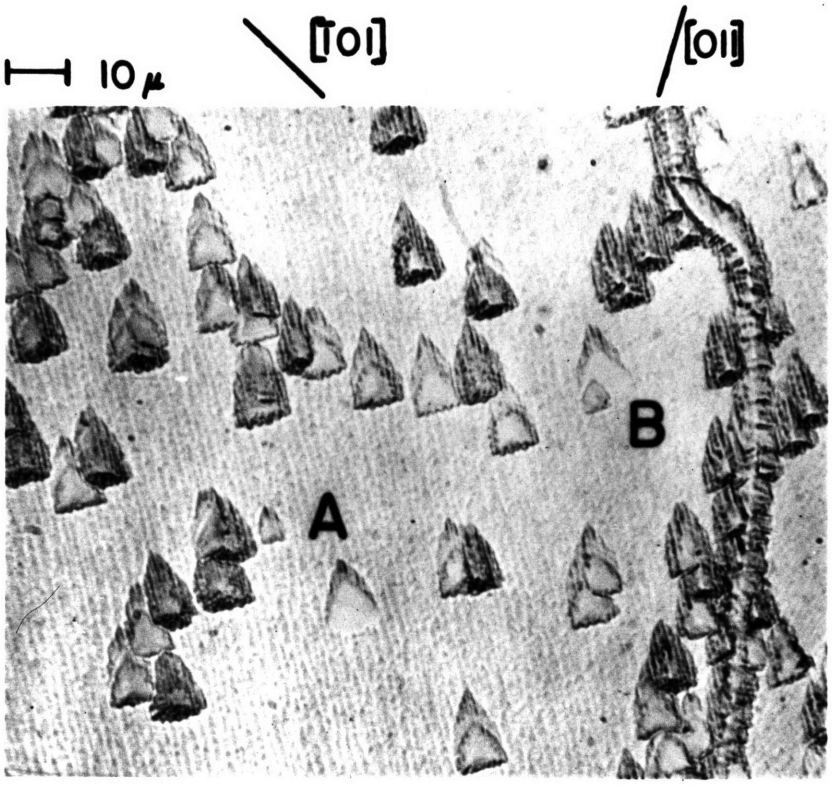

Fig. 3.2-2. Dislocation motion on the primary (A) and conjugate (B) planes, τ = 16 g/mm^2, crystal 4-8.

Table 3.2-1. Pre-yield dislocation movement on various {111} slip planes.

Resolved Stress τ on Primary System (g/mm^2)	Per Cent of Movements Observed as a Function of {111} Planes			Average Distance of Movement for Dislocations on Primary Plane (cm)
	Primary	Critical	Conjugate	
16	69	27	4	$25 \cdot 10^{-4}$
21	96	4	0	21

multiplication the difficulty of unambiguously making an association increased.

Although it could be seen that dislocation multiplication was occurring, the sources of the new dislocations could not be located. Evidence such as the occurrence on the same slip plane of separated pile-ups (which might bracket a source) was not found.

A striking feature which was observed from the lowest stresses in the pre-yield region was the development of dislocation clusters in the sub-grains. The tendency for newly generated dislocations to collect in clusters is indicated in Figure 3.2-3, the result of a double-etching, before loading and after unloading. The new pits appear preferentially in regions around the dislocations present prior to loading.

A cluster observed by etching after unloading from $\tau = 30$ g/mm^2 is shown in Figure 3.2 4. Many of the dislocations are associated pairwise one with another, that is, in dipoles. The lines of centers of many pairs make nearly a 45° angle with the primary slip direction, suggesting that these dipoles are opposite sign edge dislocation dipoles of the primary system. The cluster may be considered a multipole, having a net Burgers vector much less than the total number of dislocations in the cluster.

The multipole nature of clusters may also be seen in Figure 3.2-5, the result of an etching with black-white pit differentiation denoting positive and negative dislocations (the subject of black-white etching is discussed in Appendix A). Although a quantitative measure of the dipole concentration in a cluster can not be obtained from this photograph, it can be seen that the clusters contain both positive and negative (black and white) dislocations.

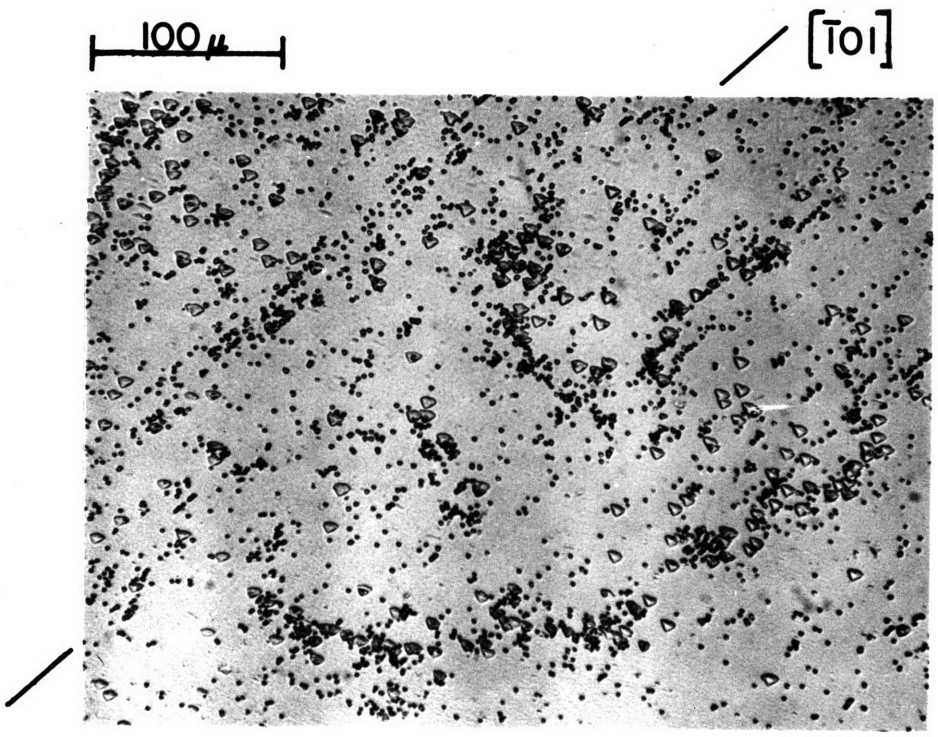

Fig. 3.2-3. Preferential formation of clusters in neighborhood of pre-existing dislocations, crystal 4-1.

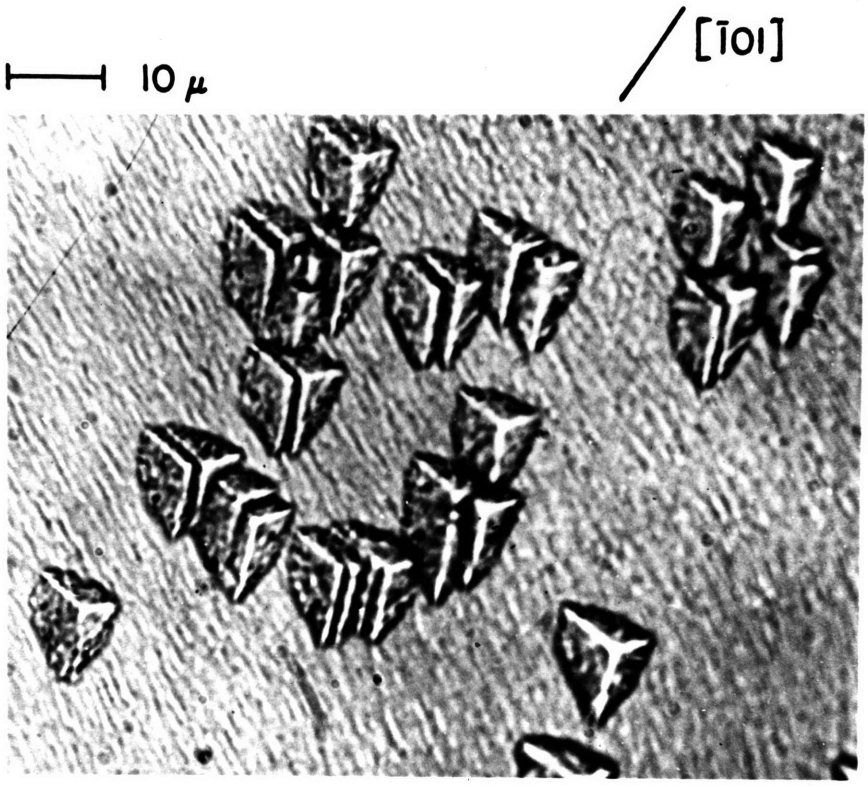

Fig. 3.2-4. A cluster in the pre-yield region, τ = 30 g/mm^2, crystal 4-8. Many of the dipoles lie at about 45° to the primary slip direction.

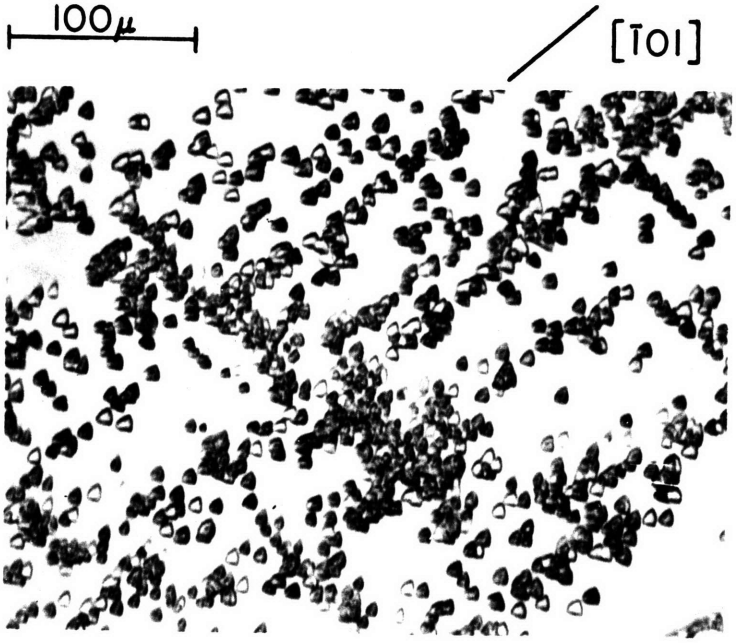

Fig. 3.2-5. Clusters composed of both positive and negative dislocations, indicated by black and white pits, crystal 5-17.

As a further check on the nature of the dipoles in clusters, the distribution of etch pit spacings has been analyzed. An edge dislocation dipole will be stable, that is, it can form and will not be driven apart by the applied stress, only if the spacing between the slip planes of the dislocations is less than a distance set by the stress level and given (Cottrell 1953, p. 152) by the relation

$$h = \frac{Gb}{8\pi(1-\nu)\tau}.$$

To analyze the dipoles a histogram was constructed by picking a particular pit and measuring the center-to-center distance to its nearest neighbor, then from that pit to its nearest neighbor, and so on until a return was made to a pit previously involved in the sequence. When this occurred, a pit not yet reached was taken as a new starting point and the procedure begun again until a pit from either current or a past sequence was reached. This procedure implied that certain separations, particularly the smaller ones, would be counted twice, but not more than twice.

A number of photographs of clusters at $\tau = 30$ g/mm^2 were analyzed in this fashion and the frequency of occurrence f of center-to-center distances observed as a function of the distance D is shown in Figure 3.2-6. The center-to-center distance corresponding to the critical interplanar spacing is indicated in the histogram. The relation between interplanar spacing h and center-to-center distance D is a geometric one,

$$h = D \cdot \cos 45° \cdot \sin 70.5°.$$

In this relation, the term cos 45° derives from the equilibrium position

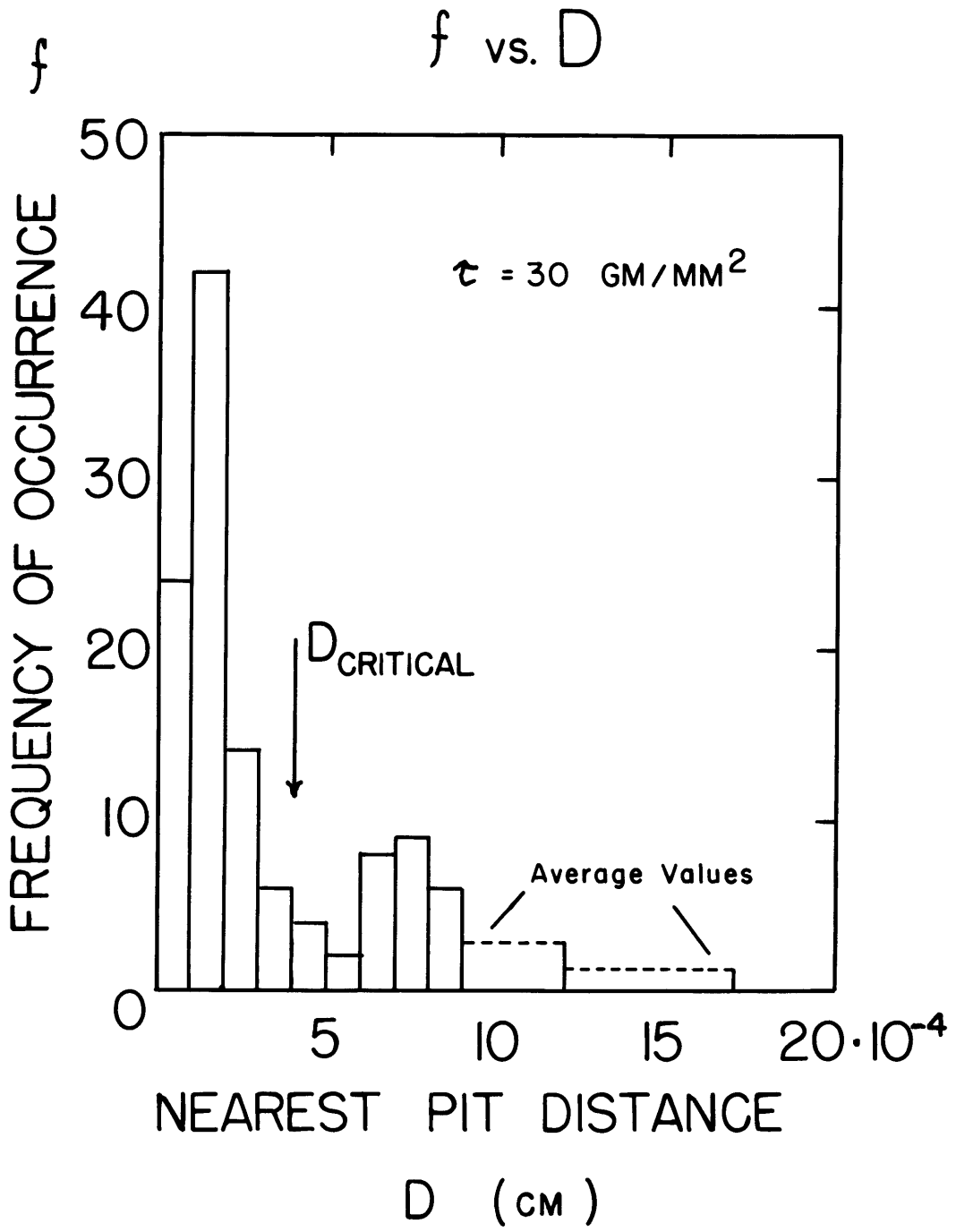

Fig. 3.2-6. Histogram of pit separation distances in pre-yield region, τ = 30 g/mm^2, crystal 4-8.

of an opposite-sign dipole (line of centers of the dislocations at 45° to the slip direction), and the term sin 70.5° derives from the angle between the $(1\bar{1}1)$ observation plane and the plane normal to the dislocation lines.

The fact that f falls off at about the critical spacing supports the hypothesis that the dislocation dipoles are the basic building blocks of the clusters. The second peak in the historgam reflects the spacing of dislocations which are not in dipoles. If all dislocations were distributed evenly, the nearest neighbor spacing would be the reciprocal square root of the etch pit density, which at $\tau = 30$ g/mm^2 was about $5 \cdot 10^5$ per cm^2. This spacing would be $14 \cdot 10^{-4}$ cm; the position of the peak at a smaller distance is a measure of the clustering.

In easy glide, the number of clusters increased from the pre-yield level, but not as rapidly as did the number of dislocations associated with each cluster. Once formed, clusters did not break up as a result of further deformation; a similar stability was observed when a crystal was subjected to a compressive strain after deformation in tension (Appendix D).

Figure 3.2-7 shows almost a complete sub-grain at $\tau = 89$ g/mm^2. The density of clusters such as those labelled A, B and C is about $2 \cdot 10^5$ per cm^2, equal to the initial density of the crystal. The tendency for clusters to show an orientation effect, either parallel or perpendicular to the primary slip direction, was observed only at stresses above the yield point.

Figure 3.2-8, an etch pit spacing histogram for $\tau = 89$ g/mm^2, shows a more pronounced dipole peak than the histrogram for $\tau = 30$ g/mm^2,

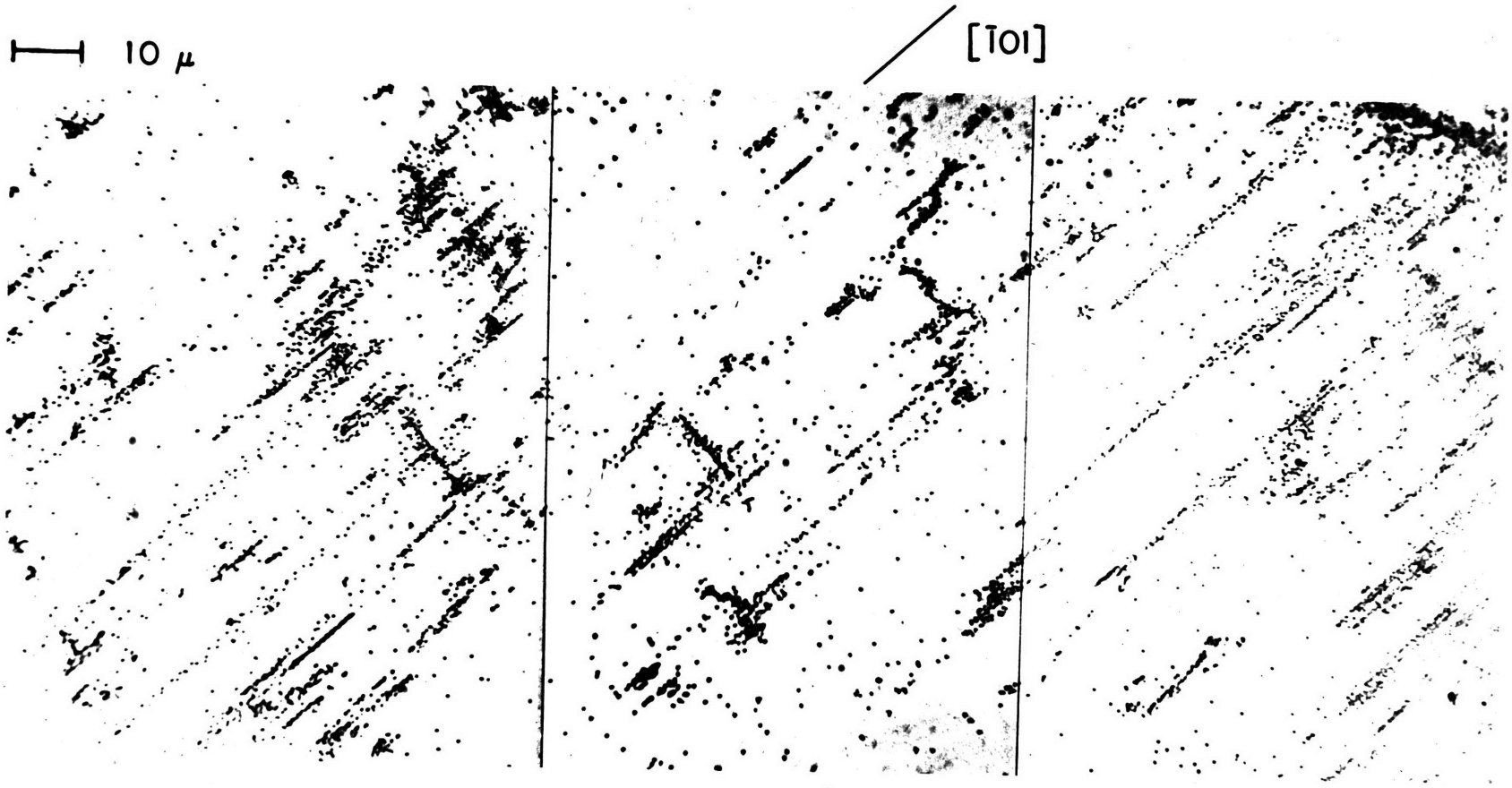

Fig. 3.2-7. Clusters in a sub-grain, τ = 89 g/mm^2, crystal 4-8.

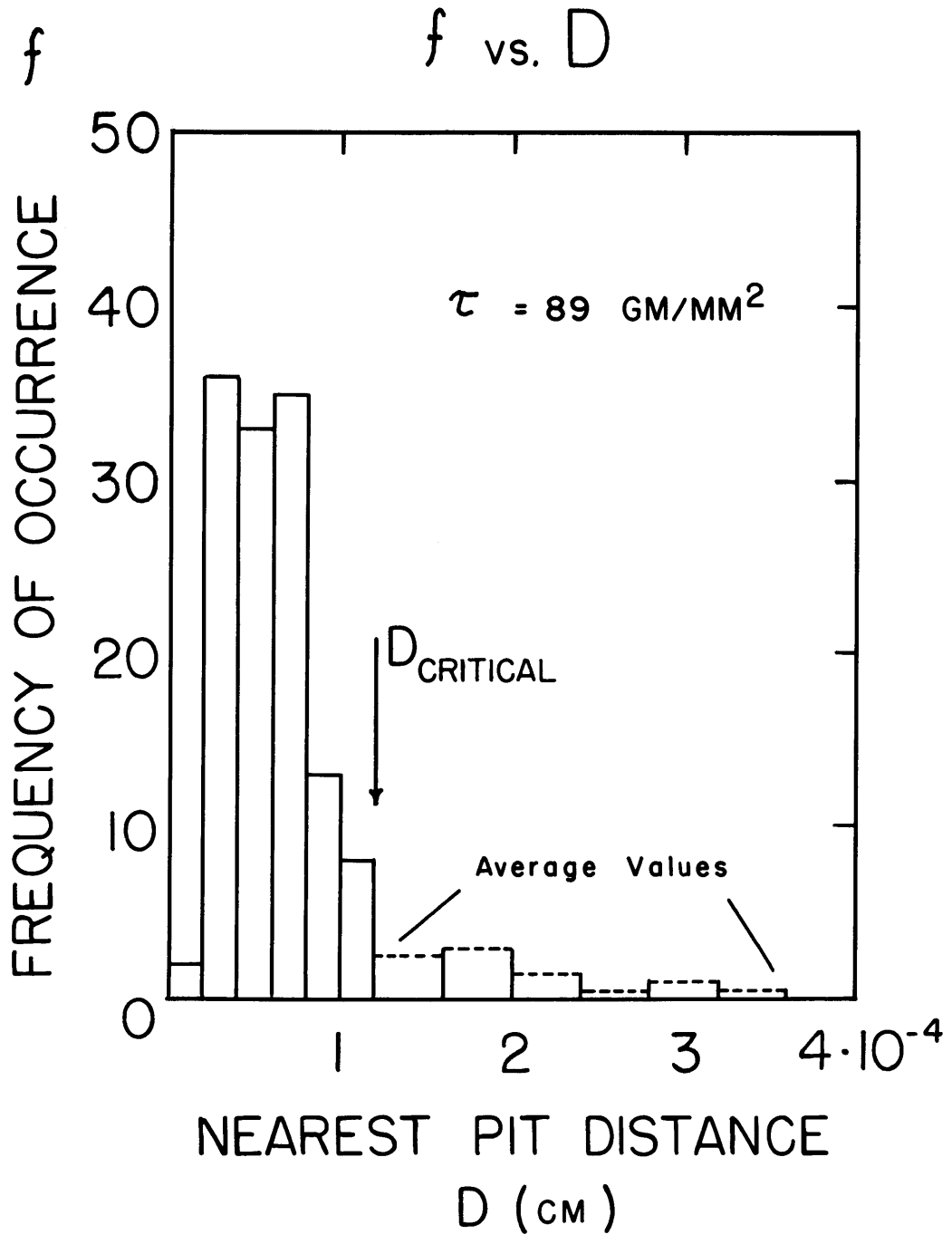

Fig. 3.2-8. Histogram of pit separation distances, τ = 89 g/mm^2, crystal 4-8.

implying that at the higher stress a greater fraction of the dislocations are in dipole configurations. In this histogram as in the previous one, the dipole peak falls off at the critical passing spacing.

A dislocation configuration of particular interest is shown in Figure 3.2-9. Streamers of this sort are frequently observed, but if the etch pits are not clearly resolvable they may be mistaken for pile-ups. This photograph, the result of a short (one second) etching, shows that the streamer consists mainly of dipoles, perhaps all on the same two parallel planes, stacked one next to another. The dipole spacing is less than the passing spacing for the stress level, 89 g/mm^2.

3.3 Microstrain Measurements

The topic of microstrain, the plastic behavior of a crystal below its macroscopic yield point, has received attention for the information it sheds on the behavior of dislocations in non-strain-hardened material. The parameters which can be measured in microstrain experiments are more or less distinct from those determined in macroscopic mechanical tests, though, of course, a successful theory of crystal plasticity must satisfactorily explain observations on both scales.

The parameters which are measured in microstrain experiments may be divided into two classes, those which are sensitive to the strain resolution and those which are not. Experimental determinations of elastic limits, either in loading or unloading, are extremely sensitive to the strain resolution employed; magnitudes of strain, such as forward plastic strain or recovered unloading strain, are relatively insensitive to strain resolution on the micro-scale, that is, a strain resolution of

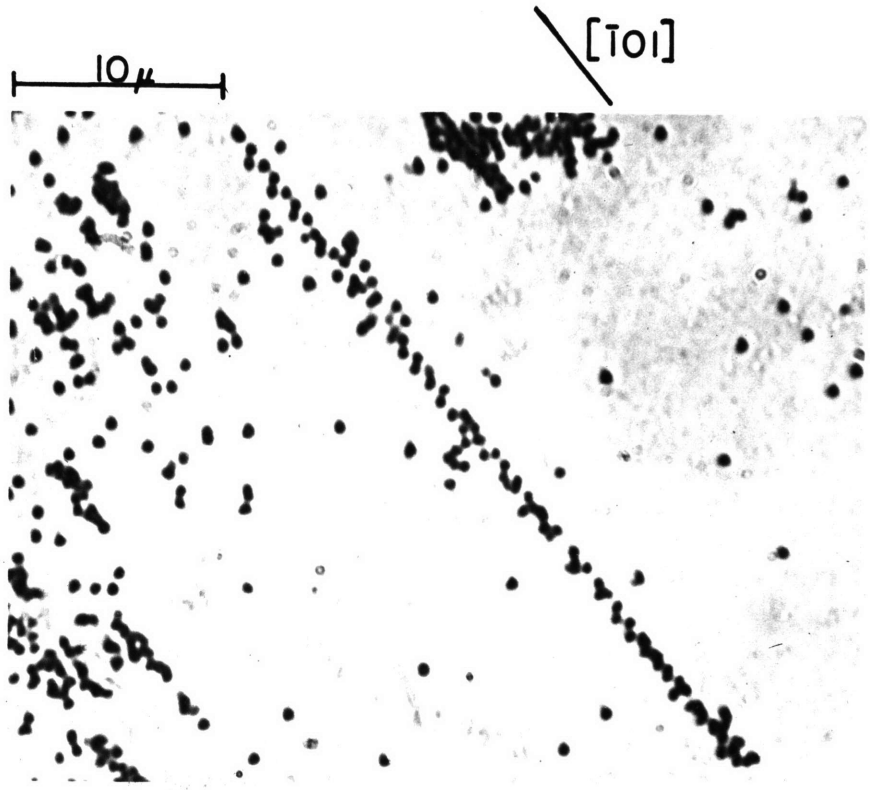

Fig. 3.2-9. Streamer composed mainly of dipoles, τ = 89 g/mm^2, crystal 4-8.

about 10^{-6}. This was the resolution in the present experiments, as well as in earlier work on copper single crystals by Rosenfield and Averbach (1962) and Bilello (1965), and on zinc by Roberts and Brown (1960).

Loading of crystals prepared in the usual manner was carried out on the testing machine equipped with a load cell. A linear variable differential transformer (Schaevitz Engineering, Model 020M-L) measured displacements in the specimen. The transformer coil housing was mounted along the specimen axis in an aluminum collar which was screwed to one grip. The core was held by an aluminum bracket which was affixed by screws to the other grip and ran the length of the specimen. The bracket was split into three pieces held together by screws, with slotted clearance holes employed so that the core could always be centered concentrically with the coil regardless of specimen length and slight variations in grip alignment. The output of the LVDT was fed into a Sanborn recorder through a phase shift network which kept the output signal in phase with the input. The load cell output was also fed into the Sanborn, from which both load and displacement signals went to an X-Y recorder. Data was analyzed from the X-Y record.

The LVDT was calibrated and checked for hysteresis with dummy specimens of aluminum and polycrystalline copper with assumed elastic moduli of 10 and $18 \cdot 10^6$ pounds per square inch, respectively. When single crystals of copper were subsequently tested, the apparent elastic modulus was always within ten per cent of the value for the particular orientation computed from the elastic coefficients given by Schmid and Boas (1950, p. 191). This value was $1.38 \cdot 10^4$ kg/mm^2. The source of elastic modulus discrepancy was thought to be due to slight misalignments

of the LVDT core.

The general form of the experiments was to load the crystal until a deviation from a linear load-elongation curve could be seen on the X-Y plot, then unload to slightly above zero load (usually to a load of about 100 grams). The crystal was then reloaded and further forward plastic strain introduced. The process was repeated until the total forward plastic strain was about $5 \cdot 10^{-3}$. Several times during the experiment the LVDT was re-nulled.

A typical load-unload cycle is shown in Figure 3.3-1, where the parameters determined from the X-Y recording have been labelled. A cumulative forward plastic strain γ was computed by adding together the incremental values γ_i.

The variation of recovered strain γ_r with forward plastic strain in crystal 5-5 is shown in Figure 3.3-2. In Figure 3.3-3, the unloading stress τ_f and the flow stress τ are shown as functions of forward plastic strain.

It was found that a single power law could not be used to characterize the stress-strain data over more than one order of magnitude in strain in the pre-yield region. This behavior differed from that reported by Roberts and Brown (1960), where stress and strain obeyed one power dependence up to the macroscopic yield point, and another thereafter.

Of the properties determined, the unloading stress is most sensitive to the strain resolution employed. Assigning a value to unloading stress involves determining when the unloading curve deviates from the elastic line, and the resolution for this is about 10^{-6} in strain. This means that dislocations may be moving even before the unloading stress drop has

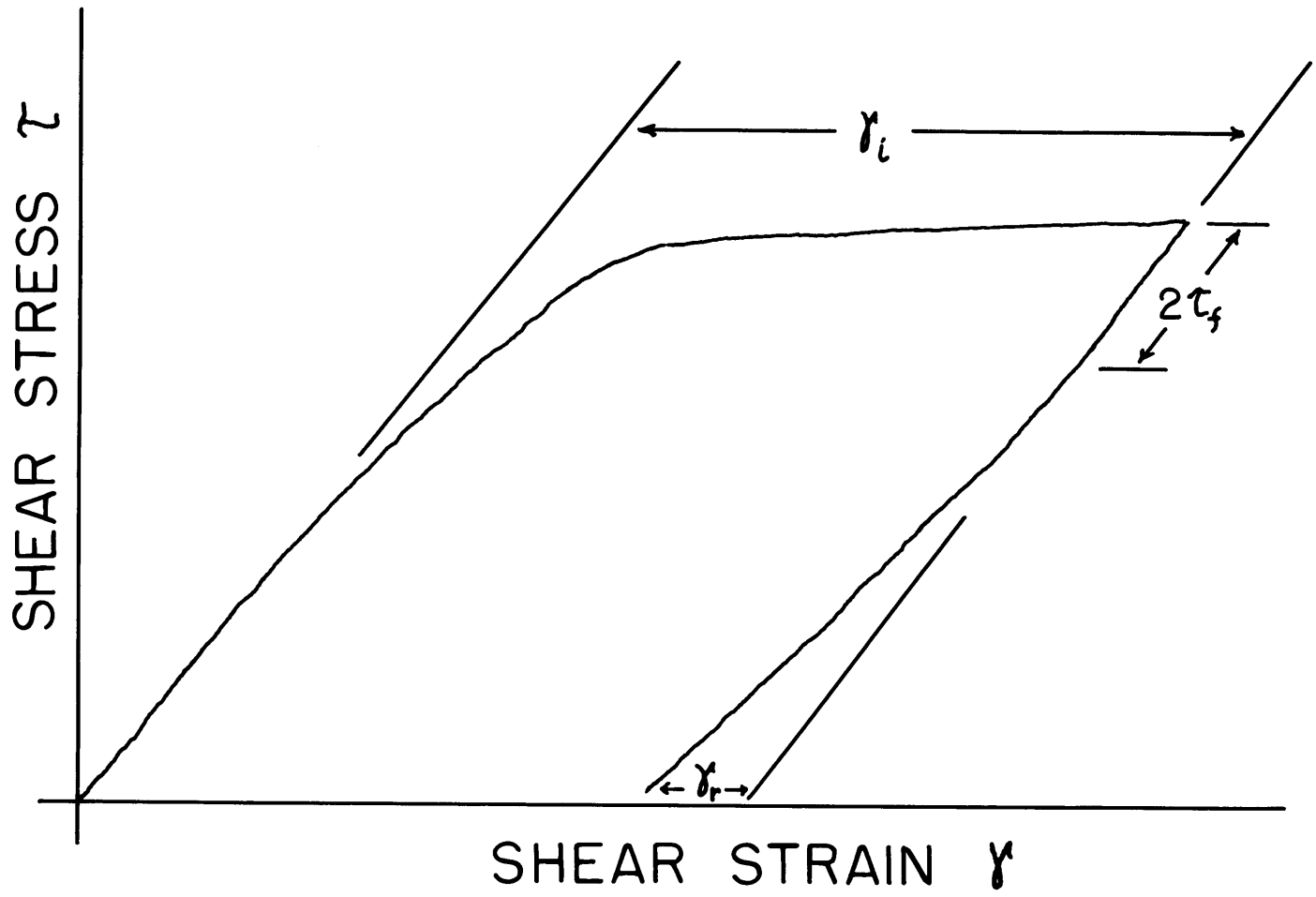

Fig. 3.3-1. Typical load-unload cycle for microstrain measurements, with parameters labelled.

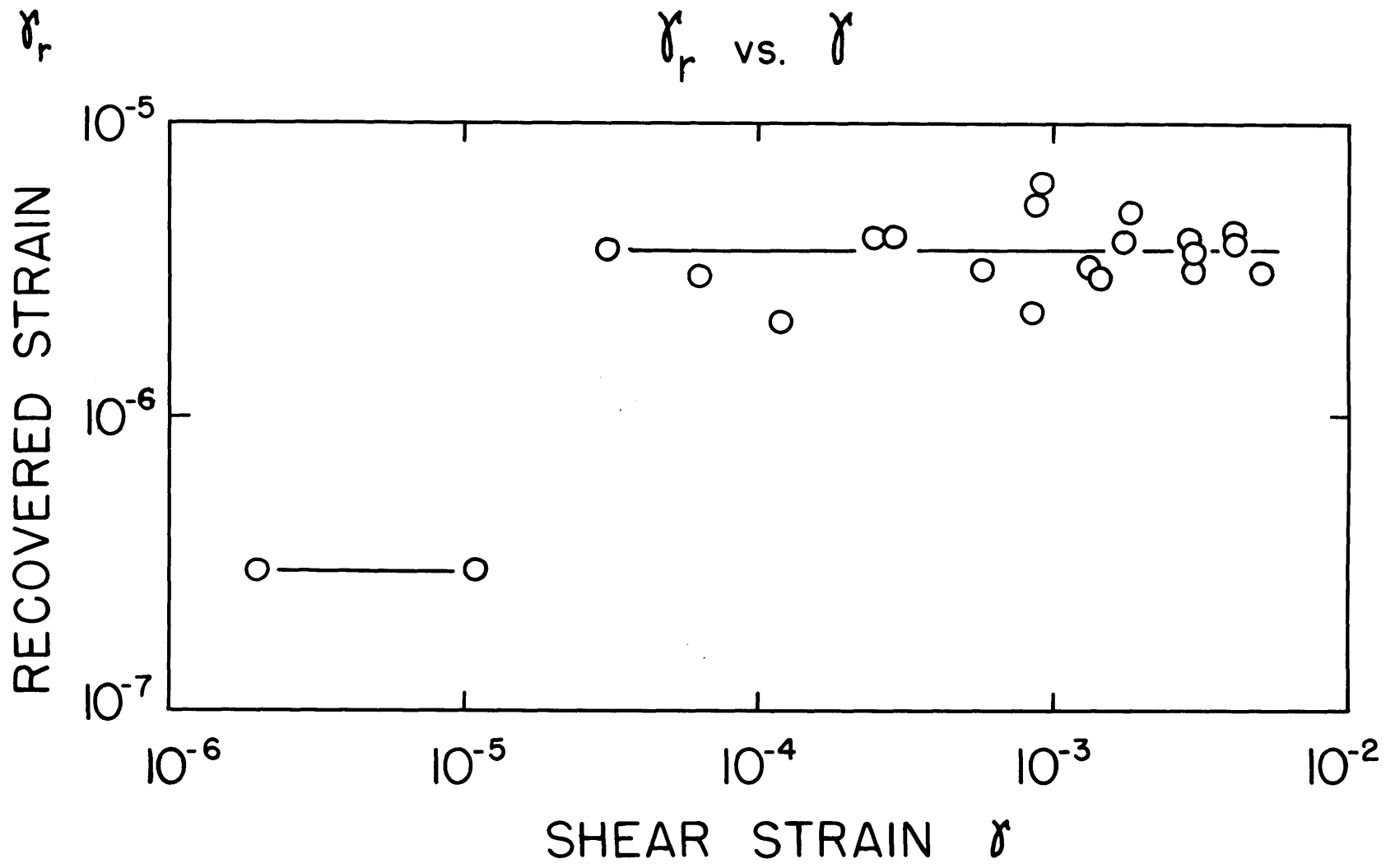

Fig. 3.3-2. Relation between recovered strain and forward strain, crystal 5-5.

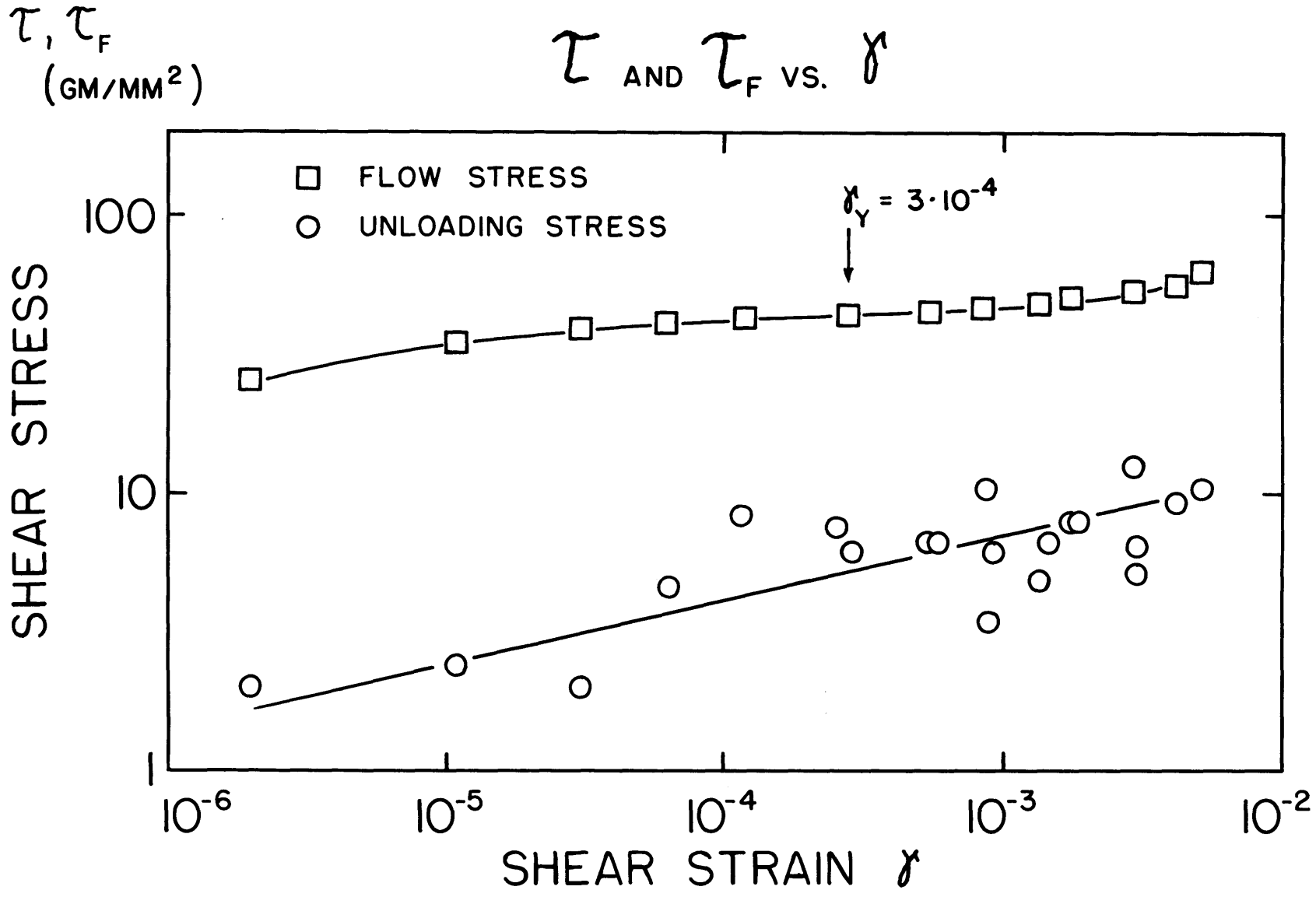

Fig. 3.3-3. Relation between flow stress, unloading stress, and forward strain, crystal 5-5.

occurred. The unloading stress measures the stress drop necessary before the combination of mobile dislocations and their relaxation distances yields a strain of about 10^{-6}.

At strains less than 10^{-5}, the magnitude of the unloading stress, about 2 g/mm^2, agrees with the stress value at which Young (1961b) first observed dislocation motion in copper with an etch pit technique. The measurements of Tinder and Washburn (1964) show that irreversible dislocation motion occurs at stresses less than 1 g/mm^2, which sets an upper limit on the lattice friction stress. The lattice friction stress on a straight dislocation segment is not subject to change with strain; the increase in the unloading stress with forward strain indicates an increase in the tightness of binding of the dislocations which are responsible for the unloading strain.

On the log τ vs. log γ plot the yield stress is taken as the stress at which the slope is minimum. It has been established that the value of the yield stress τ_y determined in this way is very nearly identical to the value τ_o obtained by extrapolating the easy glide slope to zero strain on straight τ-γ coordinates. The additional information which the log-log plot furnishes is the plastic strain at the yield stress. In Figure 3.3-3, the value of γ_y is about $3 \cdot 10^{-4}$.

3.4 Dislocation Motion Accounting for Recovered Unloading Strain

Following the microstrain experiments, of which one feature was the measurement of recovered strain γ_r, it was decided to employ a double-etching technique to determine the dislocation motion which accounted for this strain. The parameters to be determined experimentally

are found in the expression for the recovered shear strain

$$\gamma_r = bN_r x_r$$

where N_r is the density of dislocations moving during unloading, and x_r the average distance moved by the dislocations. Both N_r and x_r could be determined with the etch pit technique by etching under load and again when the load had been removed. The moving density and distances moved were determined by counting flat pits and measuring distances between such pits and fresh pits. Examples of unloading motion are shown in Figure 3.4-1.

The value N_r at a particular value of forward strain represents an average of densities counted on photographs of several regions. The value of x_r was taken as the average of about 25 back-motion distances observed and measured in the microscope. The distribution of the distances at one particular strain is shown in Figure 3.4-2, where the distances are those observed at an eyepiece magnification of 80X. Normal statistics were used to obtain 95% confidence limits on the mean, the limits being indicated by the brackets around the mean value point. It was recognized that the distribution is flatter than a normal distribution, and would perhaps be better represented by log normal statistics. However, the normal statistics give a more conservative view of the confidence limits.

Motion in opposite sense in a particular slip system was assumed to reflect the behavior of opposite sign dislocations on unloading, and not to be due to internal stress fields causing forward motion during unloading. A particular example of positive-negative dislocation motion on

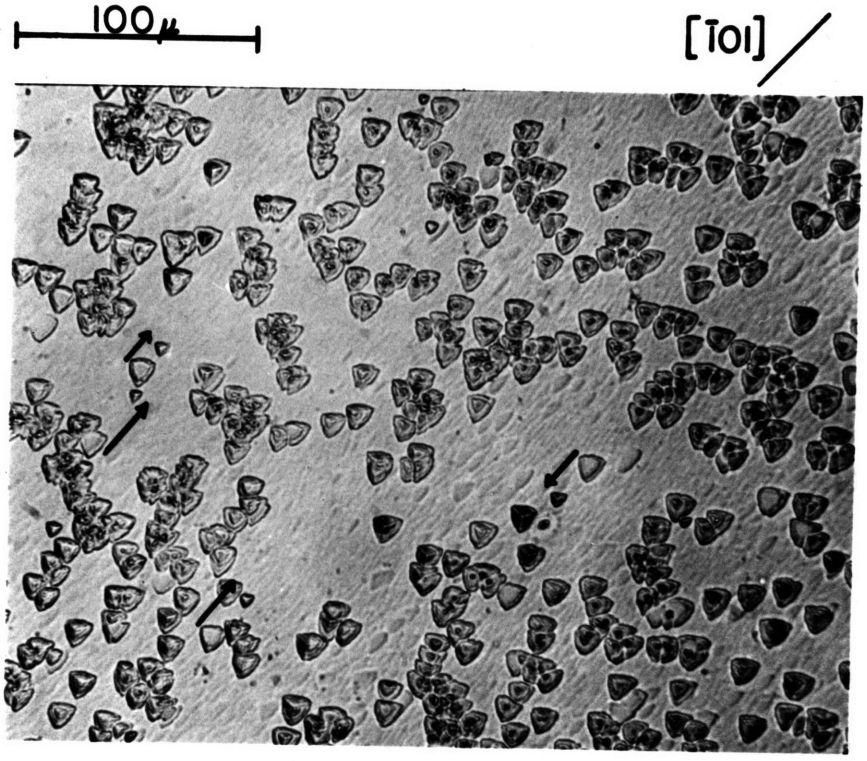

Fig. 3.4-1. Examples of dislocation motion during unloading, crystal 4-1.

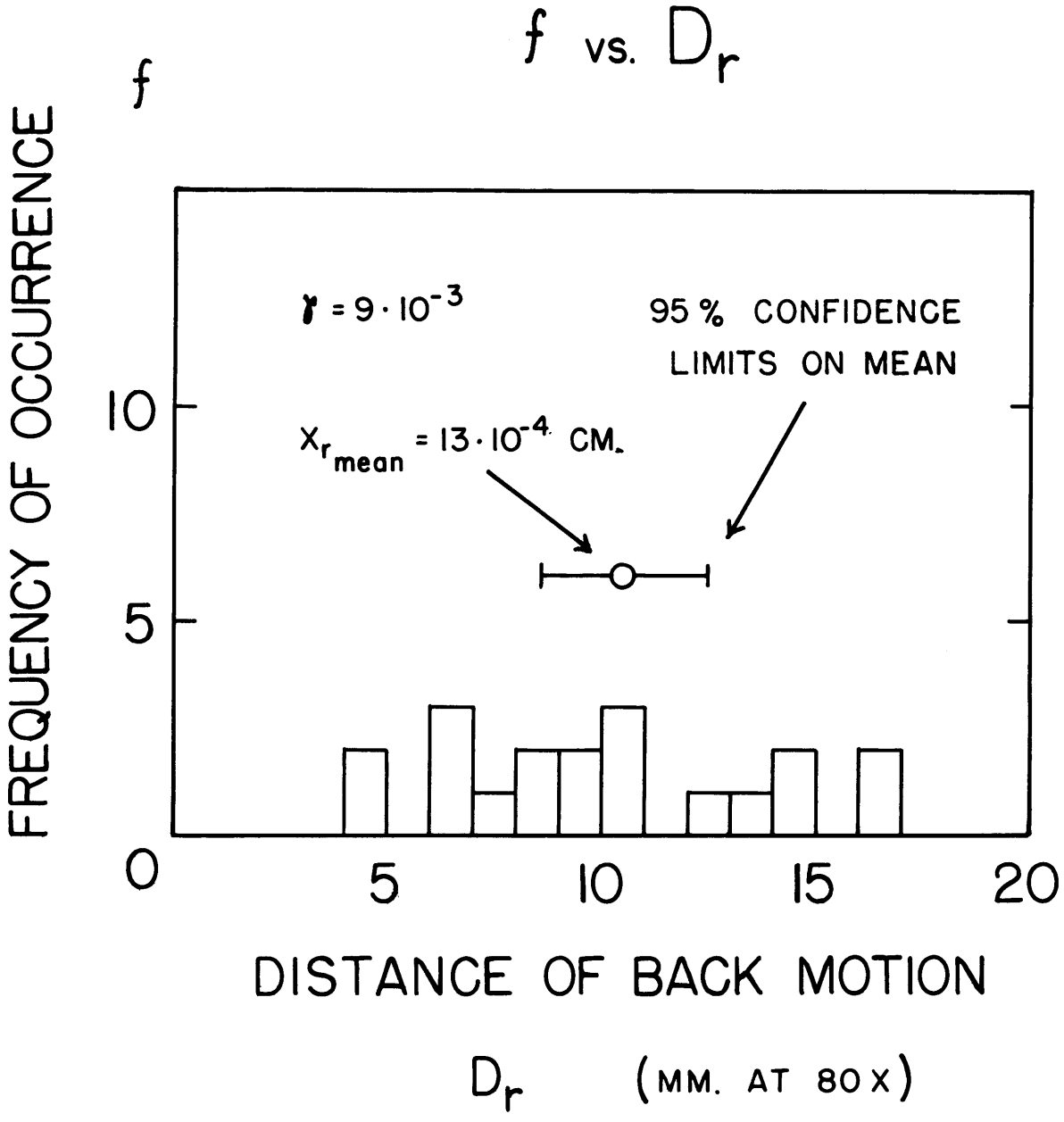

Fig. 3.4-2. Histogram of dislocation motion on unloading, $\gamma = 9 \cdot 10^{-3}$, crystal 4-3.

unloading is shown in Figure 3.4-3. The difference in sign of the moving dislocations is evident from the different appearances of the original pits; the white and black pits, differentiating positive and negative dislocations, appear different in this re-etching, the black having a more distinct dark border than the white.

From the observed N_r and x_r the recovered unloading strain could be calculated. The recovered strain was also measured directly to determine whether the computed value agreed with the true value, it being possible that the surface behavior of dislocations, which was measured with etch pits, would differ from the bulk behavior, which accounts for the directly measured recovered strain. Consequently, the recovered strain was measured directly with the LVDT as done in the microstrain experiments described in Section 3.3; the same methods for measuring load and displacement were employed.

The test procedure was to extend the crystal (4-3) a small amount, then unload to about 100 grams, obtaining the stress-strain curve and consequently the recovered strain for this forward strain increment through the LVDT. Then, without removing the crystal from the machine, it was immediately reloaded and given a small increment of forward plastic strain. The etchant (in a beaker) was brought in contact with the crystal under load for about three seconds and then removed. The crystal was unloaded and the etchant again brought into contact with the crystal, still on the machine. After ten seconds of etching the etchant was removed, and the crystal rinsed and dried. After the LVDT was removed from the crystal, the results of the double-etching were observed under the microscope. For successive strain increments the procedure was the same.

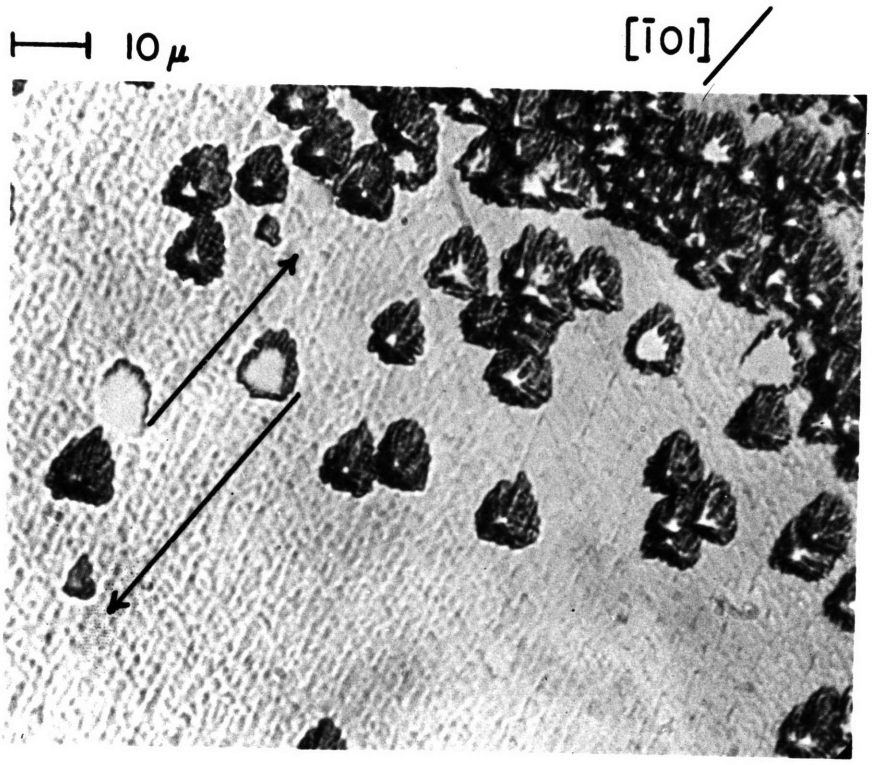

Fig. 3.4-3. Opposite sense motion of opposite sign dislocations on unloading, $\gamma = 7 \cdot 10^{-4}$, crystal 4-3.

Some general features of dislocation behavior on unloading were noted in addition to the specific information of numbers moving and distances moved. Figure 3.4-4 shows that glide polygonization, the short range alignment of dislocations in a direction perpendicular to the slip direction (Livingston 1960), occurs during the unloading of the crystal. Figure 3.4-5 illustrates the cooperative motion of a polygonized wall of dislocations under stress. The entire wall was pressed against the subboundary by the stress. It was found that most polygonized arrangements moved in a similar cooperative fashion under stress. In Figure 3.4-6, although the number of dislocations within clusters which moved during unloading cannot be ascertained, it can be seen that many dislocations in positions at the extremities of clusters and between clusters moved.

The behavior of N_r and x_r as functions of forward strain γ are shown in Figures 3.4-7 and 3.4-8, respectively. The distance of back movement, x_r, decreases with strain in what is roughly the pre-yield region, and then is constant or at least slowly decreasing in the early portion of easy glide. The density of dislocations contributing to the back-strain, N_r, is a constantly increasing function of strain and is well represented by a correlation

$$N_r \sim \gamma^{1/2}$$

which is shown with a least-square-fit line.

From these values of N_r and x_r the recovered strain was calculated and is shown in Figure 3.4-9 as a function of forward strain. Also shown are the LVDT-determined values of γ_r. The agreement of the recovered strain values is considered close enough to conclude that the measurements

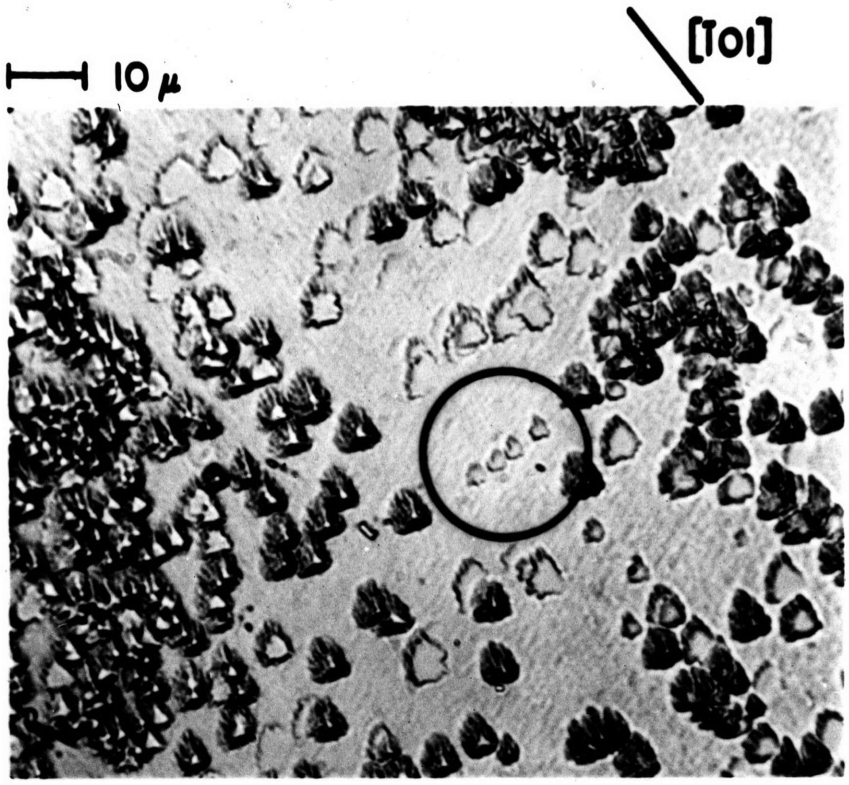

Fig. 3.4-4. Glide polygonization on unloading, crystal 4-3.

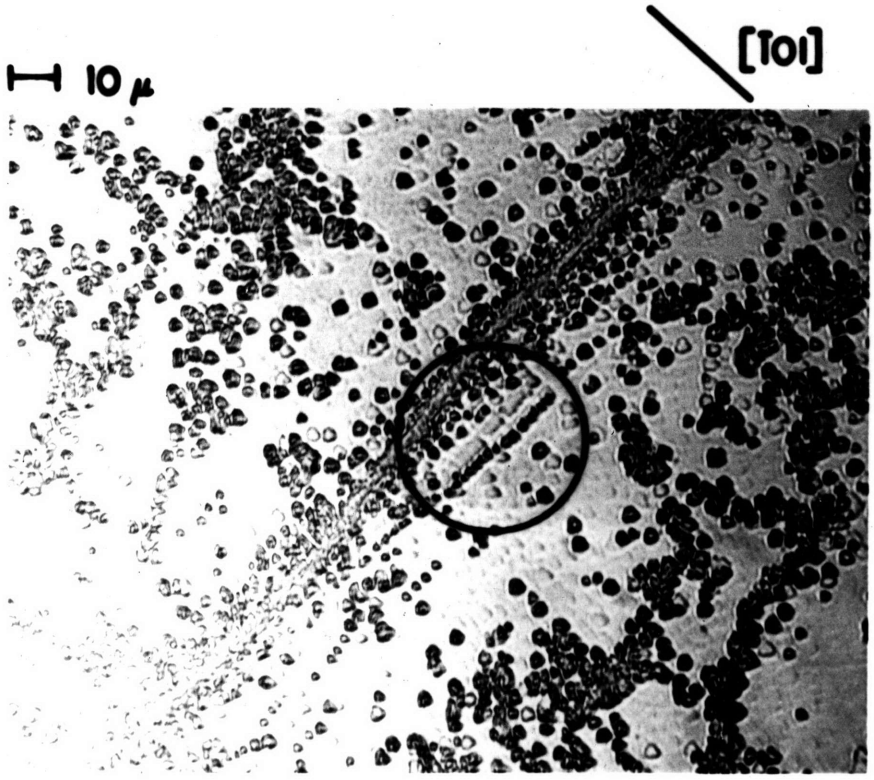

Fig. 3.4-5. Unloading relaxation of a polygonized wall of dislocations, crystal 5-5.

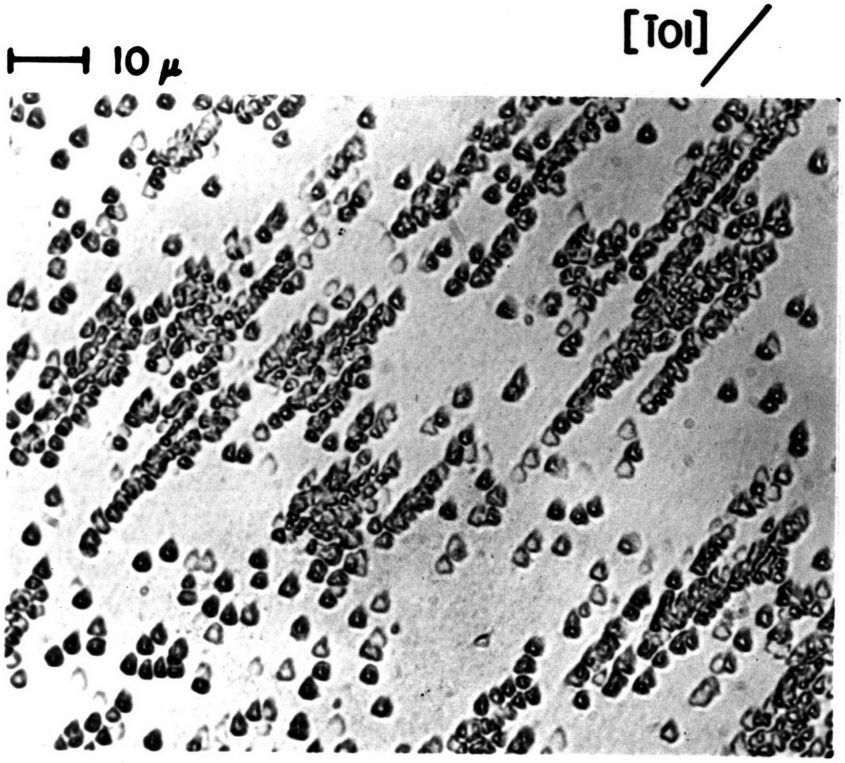

Fig. 3.4-6. Unloading motion of dislocations between clusters, crystal 4-3.

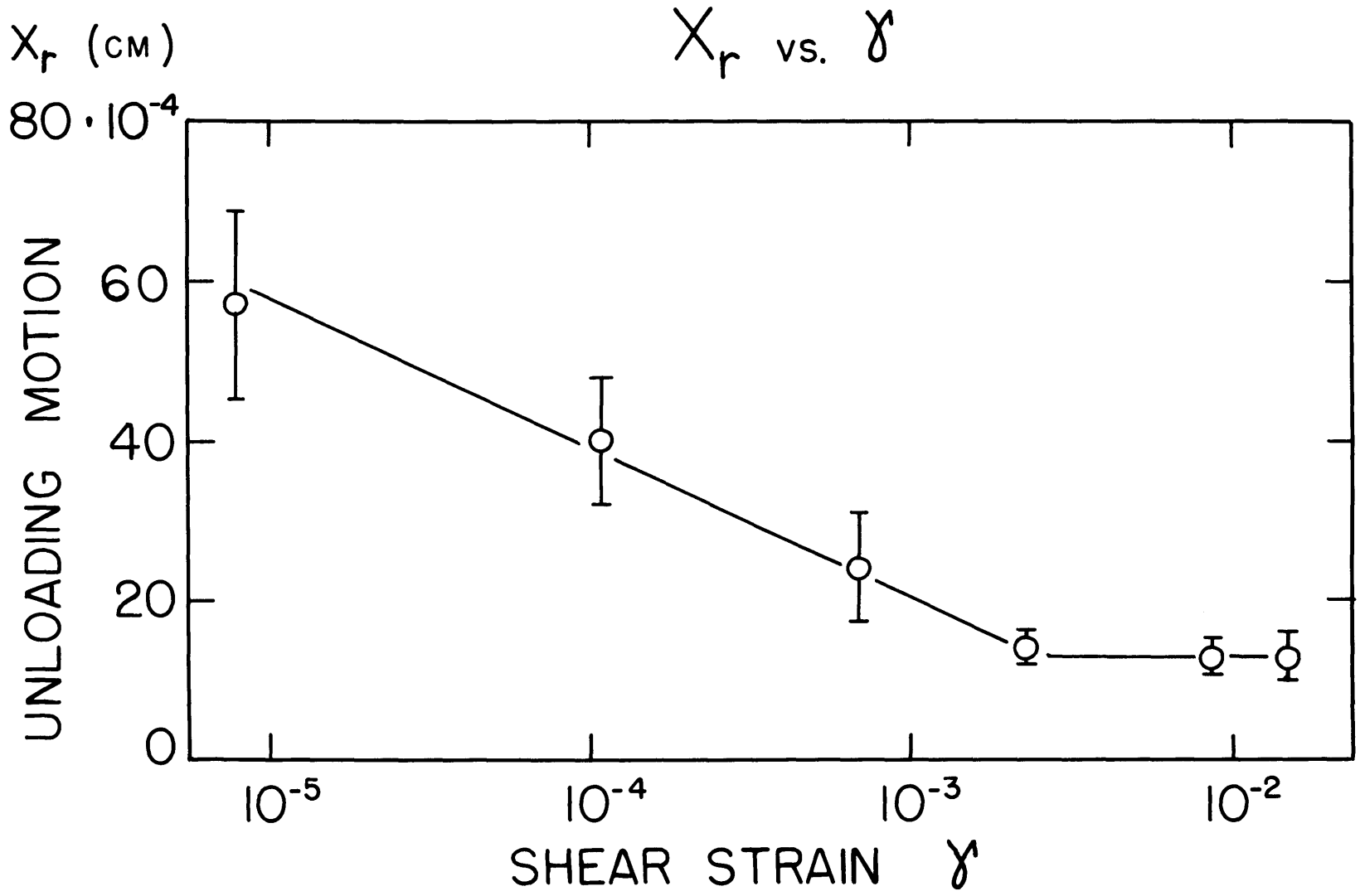

Fig. 3.4-7. Relation between distance of dislocation movement on unloading and forward strain, crystal 4-3.

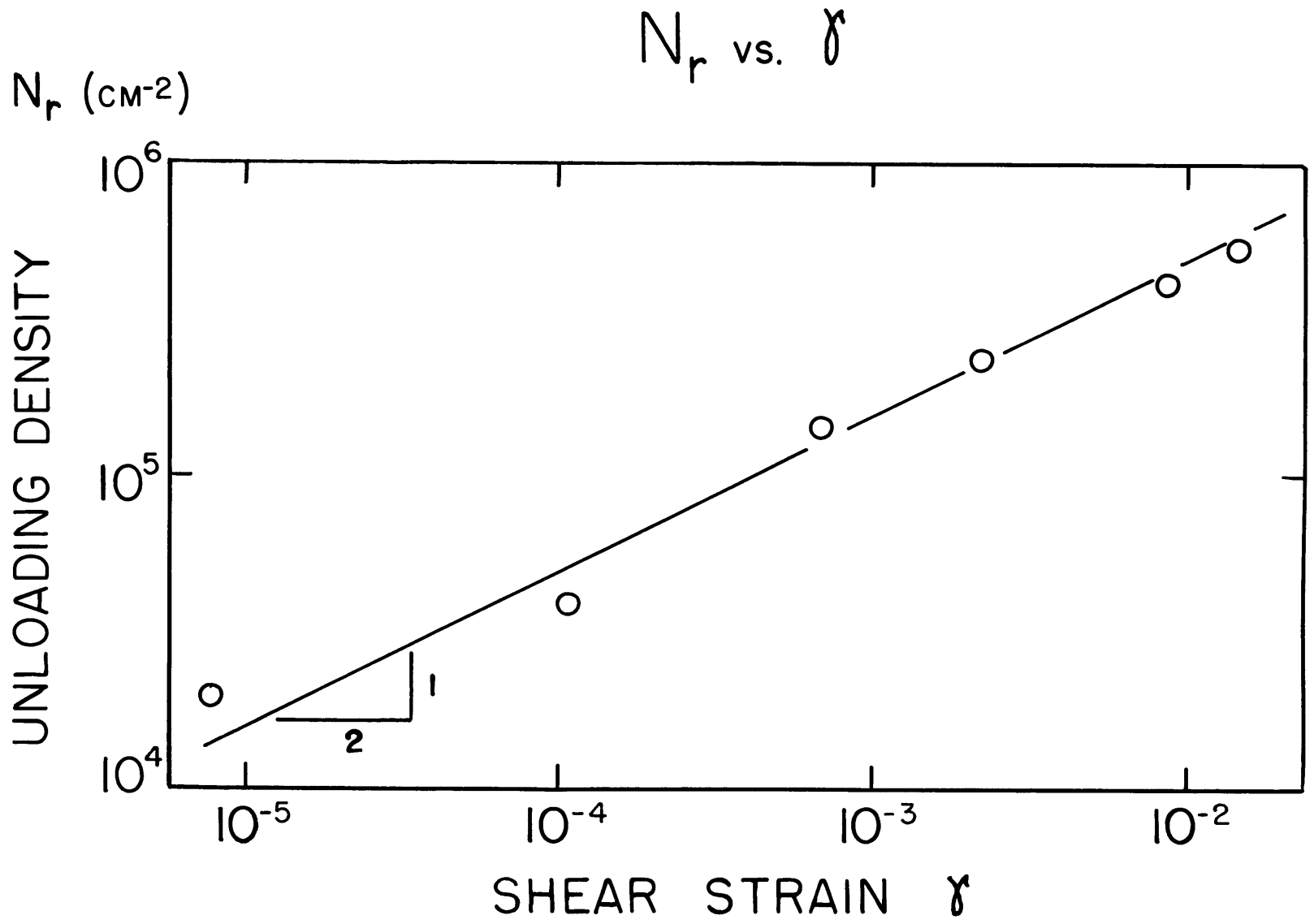

Fig. 3.4-8. Relation between density of dislocations moving during unloading and forward strain, crystal 4-3.

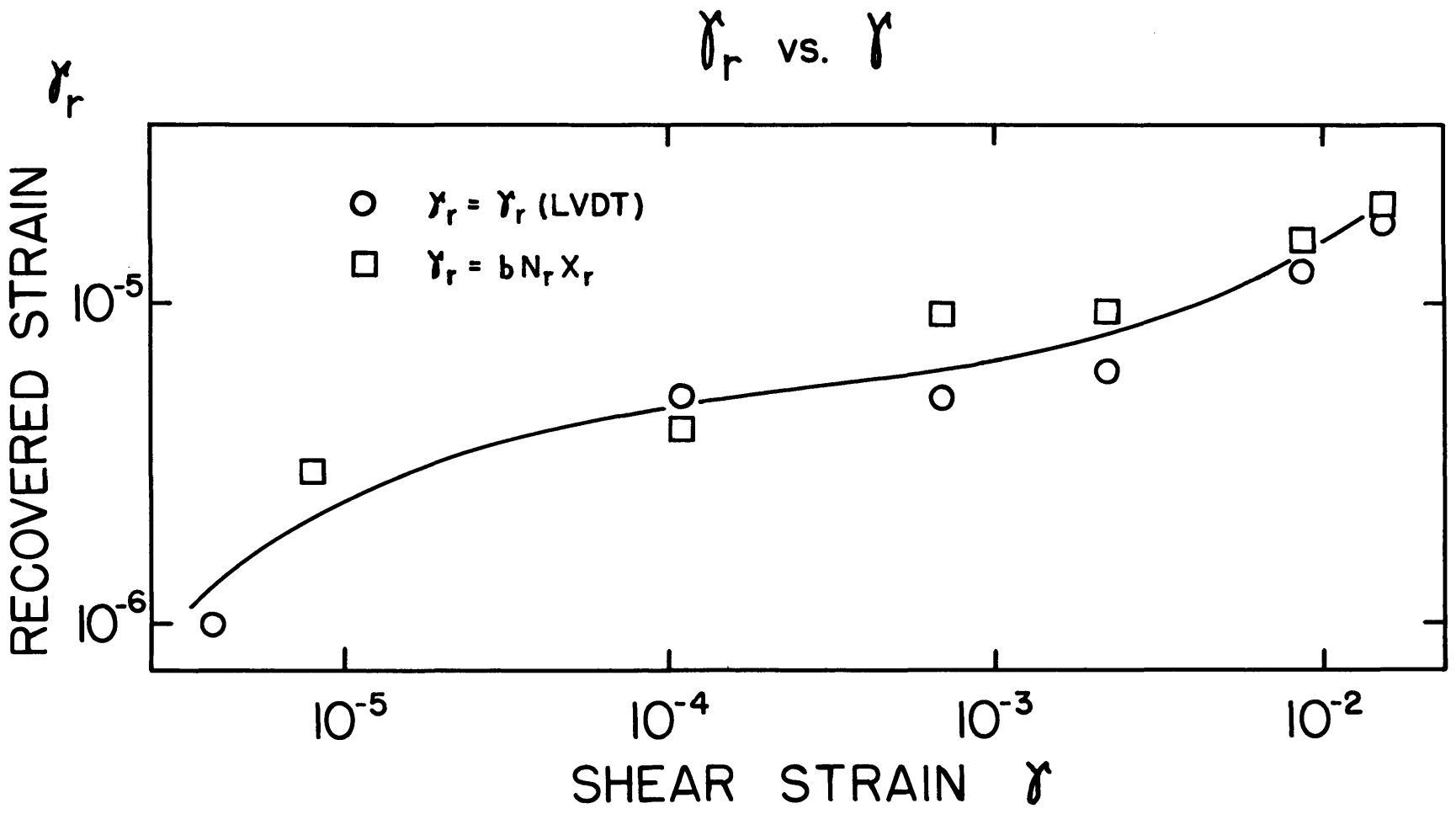

Fig. 3.4-9. Relation between recovered unloading strain and forward strain, crystal 4-3.

of pit motion on the surface are a satisfactory representation of behavior in the bulk.

Figure 3.4-10 shows the correlation between the recovered strain and the flow stress τ.

3.5 Relation of the Yield Stress to the Forest Dislocation Density

The preceding experiments have disclosed the behavior of dislocations intersecting the cross plane, most of these being dislocations of the primary system. It has been seen that transitions in the recovered strain behavior and in the form of clusters occur at the macroscopic yield stress, though no obvious mechanism for the determination of the yield stress appears from these etching studies.

The yield stress is very likely a structure sensitive property, since many investigators working with copper of essentially the same purity (99.999%) have measured widely different yield stress values. The range is from about 35 g/mm^2 (Young (1962b); this work) to several hundred g/mm^2 (Thornton, Mitchell and Hirsch (1962)). It has been pointed out earlier that the initial structures, measured by initial dislocation density, have also varied due to differences in growth and annealing procedures.

The experiments to be described were intended to determine the effect of the initial dislocation density on the yield stress. As discussed previously, the initial dislocations do not lie on slip planes and are not mobile; they may be considered to be forest dislocations, that is, dislocations which intersect the primary slip plane. Because of the uncertainties in comparing results obtained on different crystals, a method

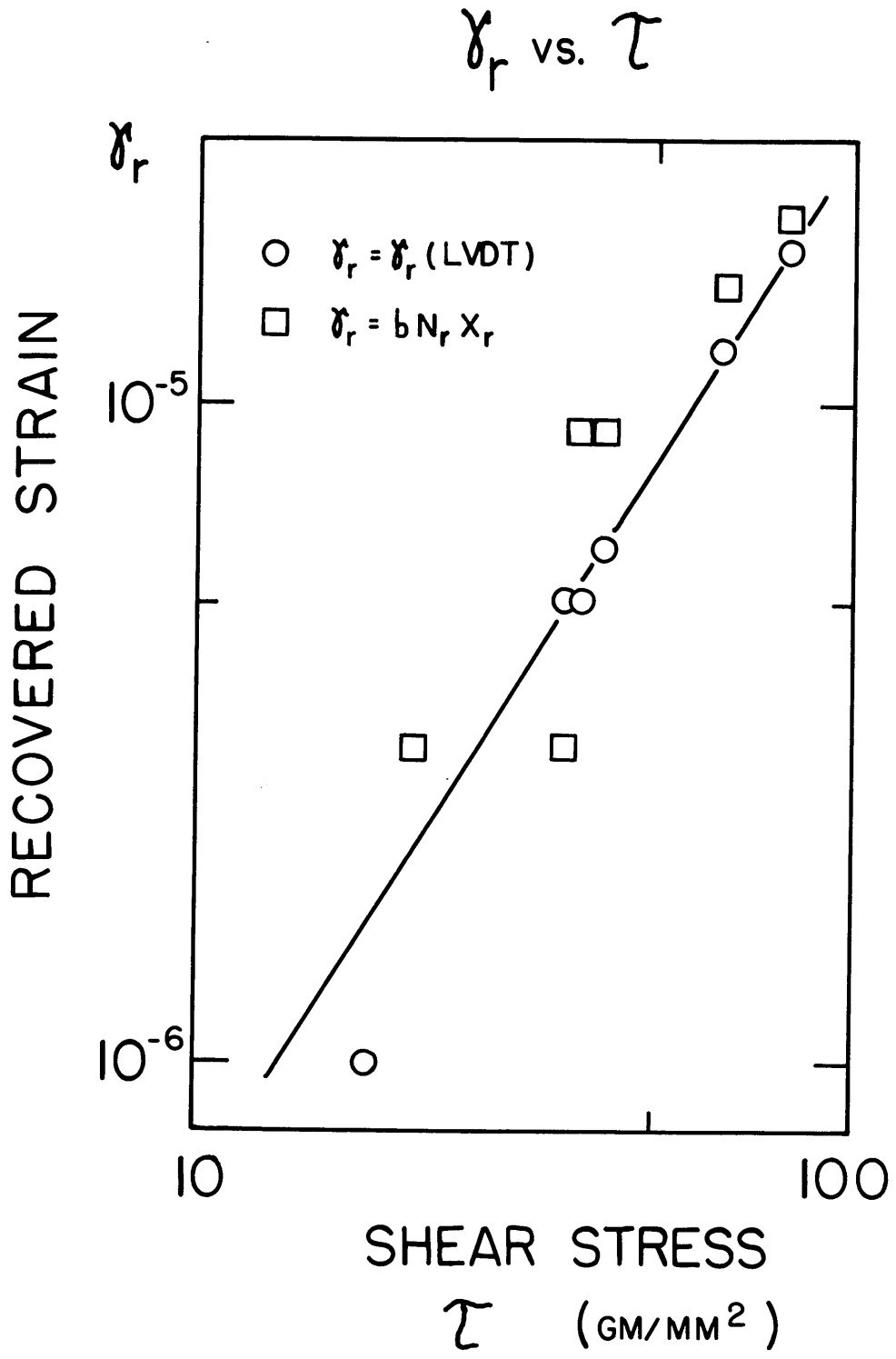

Fig. 3.4-10. Relation between recovered unloading strain and flow stress, crystal 4-3.

was developed by which the relation between yield stress and forest dislocation density could be established on one crystal; for this it was necessary to introduce a forest of known density into the crystal. This was accomplished by twisting the crystal by varying amounts prior to measuring its yield stress in tension; the torsion introduced forest dislocations preferentially into the crystal.

A relation between cumulative amount of twist and forest etch pit density N_f was established by spark-sectioning a twisted crystal on the primary plane. The result is shown in Figure 3.5-1, and the procedure is given in Appendix C. The figure also shows the etch pit density measured on the cross plane, a density which includes primary dislocations.

The procedure for determining the dependence of the yield stress on forest density was to load the crystal in tension until it yielded, to unload, then introduce a twist of ±2 degrees by means of a small twisting jig (described in Appendix C). The crystal was then reloaded in tension and the new yield point found. Four twists were applied cumulatively to each of two crystals, 4-9 and 4-10. The forest densities due to the twisting were taken directly from the twist-density plot.

The crystals were deformed in tension on the machine equipped with load and displacement cells. A continuous monitoring of the load-elongation curve was made on an X-Y recorder. When the yield point was reached, the introduction of a certain amount of plastic strain in tension was unavoidable. However, as determined from the load-elongation curve, the plastic shear strain so introduced was always less than 10^{-3}, which from the earlier multiplication experiments corresponds to a primary etch pit

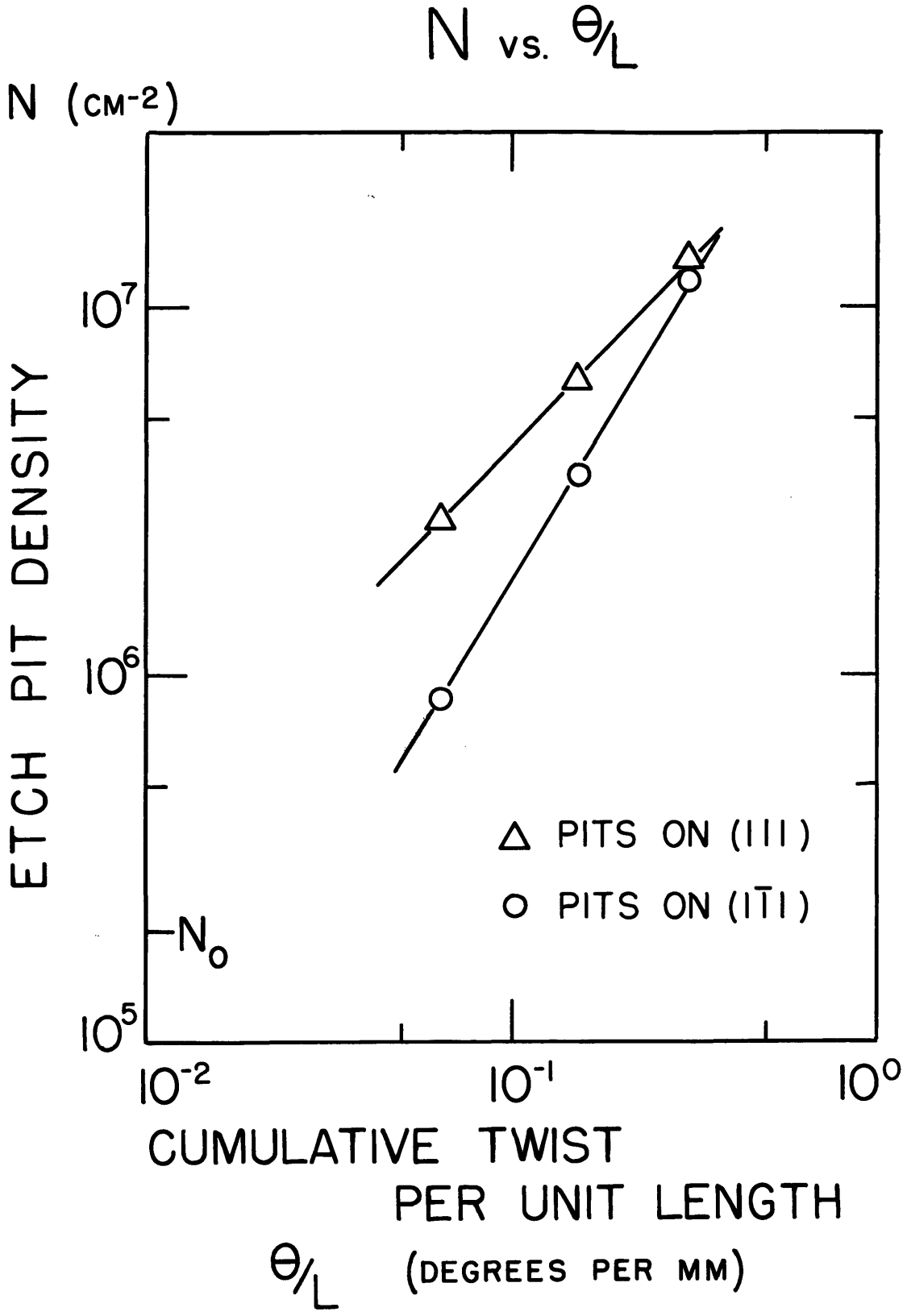

Fig. 3.5-1. Relation between etch pit density on primary and cross planes and cumulative twist per unit length, crystal 5-18.

density of less than 10^6 per cm^2. Thus the primary dislocation density for successive loadings could be considered nearly constant apart from the unknown (but small) increase due to the twisting itself.

It had been established that the initial forest density was equal to the initial density intersecting the cross plane (see Appendix B), so the initial forest density was determined by polishing and etching the cross plane prior to loading.

The result for crystal 4-10 is shown in Figure 3.5-2, with a least-square-fit straight line constructed for the data. The striking feature is that the correlating line extrapolates to a small stress, 6 g/mm^2, at zero forest density. This implies that almost the entire magnitude of the yield stress is coupled to the forest density. Using normal statistics the 95% confidence limits for the intercept were 6 ± 15 g/mm^2; however, the result for crystal 4-9 also had an intercept of 6 g/mm^2.

The equation relating the yield stress values and the forest density may be written

$$\tau_y = \tau_{yo} + \alpha_y Gb\sqrt{N_f}$$

where α_y is a coefficient which would relate to the actual mechanism by which the forest influenced the stress. For crystal 4-10, $\alpha_y = 0.62$, with 95% confidence limits ± 0.07; for crystal 4-9, $\alpha_y = 0.67$.

Although a systematic study of the relation between forest density and yield stress has not previously been reported, a relationship between flow stress and forest density has been observed in one case (Basinski and Basinski, 1964). They found that the flow stresses of two crystals, one deformed in tension to a shear strain of 5% and the other twisted

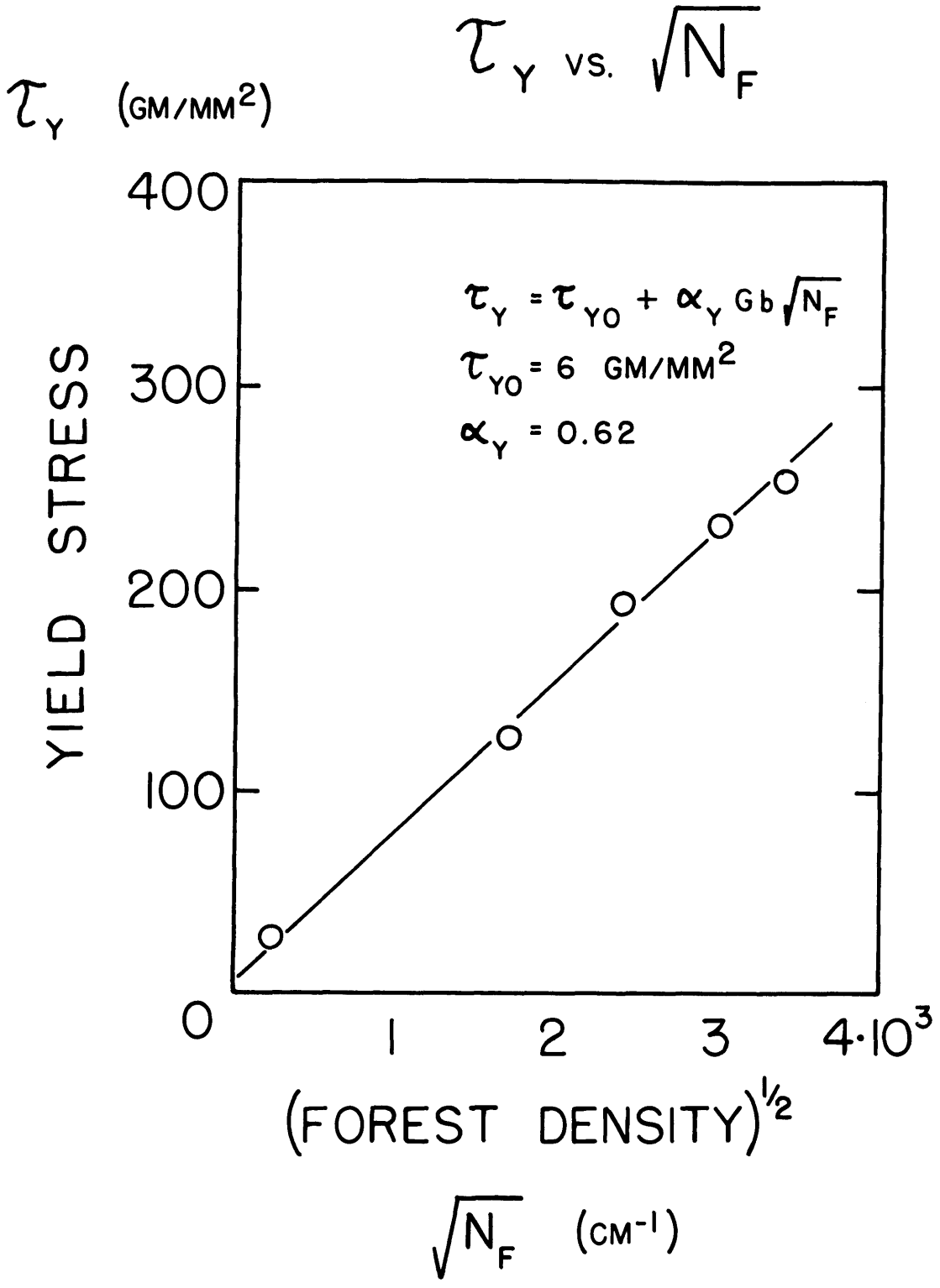

Fig. 3.5-2. Relation between yield stress in tension and square root of forest density, crystal 4-10.

and then deformed in tension to 1%, correlated well with the square root of the forest density measured after straining by a spark-sectioning and etching procedure.

Basinski and Jackson (1965a) have also reported the dependence of the tensile yield stress on pre-twist, but have not shown a relation between the pre-twist and forest dislocation density. Employing the twist-density data of Figure 3.5-1, the forest density values corresponding to the pre-twists they report were computed, and the forest density-stress plot constructed from this data gives a result consistent with the results discussed previously, α_y being 1.0. In determining N_f for these pre-twists, a correction had to be made for different specimen size, which governs the strain for a given twist per unit length. Since their specimens were 3 mm square, and the twist-density correlation had been obtained for 6 mm square crystals, the density for one of their twists was taken as that corresponding to a twist half as large in Figure 3.5-1. Their crystals were similar to ours in purity and orientation.

IV. DISCUSSION

In this section will be set forth a description of the early stages of plastic flow in a copper single crystal, a description which is suggested and supported by the preceding experimental results and pertinent results of other investigators.

An annealed crystal is divided into sub-grains of approximately one millimeter size, and within these sub-grains the initial etch pit density N_o is about $1 \cdot 10^5$ per cm^2. Merlini and Young (1966) have shown by x-ray observations that this initial density consists mainly of dislocations which do not lie on $\{111\}$ slip planes. The low initial density implies that the wavelength of the internal stress field in the annealed state is large – being the order of the distance between dislocations, i.e.,

$$\ell = \frac{1}{\sqrt{N_o}} \approx 30 \cdot 10^{-4} \text{ cm.}$$

Thw wavelength of the internal stress field is greatest in the annealed condition, and decreases with strain, that is, with increasing dislocation density or decreasing dislocation spacing.

The onset of irreversible deformation in copper has been shown by Tinder and Washburn (1964) to occur at stresses less than 1 g/mm^2. This value may be considered as an upper limit for the lattice friction stress which opposes the motion of a straight dislocation segment in an otherwise perfect lattice.

As the stress on an annealed crystal is increased from zero, etch

pit observations on the cross plane show that a small fraction of the initial dislocations move, doing so on all $\{111\}$ planes subjected to a finite stress. This motion is that of the relatively few dislocations which, after annealing, remain on the $\{111\}$ slip planes. At $\tau = 10$ g/mm^2, about five per cent ($\approx 5 \cdot 10^3$ per cm^2) of the dislocations present move. The observed distance of motion is on the order of the initial forest spacing. The strain resulting from this motion may be estimated from the usual relation

$$\gamma = bNx$$

and with $N = 5 \cdot 10^3$ per cm^2 and $x = 30 \cdot 10^{-4}$ cm, the strain is $3 \cdot 10^{-7}$. This is in agreement with the measurements of Tinder and Washburn, who found a plastic strain of $2 \cdot 10^{-7}$ at $\tau = 10$ g/mm^2 in polycrystalline copper.

At a stress τ_m in the pre-yield region multiplication of dislocations is observed from etch pit counts on the cross plane. In crystals which yielded macroscopically at about 35 g/mm^2, the value of multiplication stress was about 17 g/mm^2 (Young 1961b, also this work). Between the multiplication stress and the yield stress the increase in etch pit density is about $6 \cdot 10^5$ per cm^2.

The average distance of dislocation motion in the stress interval between multiplication and macroscopic yielding may be estimated from this density value and the value of the strain at the yield stress, which is known from microstrain measurements to be about $3 \cdot 10^{-4}$. Using the relation

$$\gamma = bNx$$

and inserting the values of N and γ just mentioned, the average distance is $200 \cdot 10^{-4}$ cm, which is about ten mean forest spacings.

In the pre-yield range the average distance of back motion of dislocations on unloading steadily decreases, from 60 to $25 \cdot 10^{-4}$ cm. Back motion is the relaxation of dislocations which at the termination of forward straining are loosely bound in the internal stress fields of the crystal, and the distance of back motion is on the order of the initial forest spacing.

Dislocation multiplication in the pre-yield region is accompanied by the formation of multipole clusters composed of edge dislocation dipoles. The usual site for formation of a cluster is at a forest dislocation, where possibly a few primary edge dislocations get caught, and then other primary dislocations are trapped in increasing numbers by elastic interactions. This is suggested by the histograms of etch pit spacings within clusters, which show a cutoff in the frequency of occurrence of spacing at the critical passing distance.

In the pre-yield region, clusters viewed by etch pits on the cross plane are rather equi-axed, that is, they do not show orientation effects such as elongation in or normal to the primary slip direction which characterize multipoles in easy glide. This may reflect a difference in operation of the sources for dislocations joining the clusters. In pre-yield, dislocation sources may send out only a few dislocations before becoming inactive; in easy glide, where slip distances are much greater, a source could send out many more dislocations, which may all end up in the same cluster, causing it to be elongated in the slip direction.

The etch pit observations of multipoles are in agreement with and

complement transmission electron microscopic (TEM) observations, which add the depth dimension missing in etch pit studies. Multipole clusters as the dominant feature of dislocation arrangement in easy glide have been found by TEM in copper by Fourie and Murphy (1962), Sharp and Makin (1964), Basinski (1964), Fourie (1964), Essmann (1965) and Steeds (1966), and in magnesium by Hirsch and Lally (1965). These observations show that clusters contain few non-primary dislocations, and have almost a total absence of primary screw dislocations, which are thought to annihilate by cross slip. The length of edge segments in clusters decreases with increasing strain. At the smallest strain (5%) studied by Essmann, the edge segment length was about $10 \cdot 10^{-4}$ cm.

From experiments in which a dislocation forest of known density was introduced into a crystal by twisting, the yield stress in tension has been found to be coupled to the forest density, by a relation

$$\tau_y = \tau_{yo} + \alpha_y G b \sqrt{N_f},$$

where $\tau_{yo} \approx 5$ g/mm^2 and $\alpha_y \approx 0.65$. The significant point about this result is that it indicates that the portion of the yield stress which is not coupled to the forest density is small. This portion, for example, would be the contribution from an impurity or friction stress mechanism. In the easy glide regime it has been established (Basinski and Basinski 1964) that the flow stress continues to be coupled to the forest density with a coupling coefficient $\alpha_f = 0.79$, which is not very different from that determined for the yield stress values. Coupling between yield stress and forest density is likely the reason that in crystals employed in etch pit investigations yield stresses have generally been lower than in crystals

employed in TEM investigations, reflecting the lower initial densities which etch pit workers obtain by annealing.

Dislocation multiplication observations in easy glide show that the etch pit density observed on the cross plane increases linearly with strain, and the 0.5 cm mean free path of primary dislocation motion calculated from the strain-density data is on the order of the specimen dimension. This is more than a factor ten greater than the motion distance calculated for the pre-yield region, indicating an important property of the yield stress, that it is the stress at which dislocations can move large distances through the forest.

Combining all these observations, the conclusion is that in the pre-yield region dislocation multiplication can commence at stresses well below the yield stress, because there are in the crystal areas where the spacing of forest dislocations is larger than the mean value. However, dislocations generated in such areas are only able to run for a short distance before meeting forest spacings which they cannot penetrate. When the yield stress is reached, essentially the whole area of a slip plane can be swept out by dislocations moving through the forest. This description has several features in common with that developed by Kocks (1966) in his statistical theory of the flow stress. He showed that for a random distribution of point-like obstacles such as forest dislocations on the slip plane, a critical stress existed for a dislocation to sweep across the plane. Because of the random distribution of obstacles, small areas of the slip plane could be swept out at stresses lower than the critical stress.

The strength of the primary dislocation-forest dislocation interaction determined the value of the coupling coefficient α, but it is not possible

to draw conclusions about the exact interaction mechanism from the observed value $\alpha_y = 0.65$. The reason is that a value of α cannot be calculated theoretically for any mechanism with a precision greater than a factor of two because of uncertainties in calculating jog energies, line energies, the effects of anisotropy, etc. It can be said that the observed value suggests that the interaction between forest and primary dislocations is a strong one which may approach the interaction needed to force extrusion in the Orowan mechanism. The coefficient for extrusion is of the order of unity, which may be seen by inserting the mean forest spacing $\ell = \frac{1}{\sqrt{N}}$ into the usual extrusion stress formula

$$\tau = \frac{Gb}{\ell} = 1 \cdot Gb\sqrt{N}.$$

The development of multipole clusters in easy glide reflects the relatively steady state behavior in this region. The number of clusters increases but slowly, while the number of dislocations in a cluster increases rapidly. At the end of easy glide the density of clusters is about $2 \cdot 10^5$ per cm^2, that is, about the initial forest density. The relative constancy in cluster numbers implies that the distance between clusters is nearly constant. This is what is reflected in the experimental finding that the distance of dislocation back motion on unloading is constant at $15 \cdot 10^{-4}$ cm in easy glide, and about equal to one-half the mean cluster spacing.

The relation between dislocation density contributing to recovered unloading strain and the square root of forward strain may be explainable in geometric terms. If the number of clusters were constant, the linear

increase in dislocation density with strain would imply that the number of dislocations per cluster increases linearly. If the clusters were geometrically similar at different values of strain, and if the dislocation density in the clusters was constant with strain, the number of dislocations on the 'perimeter' of a cluster would increase as the square root of strain. These dislocations, being the most loosely bound to the cluster, would be the ones contributing to recovered strain.

V. CONCLUSIONS

1) The yield stress (critical resolved shear stress) of a copper single crystal is determined mainly by the initial forest dislocation density, the law of coupling being

$$\tau_y = \tau_{yo} + \alpha_y Gb\sqrt{N_f}$$

where $\tau_{yo} \approx 5$ g/mm^2 and $\alpha_y \approx 0.65$, indicating a strong interaction between primary and forest dislocations.

2) The mean free path of dislocation motion in easy glide, determined by etch pit multiplication experiments, is constant and on the order of the crystal dimension, $5 \cdot 10^{-1}$ cm; in the pre-yield region the distance of motion is on the order of 10^{-2} cm.

3) The structure of primary dislocations which develops with strain consists mainly of edge dislocation dipoles collected in multipole groups. The groups grow rapidly in size but slowly in number through easy glide, where the dipole spacing is on the order of 10^{-4} cm and the spacing between groups is on the order of $20 \cdot 10^{-4}$ cm.

4) The average distance of back motion of dislocations on unloading decreases from approximately 60 to $25 \cdot 10^{-4}$ cm in the pre-yield region, finally reaching a constant value of about $15 \cdot 10^{-4}$ cm in easy glide. The dislocation density in motion during unloading increases as the one-half power of strain through the pre-yield and easy glide regimes, with a value of 10^5 per cm^2 at the yield stress.

REFERENCES

Basinski, Z. S., 1964, Discussions of the Faraday Society, No. 38, 93.

Basinski, Z. S., and Basinski, S. J., 1964, Phil. Mag., 9, 51.

Basinski, Z. S., and Jackson, P. J., 1965, Phys. Stat. Sol., 9, 805.

Bilello, J. C., 1965, "Microstrain Study of Strain Hardening in Copper," Ph. D. Thesis, University of Illinois.

Brydges, W. T., 1963, "Growth and Deformation of Magnesium Single Crystals," S.M. Thesis, M. I. T.

Cottrell, A. H., 1953, "Dislocations and Plastic Flow in Crystals" (Oxford: University Press).

Essman, U., 1965, Phys. Stat. Sol., 12, 707.

Fourie, J. T., 1964, Phil. Mag., 10, 108.

Fourie, J. T., and Murphy, R. J., 1962, Phil. Mag., 7, 1617.

Friedel, J., 1964, "Dislocations" (Oxford: Pergamon Press).

Hirsch, P. B., and Lally, J. S., 1965, Phil. Mag., 12, 595.

Hordon, M. J., 1962, Acta Met., 10, 999.

Hulett, L. D., Jr., and Young, F. W., Jr., 1965, J. Phys. Chem. Sol., 26, 1287.

Kocks, U. F., 1966, Phil. Mag., 13, 541.

Livingston, J. D., 1960, J. Appl. Phys., 31, 1071; 1962a, in "Direct Observation of Imperfections in Crystals," ed. Newkirk and Wernick (New York: Interscience), p. 115; 1962b, Acta Met., 10, 229; 1963, J. Aus. Inst. Met., 8, 15.

Merlini, A., and Young, F. W., Jr., (1966), in press.

Orowan, E., 1934, Z. Physik, 89, 635.

Polanyi, M., 1934, Z. Physik, 89, 660.

Reid, C. N., Gilbert, A., and Rosenfield, A. R., 1965, Phil. Mag., 12, 409.

Roberts, J. M., and Brown, N., 1960, Trans. AIME, 218, 454.

Rosenfield, A. R., and Averbach, B. L., 1962, Acta Met., 10, 71.

Schmid, E., and Boas, W., 1950, "Plasticity of Crystals" (London: F. A. Hughes and Co.).

Sharp, J. V., and Makin, M. J., 1964, Phil. Mag., 10, 1011.

Steeds, J. W., 1966, Proc. Roy. Soc., A292, 343.

Taylor, G. I., 1934, Proc. Roy. Soc., A145, 362.

Tinder, R. F., and Washburn, J., 1964, Acta Met., 12, 129.

Young, F. W., Jr., 1961a, J. Appl. Phys., 32, 192; 1961b, J. Appl. Phys., 32, 1815; 1962a, J. Appl. Phys., 33, 749; 1962b, J. Appl. Phys., 33, 963; 1962c, J. Appl. Phys., 33, 3553.

Appendix A

OBSERVATIONS ON ETCHING

In the course of the experiments numerous features of etching were observed which are perhaps of more interest to a study of the etching process itself than to the use of etching in studying mechanical behavior.

The etchant employed was that of Livingston (1962b), 90 parts water, 25 hydrochloric acid, 15 acetic acid and 1 bromine. Parameters other than the composition were found to affect the outcome of etching. The best etching occurred on a mirror-like polished surface which was held without agitation in a horizontal position (faced either up or down). The etching time was usually about ten seconds. The etching was insensitive to the use of tap water instead of distilled water, and to pure instead of reagent grade bromine.

The etchant reveals the sites of dislocations emerging on a $\{111\}$ surface with triangular pointed-bottomed pits, the edges of which are in $<110>$ directions, the lines of intersection of the $\{111\}$ planes. Thus the Burgers vectors (which are $<110>$) of the slip systems lie parallel to pit edges, and edge dislocations move in these directions, thus providing a useful tool in analyzing dislocation movements and cluster configurations. The sloping sides of the pit do not have rational indices. The pits are in fact quite shallow, with a width to depth ratio of about fifteen to one (Livingston 1962a). Livingston (1960) has found considerable evidence that the etch pits on $\{111\}$ faces are a reliable measure of the total number of dislocations intersecting the etching surfaces.

The result of a successful etch is shown in Figure A-1. The most noticeable feature of the pits is that they are of two basic varieties, designated black and white. This effect was first observed and explained by Livingston (1962a). In this explanation the difference in color is due to a difference in depth of the pits, the blacks being deeper such that their sloping sides reflect incident light from the microscope away from the objective to a greater extent than do the sides of the shallower white pits. Livingston also concluded that if the blacks represent positive edge dislocations, the whites represent negative ones if both are of the same slip system. This results from an asymmetry in position of the extra half-planes. With a $\{111\}$ etching surface, the other $\{111\}$ planes, which are the slip planes, meet the surface at 70.5 degrees, and consequently, if a positive dislocation has its extra half-plane in the acute angle between slip and etching planes, a negative dislocation has its half-plane in the obtuse angle. According to Livingston, this difference in position of the extra half-plane causes the difference in etching depth of the pits, the deeper pits being formed when the extra half-plane is in the acute angle; a convincing explanation for this effect has not yet been advanced.

Finer details of the etch pits may be seen in the electron micrograph, Figure A-2. A parlodion replica was made of the surface, and after shadowing with chromium was examined in a Siemens Elmiskop I microscope. A black pit appears at lower left, a white at upper right. The sides of the black pit are covered with a fine structure which has been determined, through the use of shadowing balls on the replica, to consist of tiny hills on the pit walls. Similar features appear on Young's (1962a) micrographs made from pre-shadowed carbon replicas, although

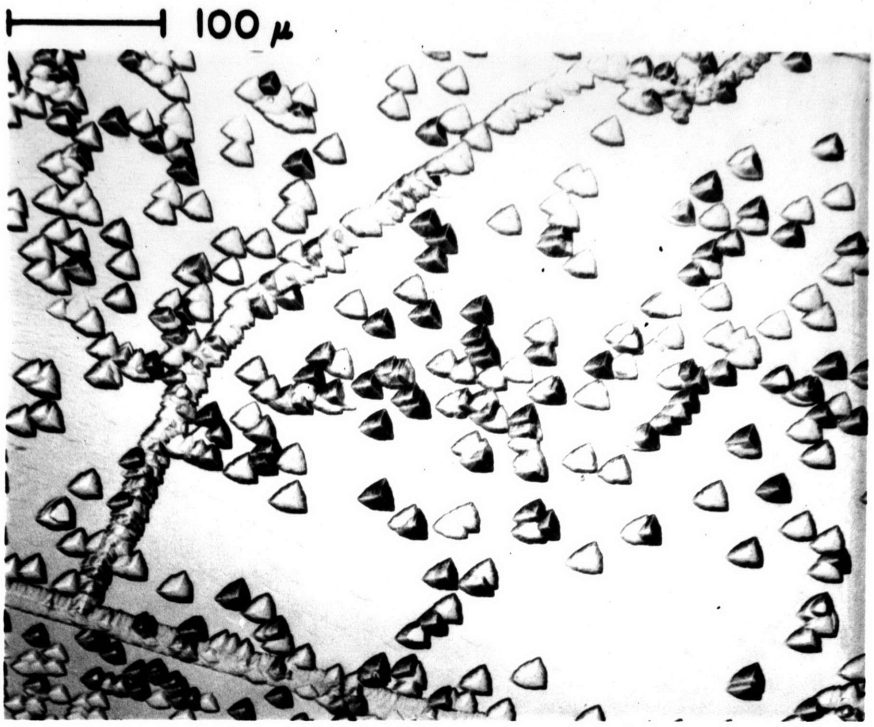

Fig. A-1. Dislocations revealed by Livingston's etch on a {111} face of copper.

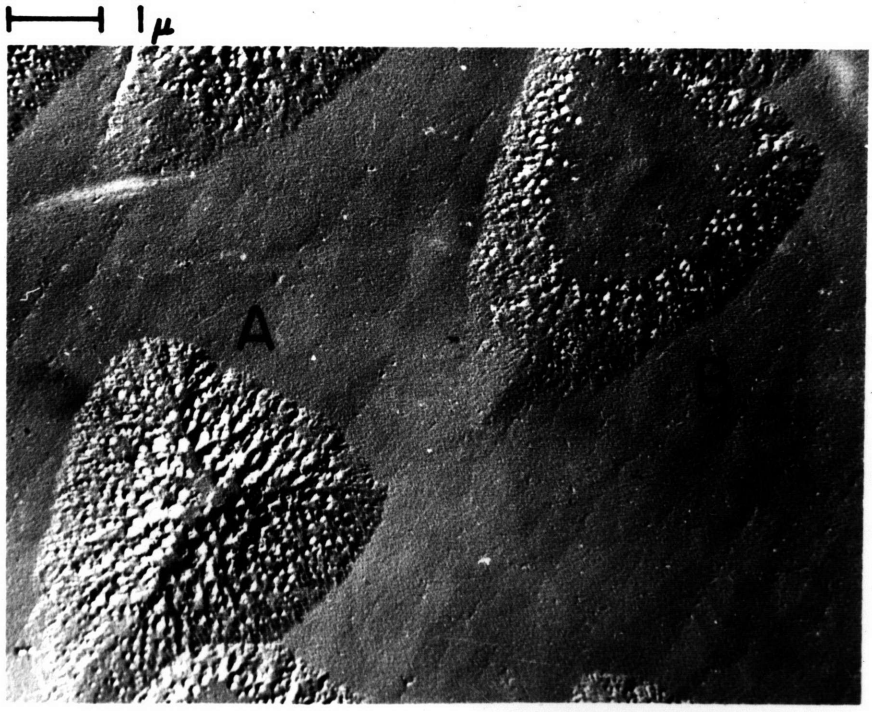

Fig. A-2. Electron micrograph of a surface replica showing fine structure of black (A) and white (B) pits.

he did not discuss them. Hills can also be seen near the edges of the white pit, a region in which it appears that the slope of the pit is steeper than near its center. The light micrograph, Figure A-1, also shows a black (high slope) region at the edges of the white pits. Apparently the small hills are formed only on slopes with a certain minimum slope.

After deformation in the easy glide regime, various etch pit configurations appear which are consistent with the idea that most of the dislocation multiplication and motion in this regime occurs on the primary system, and that blacks and whites represent positive and negative dislocations in the primary slip system. Figure A-3 illustrates one such configuration, with whites piled against one side of a sub-boundary and blacks against the opposite side, as would be expected if the pits represented opposite sign dislocations.

It may be assumed that edge dislocations on the critical and conjugate planes which meet the etching plane at the 70.5 degree $\{111\}$ interplanar angle also obey the black-white governing laws outlined above. There are, however, dislocations in the crystal which have other orientation relationships with the etching plane, and the etching behavior of such dislocations has not been established. Young* has studied the etch pits formed at various types of dislocations with different relationships to the surface, but has not been able to formulate a rule of etching behavior. The lack of such information makes it difficult to analyze sub-structure, for example, in Figure A-4, in which some of the sub-boundaries are light, others dark and some mixed, and in which one sub-grain is filled

---

*F. W. Young, Jr., personal communication.

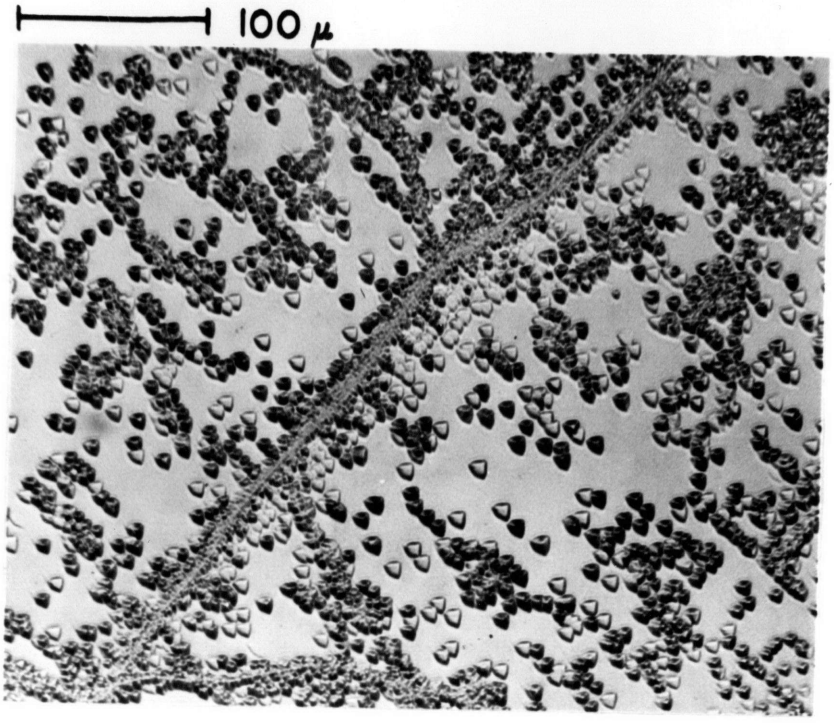

Fig. A-3. Dislocations of opposite sign, shown by black and white pits, piling up at opposite sides of a sub-boundary in easy glide.

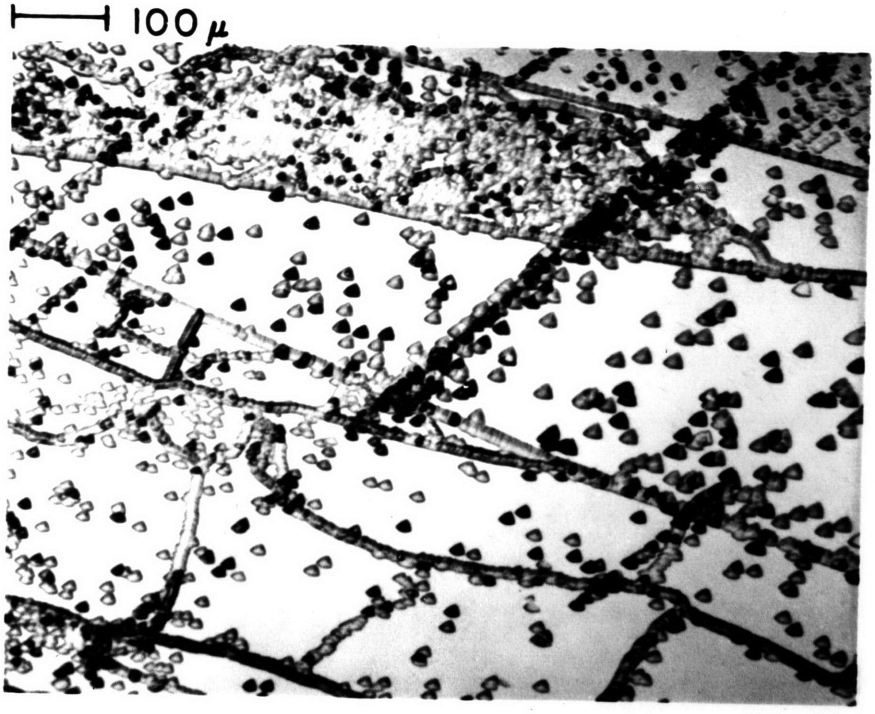

Fig. A-4. Sub-boundaries black, white, and mixed, and a sub-grain filled with white pits.

with white pits. The pits in the band along the primary slip direction show the black-white differentiation of primary edge dislocations.

Figure A-5 shows a further example of the pits formed at dislocations which are not of the primary edge type. This was the pit distribution on the cross plane following a twist of the crystal (the experiment is discussed in Appendix C). In this case the dislocations which intersect the etching face are mostly screw dislocations on the conjugate plane. It can be seen that most of the pits are of a white variety. The few blacks could mark edge dislocations. Since the crystal was twisted in one direction and then back again, both positive and negative screw dislocations were introduced, and the fact that almost all of the pits are white in nature suggests that there is no black-white effect for these screw dislocations. Applying this thought to Figure A-4 suggests that the subgrain filled with white pits is an expanded twist boundary.

The previous discussion has been concerned with the formation of etch pits at the sites of dislocations. If a crystal is etched, then strained to move some of the dislocations and then re-etched, three types of pits will be observed: where a dislocation has remained at its original site, the original pit will continue to grow with a pointed bottom; at a vacated dislocation site, the original pit will continue to grow laterally but becomes flat-bottomed; and at the sites of the dislocations which moved, or at the sites of newly created dislocations, pointed bottom pits form (Livingston 1960, Young 1961b, Livingston 1963). The black-white effect continues, but transient conditions at the start of re-etching complicate the pit forms. Figure A-6 illustrates the re-etching behavior. Pit A is a black at the site of a dislocation which remained in position; B is a

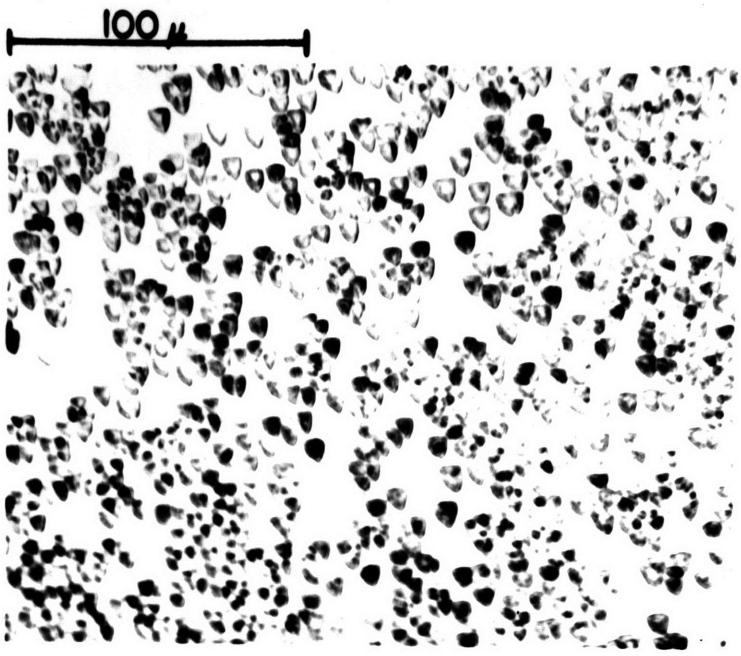

Fig. A-5. Predominantly white pits resulting from a twisting cycle.

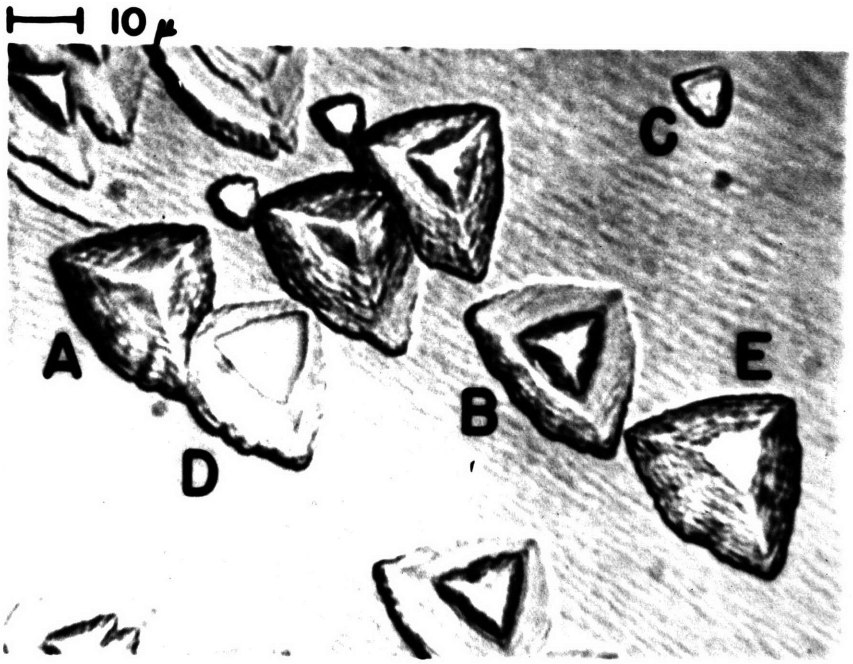

Fig. A-6. Re-etching behavior. A and B are, respectively, black and white pits at the sites of dislocations which did not move during straining; C a new pit; D and E, respectively, white and black pits where dislocations moved.

similar white pit; C is a pit (whether black or white it is difficult to tell at this small size) at a site to which a dislocation moved; D is at the site of a 'white' dislocation which moved away; and E is a similar black pit.

Whereas pit A has its expected appearance, pit B contains an annular black ring although at its center it has regained its white nature. The apparent explanation for this is that when etching (or re-etching) commences, it does so with a deep bite into the surface, forming a steep slope to the pit. As etching proceeds, this transient dies out and the pit regains its normal slope. The steep region moves away from the center as the pit grows. This explanation is shown diagrammatically in Figure A-7. The explanation implies that any white pit will have a black border; this effect has been pointed out for Figure A-1.

The reason that the flat bottoms of pits D and E are not of the same size, although the etching times were the same for both, is that the speed with which a slope discontinuity propagates in a pit is dependent on the size (angle) of the discontinuity (Hulett and Young, 1965). Because of the difference in slope of the sides of black and white pits, the angle of discontinuity to the flat bottom is different in the two cases.

An additional feature of re-etching is that the surface of the crystal is much more likely to develop ledges and other markings than it is on a first etching, the reason possibly being that the first etching leaves some deposit on the surface. An example of such a ledged, roughened surface is shown in Figure A-8. In this photograph the internal surfaces of the pit have also become roughened.

The etching behavior considered previously has been for dislocations at rest. Experiments have also been performed in which a crystal

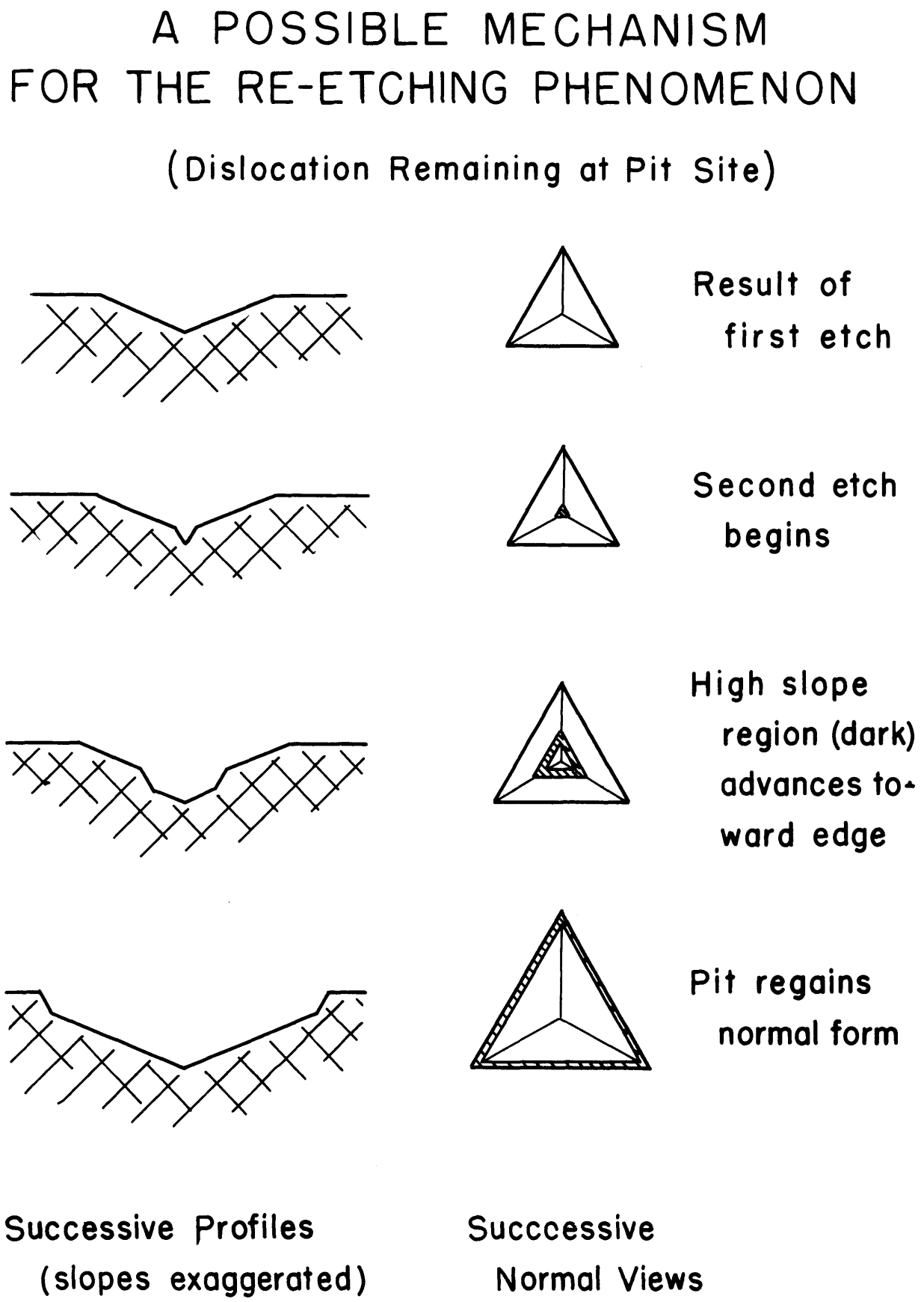

Fig. A-7. A possible mechanism for re-etching behavior.

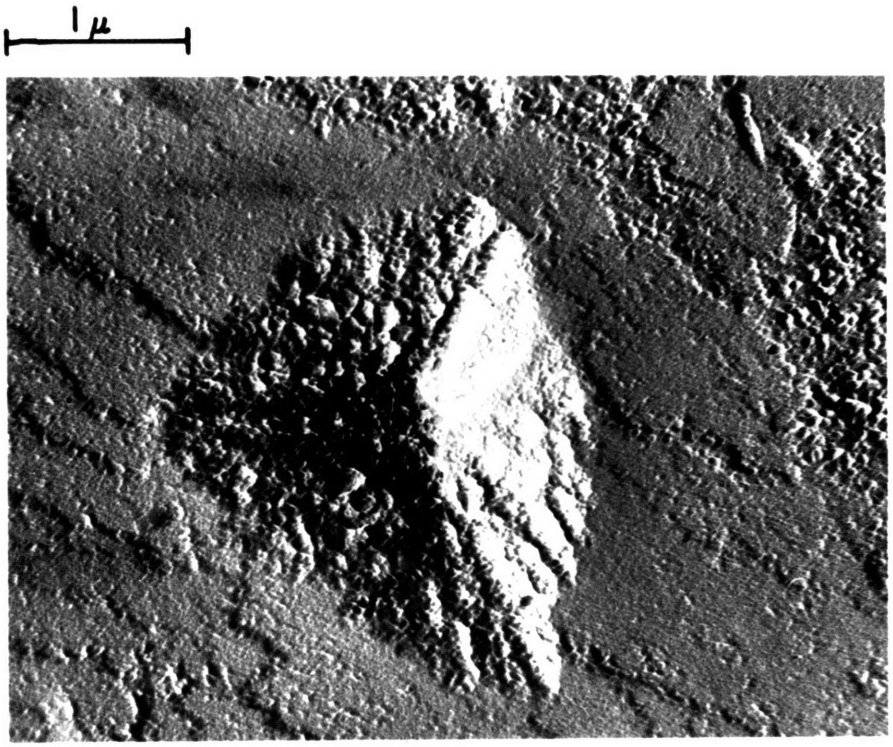

Fig. A-8. Electron micrograph of a surface replica showing fine structure of pit and ledges on surface following re-etching.

was etched while it was being strained above the yield stress. If the initial and final dislocation positions were linked by a continuous trail of pits or by a sequence of isolated pits (as was observed by Young (1961b) below the macroscopic yield stress), the technique could be used to measure mobile densities and slip distances reliably. The procedure was to preload the crystal, bring the etching bath into contact with it and etch ten seconds, strain and etch for about 20 seconds, stop straining and etch an additional ten seconds.

The result was that between the initial and final position pits, no trails or other pits were visible by light microscopy; it is possible that trails did form but were too shallow to be detected. A similar negative result was obtained when etching was attempted during unloading. If it is correct that no trails formed, the conclusion is that an incubation period is necessary for etching to commence, so that a moving dislocation can not be etched.

The average velocity of dislocations in motion during etching was estimated to be $3 \cdot 10^{-4}$ cm/sec. This estimate was made according to the equation for strain rate,

$$\dot{\gamma} = bN_m v$$

where v is the average velocity of a dislocation density N_m in motion at any instant. The strain rate was determined from LVDT displacement measurements and was $9 \cdot 10^{-7}$ per second. The mobile density was taken as 10^5 per cm^2, which could be an underestimate by no more than a factor of ten, since the total density was about 10^6 per cm^2; it could be an overestimate by at least as much.

Until now this discussion has concerned the etching of {111} surfaces, the type for which Livingston (1962b) reported the etchant successful. It has been found that the etchant also works on {100} surfaces. Young (1961a) successfully etched dislocations on the {100} face with a modified {111} etch, but etching of {100} has never been employed in connection with a deformation investigation. The observations to be described were made on a crystal grown in the usual way, but one which did not take on the seed orientation, growing instead with two opposite faces one degree off (100) and with an axis nine degrees from [011] on the tie line to (001). Prior to etching the crystal was given the usual electropolishing.

Figure A-9a shows the result of etching the virgin crystal. Both black and white pointed-bottom pits appear (A and B), as well as several other pit forms which have not been analyzed. It is likely that the explanation of black-white pitting is the same for {100} as for {111} surfaces, since in both cases the slip planes intersect the etching surface non-perpendicularly (in the {100} case the angle is 54.7°).

The crystal was deformed in tension and yielded at a resolved shear stress of 39 g/mm^2. Figure A-9b shows multipole groups forming after $2 \cdot 10^{-3}$ shear strain. Again, in addition to the strong black-white pitting, other types of pits appear. Clusters after a shear strain of $8 \cdot 10^{-3}$ are shown in Figure A-9c. The clusters do not show the orientation effects found for single-slip crystals, although it seems that the formation of multipoles is a feature common to deformation of either orientation.

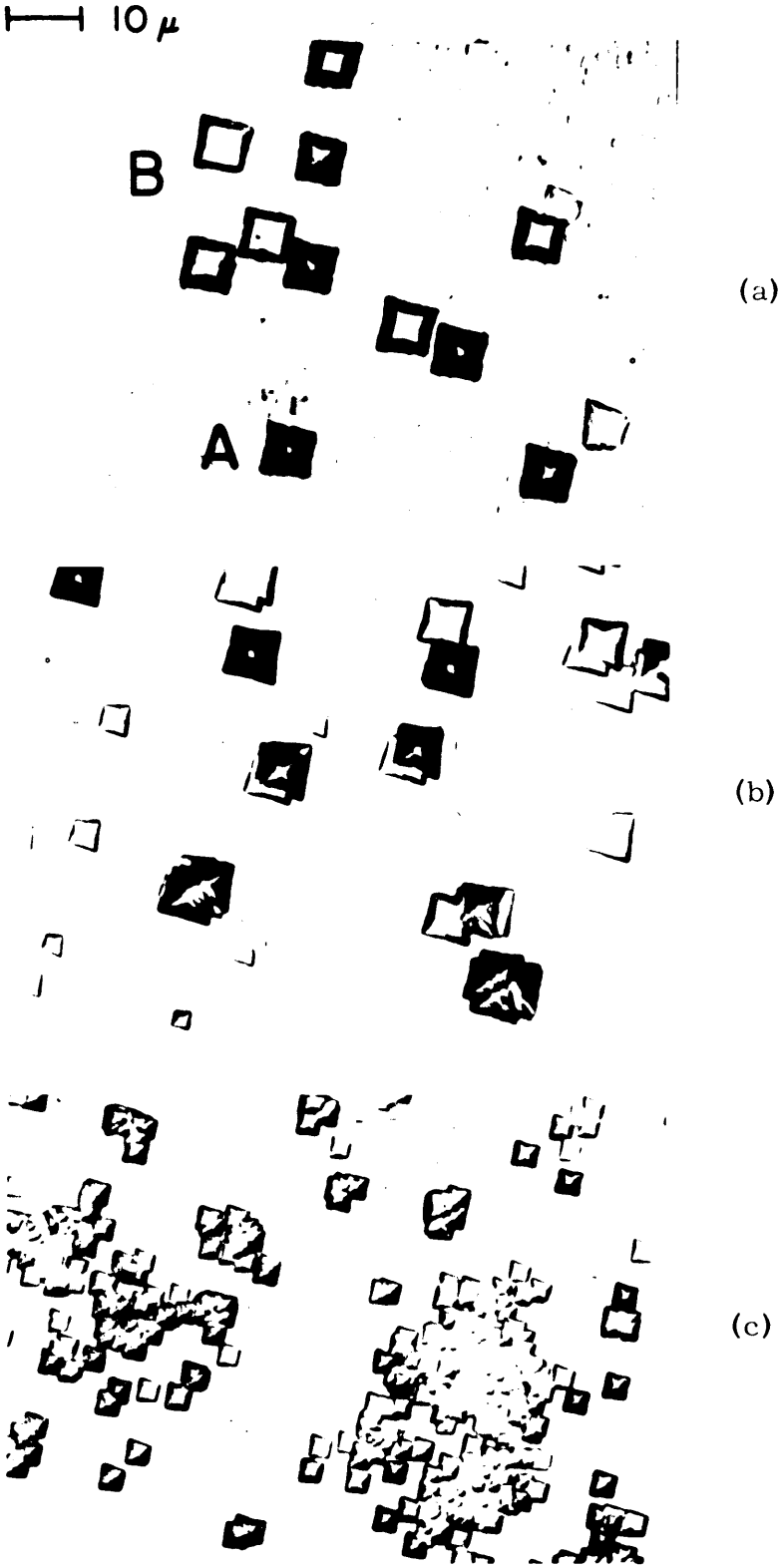

Fig. A-9. Dislocations revealed by Livingston's (1962b) etch on a {100} surface of copper. (a) Virgin crystal showing black (A) and white (B) pits; (b) after $2 \cdot 10^{-3}$ strain; (c) after $8 \cdot 10^{-3}$ strain.

Appendix B

DAMAGE DUE TO SPARK CUTTING

Although the spark cutting method is widely considered to be the most strain-free method of metal machining, considerable damage is introduced into a copper crystal by a spark cutting operation when this damage is measured on the scale of dislocation densities in virgin crystals.

The depth of damage was studied on a crystal (5-13) subjected to the same cutting operation later employed to expose the primary slip plane for etching to determine the relation between applied twist and dislocation density (Appendix C). The machine employed was a Servomet Model SMC made available by the Materials Division of the Civil Engineering Department, M. I. T. The crystal was glued with Duco cement into a brass jig which aligned the primary slip plane with a .030 inch-thick brass plate electrode which descended toward the crystal under the action of the servomotor in the machine. Kerosene was used as the dielectric medium and was directed through the cut by a jet under the liquid surface. Cuts were made on speed setting '7', the slowest available. The time of a cut was about ten hours. When the crystal had been parted, it was removed from the machine and the cement dissolved in acetone.

The spark-cut primary plane, while nominally flat, was so irregular on a fine scale that it could not be etched without electropolishing. The damage as a function of depth from the spark-cut surface was determined by alternately polishing and etching the crystal. The polishing rate had been previously determined on other crystals, and for the polishing conditions

employed (5.0 volts) was five microns per minute.

The etch pit density versus depth data, Figure B-1, indicates that in the spark cutting operation dislocations were introduced into the crystal to a depth of about 0.7 mm, at which point the density had fallen to about $1 \cdot 10^5$ per cm^2. This was also the density observed on the cross plane prior to the spark cutting operation, and the fact that the density on the spark-cut primary plane fell to the same value implies that the initial dislocation density of the crystal is the same whether measured on the primary or cross planes.

The depth of damage was also measured after spark-cutting by etching the cross plane. The etch pit density observed in this way decreased with distance from the cut surface, and the depth of damage estimated by this method agreed with that determined as described above.

The sequence of photographs in Figure B-2, corresponding to the data points of Figure B-1, shows that near the cut surface the damage consisted of a cell structure of dislocations breaking down with increasing distance from the cut toward the isolated-pit density characteristic of virgin material.

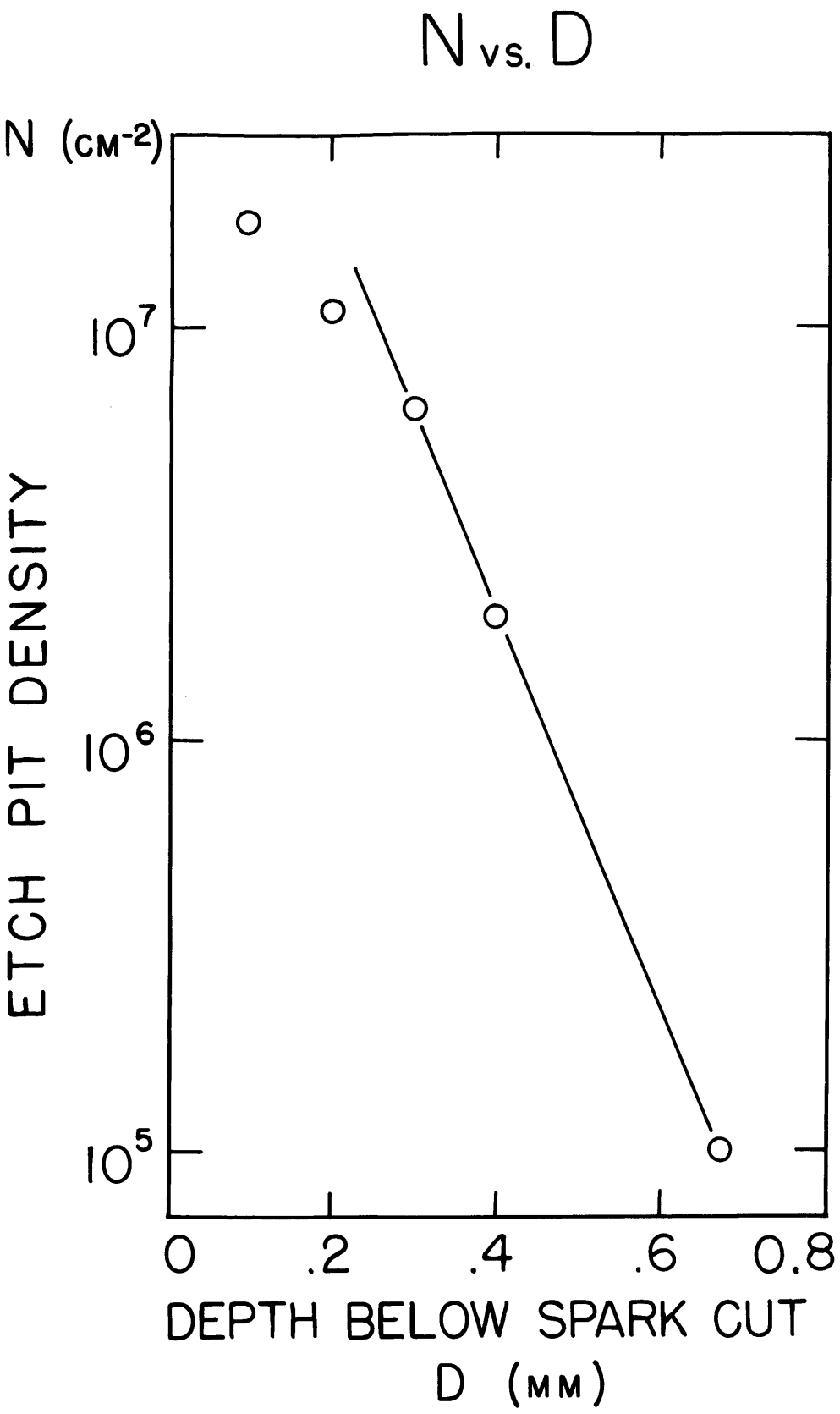

Fig. B-1. Relation between etch pit density on primary plane exposed by spark-sectioning and distance below the cut.

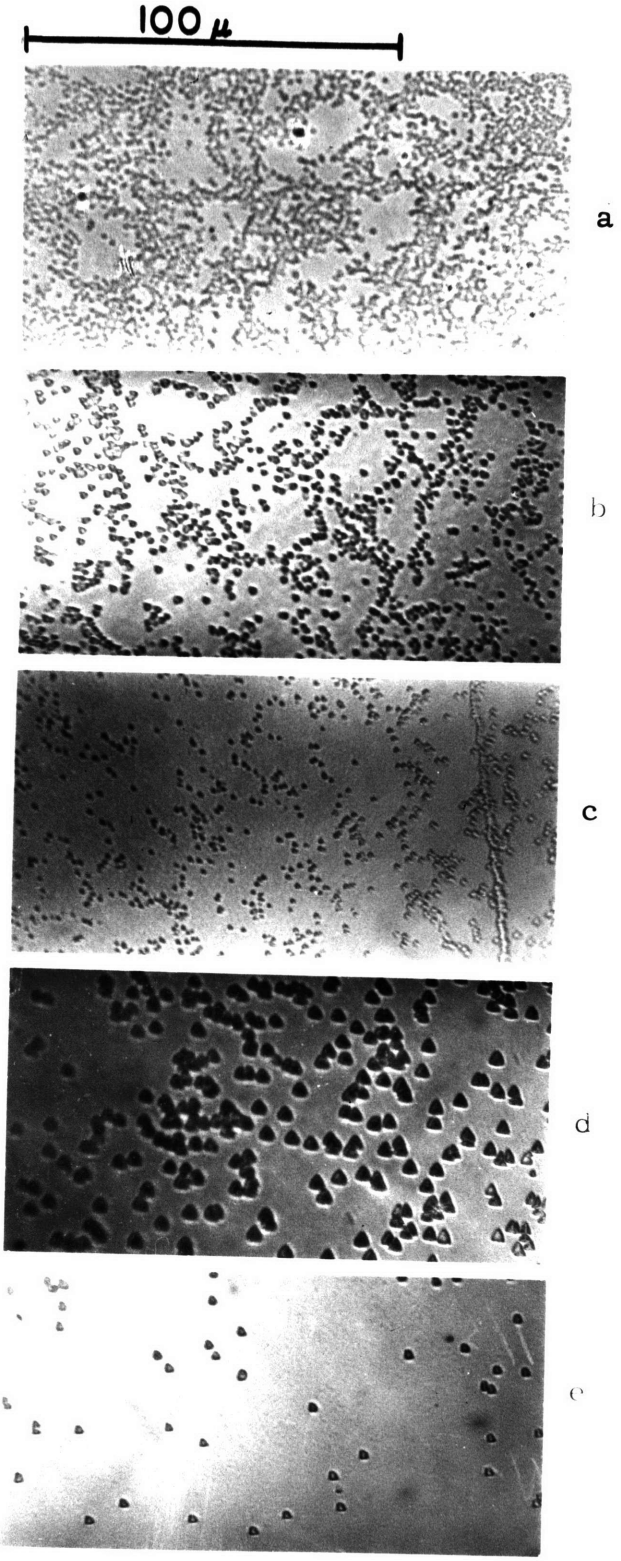

Fig. B-2. Etch pits at successive depths below spark-cut primary plane. (a) 0.1 mm; (b) 0.2; (c) 0.3; (d) 0.4; (e) 0.7.

Appendix C

DISLOCATION DISTRIBUTION INTRODUCED BY TWISTING THE CRYSTAL

The dislocation distribution introduced into a crystal by twisting was determined by sectioning a twisted crystal (5-18) along the primary plane by spark cutting, and then etching the plane thus exposed as well as the $\{111\}$ side faces of the crystal. Etch pit densities on these faces were plotted as functions of twist in Figure 3.5-1.

Prior to twisting, the crystal was glued into standard grips, in which condition it was accommodated in a small hand-operated twisting machine. The twisting device consisted of a steel block grooved to hold one specimen grip, the other grip resting in a similarly grooved collar which could be rotated with respect to the block, the axis of rotation being concentric with the crystal axis.

After the first twist of two degrees forward and two degrees back, the cement was dissolved in acetone and the crystal mounted for spark cutting as described in Appendix B. The first cut was taken two specimen thicknesses away from one grip. The smaller end of the crystal was then taken for polishing and etching, and the remaining longer section glued back into the grips and another twist given in the same manner as the first. The $3\frac{1}{2}$-inch length of the original crystal allowed for three such sectionings to be carried out, the final cut being midway between grips and still two specimen thicknesses from each. All three twists were $\pm$two degrees, which meant that the twist per unit length increased in the

series. In computing θ/L, a twist of two degrees forward and two back counted as four degrees.

The specimens generated by the above procedure were electropolished both to provide a good surface for etching and to remove the layer of damage resulting from spark cutting. In mind of the results of the damage experiment described in Appendix B, at least 0.7 mm was polished off before etching.

The amount of twist to be applied was chosen from a consideration of the amount of strain it would produce, and the increase in dislocation density that might reasonably be expected to result from such a strain. Using as an approximation the torsion formula for circular bars,

$$\gamma = r \frac{d\theta}{dz}$$

and taking Livingston's (1962b) result that in a double-slip tensile configuration a strain of one percent increased the dislocation density to nearly 10^7 per cm^2, an initial twist of ±2 degrees was calculated to provide a surface shear strain of one-half of one percent. This twist proved satisfactory and the same angular amount was chosen for the subsequent twists.

The stress state in torsion is quite different from that in tension, since in torsion the primary slip plane is little stressed, lying as it does at nearly 45° to the axis. The conjugate plane, which is nearly perpendicular to the axis, is highly stressed in torsion.

The idea with which the twisting experiments were undertaken, that the dislocations threading the primary plane (forest dislocations) could be increased relative to the primary density, was born out by the etch pit measurements. The unusual feature of the twist-density plot, that

the densities measured on the primary and cross planes become equal at one twist level, was reproduced on a second crystal (4-2). The fact that the etch pit density on the cross plane increases more rapidly with twist than the density on the primary plane reflects a changing distribution of slip on the various systems.

Although no detailed observations were made on the dislocation structures produced by twisting, evidence was seen for the development of a cell structure, Figure C-1. The vertical cell walls lie roughly along the $[\bar{1}01]$ line of intersection of the primary plane and the cross plane. The other walls are not as closely oriented to intersection directions.

The etch pit counts were made in regions roughly midway between the specimen surface and axis, although it was noted that the distribution of etch pits on the primary plane was reasonably uniform. Uniformity in dislocation distribution across the primary plane of a spark-cut twisted crystal has also been reported by Basinski and Basinski (1964), and is analogous to Livingston's (1962a) finding an absence of an elastic core in bent specimens.

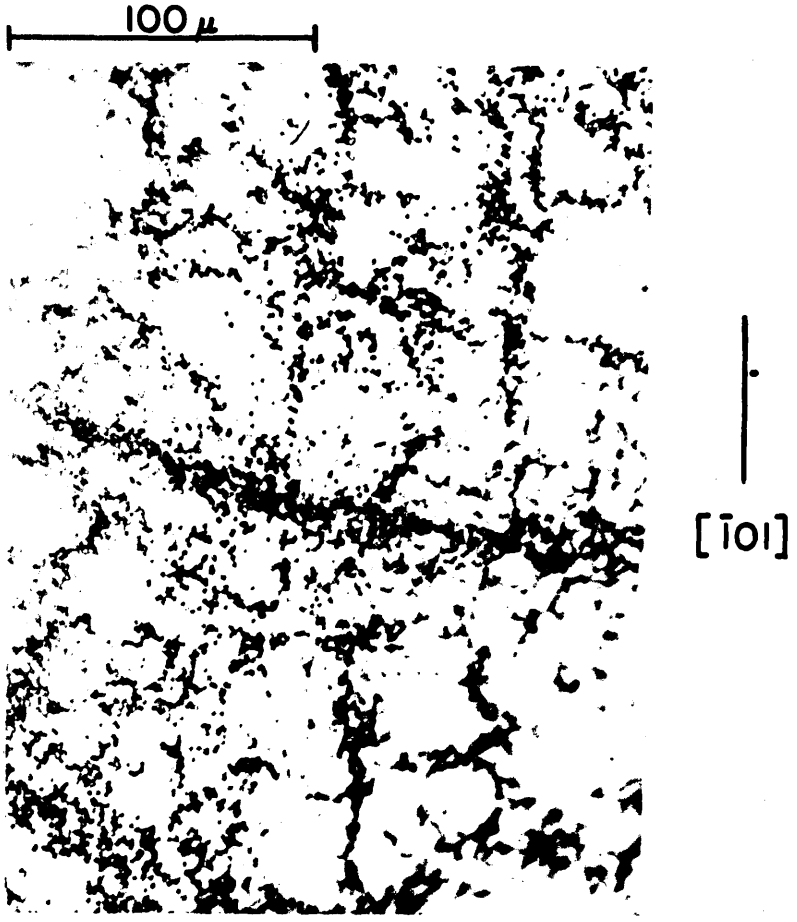

Fig. C-1. Etch pit distribution on cross plane after twisting crystal.

Appendix D

BEHAVIOR IN ALTERNATING TENSION AND COMPRESSION

In addition to studying the stability of dislocation groupings on unloading, as described previously, it was attempted to determine the behavior on reverse loading. It was found that clusters formed in tensile loading remained on subsequent compressive loading, but the occurrence of extensive slip on the critical and conjugate planes complicated the experiment.

Loading was carried out in a small hand-operated machine equipped with a load cell with the specimen mounted rigidly between crossheads. No provision was made for rotation of the grips to accommodate specimen rotation during deformation, as had been done in the regular tensile experiments. The specimen length was one inch between the grips into which the crystal was glued. The crystal was loaded to a resolved shear stress of 42 g/mm^2 in tension and 54 g/mm^2 in compression, both stresses being sufficient to cause extensive dislocation multiplication. It was estimated that a plastic shear strain of about $1 \cdot 10^{-3}$ was introduced in tension, and $2 \cdot 10^{-3}$ in compression. The crystal was polished and etched in the annealed condition prior to testing, and again after both the tensile and compressive deformations.

The photographs of Figure D-1 illustrate both the stability of clusters and the occurrence of extensive non-primary slip. The cluster A formed after the tensile half-cycle clearly remains at least as extensive after the compressive half-cycle. The etch pit band B' corresponding to

Fig. D-1. Etch pits in same region on virgin crystal (a), after tensile half-cycle (b), and after compressive half-cycle (c). The cluster (A) formed in tension remains after compression (A'). Etch pit band B' is formed by critical plane dislocations.

slip on the critical plane was formed on the compressive half-cycle, but similar evidence of slip on both critical and conjugate planes was also seen after the tensile portion of the deformation. It was, however, much more pronounced in compression.

The occurrence of extensive non-primary slip was probably due to the specimen size and manner of gripping. The length of the specimen was such that every single critical plane in the crystal would pass through one end-effect region of the crystal, that is, the region less than one specimen thickness from the grip. The constraint of grip rigidity also may have contributed to activating slip on non-primary systems.

Appendix E

DISLOCATION ETCHING OF MAGNESIUM

Prior to the experiments on copper, attempts were made to develop for magnesium an etchant which would reveal both fresh and grown-in dislocations. The result was that although grown-in dislocations were sometimes revealed, fresh dislocations could not be etched.

Although there is no general theory of etching which would enable one to produce directly a workable formula, certain basic principles have been suggested by Young (1961a). These are that the etchant should be capable of oxidizing the metal, and should contain a 'poisoning agent', often a halide ion, to retard lateral growth of the pit.

Etching was carried out on $\{10\bar{1}0\}$ faces obtained by acid sawing from a large single crystal (the technique has been described previously (Brydges 1963)). The specimens were annealed at 390°C for 11 hours and were electropolished to provide a smooth surface. Electropolishing was done either in a solution of hydrochloric acid and butyl cellosolve, or in a solution of 40% ethyl alcohol, 40% orthophosphoric acid and 20% water.

Both chemical and electrolytic etching were tried with hydrochloric acid-based solutions containing chloride, fluoride, or iodide ions introduced by adding metallic salts. Solutions with oleic, palmitic, hydrofluoric, iodic and hydrobromic acids, and basic solutions containing ammonium hydroxide with various halide ions, were also tested. In most cases there was some attack or pitting of the surface, but in only one case

was the formation such as to suggest that dislocations were being preferentially etched. None of the etching solutions passed a scratch test, in which before etching the crystal surface was scratched with a pin so that a high density of fresh dislocations would be introduced in a known region. An etch which revealed fresh dislocations would be expected to show a high pit density around the scratch, but none did.

Figure E-1 shows pits which may correspond to grown-in dislocations (deduced from the apparent sub-boundaries and pit alignments). The etching procedure was immersion for twenty minutes in 100 milliliters of 0.01 normal hydrochloric acid with the addition of one drop of a weak zinc fluoride solution (the use of the fluoride ion was suggested by Young*). This etch was insensitive to the scratch test.

*F. W. Young, Jr., personal communication.

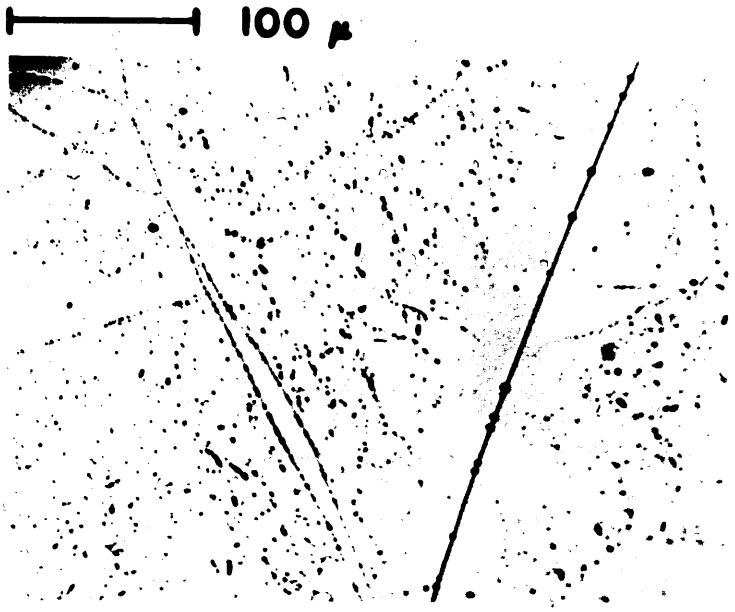

Fig. E-1. Etching of magnesium. The composition of the etchant was 100 ml 0.01 N HCl with one drop of a weak zinc fluoride solution.

ACKNOWLEDGMENTS

In the course of this thesis the author benefited from the advice and assistance of numerous persons in addition to his thesis adviser, Professor A. S. Argon, and committee members, Professors E. Orowan and R. B. Williamson. The following are especially thanked: Professor F. A. McClintock, Dr. J. D. Livingston, Dr. F. W. Young, Jr., William Henry, and Robert Leonard.

The National Science Foundation supported the work.

BIOGRAPHICAL NOTE

The author, William Thomas Brydges III, was born December 30, 1940 in Oak Park, Illinois. He attended public schools in Illinois, and graduated from Springfield High School, Springfield, Illinois in 1958.

Since 1958 he has studied at the Massachusetts Institute of Technology, from which he received the degrees of Bachelor and Master of Science in Mechanical Engineering in 1963. While at M. I. T. he has held research and teaching assistantships, and a National Science Foundation Traineeship.

Societies of which he is a member include Sigma Xi, Tau Beta Pi, Pi Tau Sigma, the American Society for Metals, and the Society for the History of Technology.

The author's wife is the former Ellen Morse of Northfield, Vermont. A son, William Charles, was born October 6, 1966.